MCR-75-21
Contract NAS8-30592

Final
Report

May 1975

Acquisition System Environmental Effects Study

MARTIN MARIETTA

MCR-75-21

Contract NAS8-30592

Final
Report

May 1975

ACQUISITION SYSTEM ENVIRONMENTAL EFFECTS STUDY

Approved

R. P. Warren
Program Manager

MARTIN MARIETTA CORPORATION
P.O. Box 179
Denver, Colorado 80201

FOREWORD

This document is submitted to the National Aeronautics and Space Administration, Marshall Space Flight Center, in accordance with the Data Requirements description of Contract NAS8-30592. The work was performed in the Propulsion Section of the Aerothermal and Propulsion Engineering Department of the Martin Marietta Corporation. The work was administered under the technical direction of Mr. George Young, NASA-MSFC Technical Monitor. The Martin Marietta contract manager was initially Mr. G. R. Page who was succeeded by Mr. R. P. Warren when Mr. Page left the Martin Marietta Corporation.

Individuals who contributed heavily to this work were: Mr. J. R. Butz who was involved in both the analytical and experimental aspects of all of the phases of the contract; Mr. J. Marino who, as the laboratory supervisor, was instrumental in the test coordination and without whom the testing would not have occurred in the smooth fashion that it did; Mr. C. D. Maytum who contributed heavily to the interpretation and analysis of the vibration data; Mr. R. G. Wilson who prepared the Phase III test procedures; Mr. D. J. Brown who was responsible for the implementation of all instrumentation requirements; Mr. J. D. Carpenter who performed the flow transient analysis; and Mr. R. Spurrier who served as technician.

CONTENTS

I. INTRODUCTION

Capillary acquisition devices are utilized within liquid tankage which must operate under reduced or zero gravity conditions such as are encountered in a variety of orbital and extra orbital missions. These devices insure that a single phase outflow of either liquid or gas is available on demand. Common usages would include propellant tankage, fuel cell reactants, coolant supply and life support fluids. These devices which utilize the liquid-vapor interfacial surface tension may be designed for use with both normal and cryogenic fluids. Fine-mesh screens are generally utilized in the construction of the capillary devices which are required to operate in the larger adverse acceleration range.

The basic objective of this study has been to quantify the effects of vibration, warm gas exposure, and feed system startup/shutdown fluid dynamics on capillary screen propellant retention capabilities. Previous technology efforts have definitely established such effects as potentially severe design constraints on the utilization of capillary acquisition systems for zero-g engine restarts. The objective here has been to extend the existing technology to the point where quantitative conclusions in terms of design criteria may be drawn.

The effects of vibration on capillary stability have been investigated experimentally by McDonnell Douglas, Eastern Division, with a spherical screen device (Ref. 1.1), by McDonnell Douglas, Western Division, with small planer screen samples (Ref. 1.2), and by Martin Marietta with an annular cylindrical device (Ref. 1.3). The results with the spherical screen device obtained for random vibration and for sinusoidal vibration at frequencies below 14 Hz were predictable from a simple hydrostatic theory. The observed stability exceeded the hydrostatic predictions for

sinusoidal vibrations at frequencies in the range of 14 to 150 Hz. Destruction of the capillary stability was observed at frequencies in the range of 150 to 300 Hz. This was attributed to a resonant condition. The results reported in Reference 1.2 showed substantial bubble point reductions but were not correlated by the hydrostatic theory. The data obtained by Martin Marietta was predictable by the simple hydrostatic theory.

The fluid transients that occur during the startup/shutdown phases of a typical propulsion system present an area of concern for the design of a capillary acquisition system. Hydraulic transients produce pressure surges when propellant outflow is initiated and terminated. The pressure surges could be large enough to cause ingestion of gas into the controlled liquid volume of the acquisition device. During the startup phase, the rapid acceleration of propellants from the device could produce a pressure drop within the device resulting in a pressure differential across the screen that could exceed the retention capability of the screen. During the shutdown phase, a water hammer pressure surge may cause propellant spillage from the controlled liquid volume of the device while gas ingestion may result from the rarefaction wave.

Considerable analyses and data are available on the behavior of propellants during initiation and termination of flow as applied to the design of propellant storage and feed systems. However, for an acquisition system that requires a close control of pressure differentials across capillary barriers, analytical and experimental data is limited. The most significant recent study in this potential problem area was conducted by Rockwell International under Contract NAS7-200 (Ref. 1.4). This program was, however, terminated prematurely and correlation of the test

and analytical data was not accomplished.

Although there has been much discussion, there is very little experimental data existant in the area of warm gas effects on cryogenic acquisition devices. Martin Marietta has built and tested, under Contract NAS9-12182, a liquid hydrogen acquisition device (Ref. 1.5). Liquid hydrogen was successfully outflowed from a screen device against one earth gravity. Most of the testing had been accomplished with cold pressurant gas bubbled in through the liquid. One test was run, however, with warm, 83K (150R), hydrogen pressurant and the screen device appeared to perform well. In contrast to this, McDonnell Douglas under Contract NAS8-27571, has experienced breakdown when a screen device has been exposed to warm pressurant gas; both hydrogen and helium (Ref. 1.6). The Martin Marietta screen device consisted of multiple layers of 325 x 2300 Dutch-twill screen, whereas the McDonnell Douglas device consisted of a single layer of 250 x 1370 screen.

II. SUMMARY

The experimental vibration studies conducted under the first phase of this contract have been structured to determine the effective acceleration at the screen for a given input acceleration and to determine what effect this effective acceleration, vibration frequency and screen mesh have on capillary stability. The test model for these tests consisted of a vertical screen which separated liquid (alcohol) and gas regions within a transparent channel. This model was mounted on a shaker table and subjected to both random and sinusoidal vibrations in directions which were both normal and parallel to the screen surface.

The startup/shutdown studies which were done under Phase II of this contract, had the objective of defining the severity of a flow transient which would result in a destabilization of the liquid vapor interface at the screen surface such that vapor would be ingested into the liquid outflow channel. Two test models were utilized. One of these, a four-channel device, which was available from a previous program, was utilized with methanol as the test fluid. The other model, an eight-channel device, also available from a previous program (Ref. 1.5), was tested with liquid hydrogen.

Under Phase III of this contract the effects of warm pressurant gas on a liquid hydrogen acquisition device were evaluated. The eight-channel test model was utilized with both hydrogen and helium pressurants. The objective was to determine under what conditions of heating and exposed screen surface, would screen dryout occur for two orientations of the tank.

Details of each task are included in Sections III, IV, and V. Some of the major findings are listed here.

1. The performance of a capillary acquisition device subjected to wide band random vibrations or sinusoidal vibrations

which are well above the resonant frequency of the device can be predicted using hydrostatic theory.

2. Pressure differentials far in excess of the screen bubble point but of short duration (1-7 ms) did not lead to gas ingestion into the screen device.

3. With the proper operating procedures, a capillary screen device with either warm hydrogen or helium pressurant can be utilized to provide gas-free liquid outflow when there are no stagnant liquid regions within the acquisition device. This includes operation in adverse acceleration environments up to one g. Further testing is required to define the operating procedures which would allow operation with stagnant liquid regions.

III. VIBRATION EFFECTS

A. DESCRIPTION OF TEST ARTICLE

The test model consisted of a transparent, cast polyester, single channel fabricated in two parts and assembled with a test screen specimen sandwiched between the halves, as shown in Figure 3.1 There are two ports at the top and one at the bottom of each half. The model is mounted vertically in a holding fixture (see Figure 3.1). Six screen specimens were tested. These consisted of a test screen and support plate which are resistance welded to a stainless steel frame. Solder is used to repair weak points in the weld and imperfections in the screen. The measured bubble points for these screens are listed in Table 3.1.

The dimensions of the screen specimens were 6.3 x 40 cm (7.5 x 15.6 inches). The thickness of the liquid layer adjacent to the screen was 1.3 cm (0.5 inch). The thickness of the ullage layer was, in some cases, 1.3 cm (0.5 inch), and in others, 2.54 cm (1.0 inch).

The test system flow and instrumentation schematic is shown in Figure 3.2. Valves and plumbing are provided to accomplish the fill, vent, pressurization, and outflow functions. The shaker system is rated at 26,700 Newtons (6000 lb force), and has a frequency range of 5-2000 Hz, with a variable octave sweep rate.

Instrumentation includes a manometer, Kulite miniature pressure transducer, and four accelerometers. The manometer was used to measure an initial differential pressure before each test. The transducer monitored pressure on the liquid side of the channel during testing and the output was recorded on a visicorder oscillograph. Accelerometer locations are shown, for

Table 3.1: Measured Retention Pressures (Bubble Points) of Test Screen Configurations

Configuration No.	Screen Mesh	No. Layers	Measured Capillary Retention Pressure* ΔP_c, cm H_2O	(in. H_2O)	Support Configuration
1	325 x 2300	1	63.5	(25.0)	Perforated Plate**
2	325 x 2300	2	127.0	(50.0)	Perforated Plate
3	325 x 2300	2	111.7	(44.0)	100 x 100 Square Mesh Screen
4	200 x 1400	1	44.5	(17.5)	Perforated Plate
5	200 x 1400	2	80.0	(31.5)	Perforated Plate
6	80 x 700	1	15.8	(6.2)	Perforated Plate

NOTES: *Measured in methanol.

**Perforated plate for all configurations is .0685 cm (.027 in.) thick with 50% open area.

the first series of tests, in Figure 3.2. Not all of these locations were utilized in all tests. The locations which were utilized for the first test series are listed in Table 3.2. Accelerometer number 5 is adhered to the perforated plate on the side opposite the screen. For the second test series, accelerometer locations 2 through 5 were not used. For the first eight tests of the second series, from one to three accelerometers were adhered directly to the screen as is shown in Figure 3.3 and listed in Table 3.3. Accelerometer output was recorded on magnetic tape and the data, after processing, was plotted in graphic form.

Table 3.2: Summary of Vibration Test Results, First Series

Test No.	Screen Config. No.	Hydrostatic Head cm	(in.)	ΔP_i + Head H_2O cm	(in.)	Acceleration Environment Type	Direction	Input G	Frequency	Location	Dir
1a	1	39.6	(15.6)	53.34	(21.0)	Random	Vertical	0.6, 1.0, 1.5	5-2000 Hz	#1, #3, #4	Ver
1b	1	39.6	(15.6)	53.34	(21.0)	Random	Vertical	0.6, 1.0, 1.5, 2.0, 2.5, 3.0, 3.5, 4.0	5-2000 Hz	#1, #3, #4, #5	Ver
1c	1	39.6	(15.6)	45.72	(18.0)	Random	Vertical	0.6, 1.0, 1.5, 2.0, 2.5, 3.0, 3.5, 4.0	5-2000 Hz	#1, #3, #4	
1d	1	39.6	(15.6)	58.42	(23.0)	Random	Vertical	0.6, 1.0, 1.5, 2.0, 2.5, 3.0	5-2000 Hz	#1, #3, #4	
1e	1	39.6	(15.6)	58.42	(23.0)	Random	Vertical	0.6, 1.0, 1.5, 2.0, 2.5, 3.0	5-2000 Hz	#1, #3, #4, #5	Hor
2	1	30.5	(12.0)	24.38	(9.6)	Random	Vertical	0.6, 1.0, 1.5, 2.0, 2.5	5-2000 Hz	#1	
3	1	20.3	(8.0)	16.0	(6.3)	Random	Vertical	1.5, 2.0, 2.5, 3.0, 3.5	5-2000 Hz	#1	
4	2	39.6	(15.6)	53.34	(23.0)	Random	Vertical	0.6, 1.0, 1.5, 2.0	5-2000 Hz	#1	
5	2	39.6	(15.6)	101.6	(40.0)	Random	Vertical	2.0, 2.5, 3.0, 3.5	5-2000 Hz	#1	
6	3	39.6	(15.6)	101.6	(40.0)	Random	Vertical	1.0, 1.5, 2.0, 2.5, 3.0	5-2000 Hz	#1	
7	4	20.3	(8.0)	16.0	(6.3)	Random	Vertical	0.6, 1.0, 2.0, 2.5	5-2000 Hz		
8	5	30.5	(12.0)	24.38	(9.6)	Random	Vertical	1.5, 2.0, 2.5, 3.0	5-2000 Hz	#1	
9	6	7.62	(3.0)	5.84	(2.3)	Random	Vertical	0.6, 1.0, 2.0, 2.5	5-2000 Hz		
10	7										
11a	1	39.6	(15.6)	48.26	(19.0)	Sine	Vertical	0.5, 1.0, 1.5, 2.0, 2.5, 3.0	5-2000 Hz	#1, #3, #4, #5	Ver
11b	1	39.6	(15.6)	58.42	(23.0)	Sine	Vertical	0.5, 1.0, 1.5, 2.0	5-2000 Hz	#1, #3, #4	
11c	1	39.6	(15.6)	58.42	(23.0)	Sine	Vertical	0.5, 1.0, 1.5, 2.0	5-2000 Hz	#1, #3, #4	
12	1	30.5	(12.0)	24.38	(9.6)	Sine	Vertical	0.5, 1.0, 1.5, 2.0,	5-2000 Hz	#1	
13	2	39.6	(15.6)	101.6	(40.0)	Sine	Vertical	1.5, 2.0, 2.5, 3.0	5-2000 Hz	#1	
14	3	39.6	(15.6)	53.34	(21.0)	Sine	Vertical	0.5, 1.0, 1.5, 2.0	5-2000 Hz	#1	
15	4	20.3	(8.0)	16.0	(6.3)	Sine	Vertical	0.5, 1.0, 2.0, 2.5	5-2000 Hz	#1	
16	5	30.5	(12.0)	24.38	(9.6)	Sine	Vertical	1.5, 2.0, 2.5, 3.0	5-2000 Hz	#1	
17	6	7.62	(3.0)	5.84	(2.3)	Sine	Vertical	0.5, 1.0, 2.0, 2.5	5-2000 Hz	#1	
18	7										

*DCWT - Data correlates with hydrostatic theory.

**NCWT - Data does not correlate with hydrostatic theory.

+ΔP_i - Initial pressure differencial across screen. (Ullage side minus liquid side)

FOLDOUT FRAME

	Frequency	Location	Direction #5	Pressure Data	Comments
	5-2000 Hz	#1, #3, #4	Vertical	No	DCWT* at all g levels.
	5-2000 Hz	#1, #3, #4, #5	Vertical	No	DCWT at all g levels.
	5-2000 Hz	#1, #3, #4		No	DCWT at all g levels.
	5-2000 Hz	#1, #3, #4		No	DCWT at all g levels.
	5-2000 Hz	#1, #3, #4, #5	Horizontal	No	DCWT at all g levels.
	5-2000 Hz	#1		No	DCWT at all g levels.
	5-2000 Hz	#1		No	DCWT at all g levels.
	5-2000 Hz	#1		Yes	NCWT** at all g levels.
	5-2000 Hz	#1		Yes	DCWT at all g levels, however, suspect dryout of first screen
	5-2000 Hz	#1		Yes	DCWT - suspect dryout of first screen.
	5-2000 Hz			No	DCWT at all g levels.
	5-2000 Hz	#1		Yes	DCWT at all g levels.
	5-2000 Hz			No	DCWT at all g levels. No test results due to bad screen/plate.
	5-2000 Hz	#1, #3, #4, #5	Vertical	No	NCWT at 0.5 and 1.0 g's low frequency (30-250 Hz); DCWT at all other g levels.
	5-2000 Hz	#1, #3, #4		No	NCWT at 0.5 and 1.0 g's low frequency (30-100 Hz); DCWT at other g levels.
	5-2000 Hz	#1, #3, #4		No	NCWT at 0.5 and 1.0 g's low frequency (30-105 Hz); DCWT at other g levels.
	5-2000 Hz	#1		No	NCWT at 0.5 and 1.0 g's low frequency (30 Hz); DCWT at other g levels.
	5-2000 Hz	#1		Yes	NCWT at 1.5 and 2.0 g's; DCWT at 2.5 and 3.0 g's.
	5-2000 Hz	#1		Yes	NCWT at all g levels-suspect dryout of first screen.
	5-2000 Hz	#1		No	NCWT at 1g, low frequency (90-100 Hz); DCWT at other g levels.
	5-2000 Hz	#1		Yes	NCWT at 1.5 and 2.0 g's, low frequency (20-30 Hz); DCWT at other g levels.
	5-2000 Hz	#1		No	NCWT at all g levels. No test results due to bad screen/plate specimen.

de)

FOLDOUT FRAME

2

Table 3.2: Summary of Vibration Test Results, First Series (continued)

Test No.	Screen Config. No.	Hydrostatic Head cm	(in.)	ΔP_i + Head H_2O cm	(in.)	Acceleration Environment Type	Direction	Input G	Frequency	Location	Di
19	6	7.62	(3.0)	5.84	(2.3)	Random	Horizontal	3.5, 4.0, 4.5, 5.0	5-2000 Hz	#1, #3, #4	
20	6	15.24	(6.0)	12.19	(4.8)	Random	Horizontal	3.5, 4.0, 4.5, 5.0, 5.5, 6.0	5-2000 Hz	#1, #3, #4	
21	6	16.76	(6.6)	12.45	(4.9)	Random	Horizontal	2.0, 2.5, 3.0, 4.0	5-2000 Hz	#1, #3, #4	
22	6	15.24	(6.0)	12.19	(4.8)	Sine	Horizontal	2.5, 3.0	5-2000 Hz	#1, #3, #4	
23[2]	4					Random	Vertical	2.0, 3.0, 4.0	5-2000 Hz	#1	
24[2]	6					Random	Vertical	2.0, 2.5, 3.0	5-2000 Hz	#1	

*DGWT - Data correlates with hydrostatic theory.

**NGWT - Data does not correlate with hydrostatic theory.

+ΔP_i - Initial pressure differential across screen. (Ullage Pressure)

2 - Flow Tests

FOLDOUT FRAME

(continued)

nt	Frequency	Location	Direction #5	Pressure Data	Comments
.0	5-2000 Hz	#1, #3, #4		Yes	DCWT* at all g levels.
.0,	5-2000 Hz	#1, #3, #4		Yes	DCWT at all g levels.
.0	5-2000 Hz	#1, #3, #4		Yes	DCWT at all g levels.
	5-2000 Hz	#1, #3, #4		Yes	NCWT** at low frequencies (45 to 50 Hz); DCWT at higher frequencies
	5-2000 Hz	#1		Yes	NCWT at all g levels - outflow periods were too
	5-2000 Hz	#1		Yes	brief to get good data for correlation.

FOLDOUT FRAME

2

Table 3.3: Summary of Vibration Test Results, Second Series

Test No.	Screen Config.	Hydrostatic Head cm (in.)	Test Fluid Type	Acceleration Environment				Accelerometer Data	
				Type	Direction	Input G	Frequency	Location	Directio
2-1	4	Model Dry	None	Sine	Vertical	0.5, 1.0, 1.5, 2.0, 2.5, 3.0, 3.5, 4.0	15-2000 Hz	P.P./Screen (3 Places)	Vertical
2-2	4	39.62 (15.6)	Iso-propanol	Sine	Vertical	0.5, 1.0, 1.5, 2.0 2.5, 3.0, 3.5, 4.0	15-2000 Hz	P.P./Screen (3 Places)	Vertical
2-3	4	Model Dry	None	Sine	Vertical	0.5, 1.0, 1.5, 2.0, 2.5, 3.0	15-2000 Hz	P.P./Screen (2 Places)	Vertical
2-4	4	39.62 (15.6)	Iso-propanol	Sine	Vertical	0.5, 1.0, 1.5, 2.0, 2.5, 3.0	15-2000 Hz	P.P./Screen (2 Places)	Vertical
2-5	4	Model Dry	None	Sine	Vertical	0.5, 1.0, 1.5, 2.0, 2.5, 3.0	15-2000 Hz	P.P./Screen (1 Place)	Vertical
2-6	4	39.62 (15.6)	Iso-propanol	Sine	Vertical	0.5, 1.0, 1.5, 2.0, 2.5, 3.0	15-2000 Hz	P.P./Screen (1 Place)	Vertical
2-7	4	Model Dry	None	Sine	Vertical	0.5, 1.0, 1.5, 2.0, 2.5, 3.0	15-2000 Hz	P.P./Screen (3 Places)	Horizont
2-8	4	39.62 (15.6)	Iso-propanol	Sine	Vertical	0.5, 1.0, 1.5, 2.0, 2.5, 3.0	15-2000 Hz	P.P./Screen (3 Places)	Horizont
2-9	1	39.62 (15.6)	Methanol	Random	Vertical	0.7, 0.9, 1.0, 1.2	5-2000 Hz	Shaker Input	Vertical
2-10	1	39.62 (15.6)	Methanol	Sine	Vertical	0.5, 1.0, 1.5	15-2000 Hz	Shaker Input	Vertical
2-11	1	30.48 (12.0)	Methanol	Random	Vertical	0.5, 1.0, 1.2, 1.4, 1.5, 1.6, 2.0, 2.5, 3.0	5-2000 Hz	Shaker Input	Vertical
2-12	2	39.62 (15.6)	Methanol	Random	Vertical	1.0, 2.0, 2.5, 3.0, 3.5	5-2000 Hz	Shaker Input	Vertical
2-13	2	30.48 (12.0)	Methanol	Random	Vertical	1.0, 2.0, 2.5, 3.0, 3.5	5-2000 Hz	Shaker Input	Vertical
2-14	6	15.24 (6.0)	Methanol	Random	Horizontal	2.0, 2.5, 3.0, 3.5, 4.0	5-2000 Hz	None	None
2-15	6	13.0 (5.1) 7.9 (3.1)	Methanol	Random	Horizontal	1.0, 1.5, 2.0	5-2000 Hz	None	None
2-16	1	39.6 (15.6)	Methanol	Sine	Vertical	0.5, 1.0, 2.0	15-2000 Hz	None	None
2-17	1	39.6 (15.6)	Methanol	Random	Vertical	1.0, 2.0, 3.0	5-2000 Hz	None	None
2-18	1	39.6 (15.6)	Methanol	Sine	Vertical	0.5, 1.0	1000, 700, 500, 300, 150, 100, 70, 40 Hz	None	None
2-19[2]	6	(Outflow)	Methanol	Random	Vertical	1,0, 2.0	5-2000 Hz	Shaker Input	Vertical

FOLDOUT FRAME

Frequency	Accelerometer Data		Pressure Data (Visicorder)	Comments
	Location	Direction		
15-2000 Hz	P.P./Screen (3 Places)	Vertical	No	Tests 1 through 8 (except for Test 2) were successful and objectives were achieved.
15-2000 Hz	P.P./Screen (3 Places)	Vertical	No	Test 2 was not successful because the bottom accelerometer got wet and no data was obtained. The successful test data was used to measure natural frequencies of the plate/screen configuration and evaluate the effects of accelerometer mass.
15-2000 Hz	P.P./Screen (2 Places)	Vertical	No	
15-2000 Hz	P.P./Screen (2 Places)	Vertical	No	
15-2000 Hz	P.P./Screen (1 Place)	Vertical	No	
15-2000 Hz	P.P./Screen (1 Place)	Vertical	No	
15-2000 Hz	P.P./Screen (3 Places)	Horizontal	No	
15-2000 Hz	P.P./Screen (3 Places)	Horizontal	No	
5-2000 Hz	Shaker Input	Vertical	Yes	Test objectives were achieved; good film data obtained on Tests 9 and 10.
15-2000 Hz	Shaker Input	Vertical	Yes	
5-2000 Hz	Shaker Input	Vertical	Yes	Different PSD curve evaluated; no significant difference observed in results between the new and original curves.
5-2000 Hz	Shaker Input	Vertical	Yes	Better results were generally obtained with these double layer screen tests than with the original tests.
5-2000 Hz	Shaker Input	Vertical	Yes	
5-2000 Hz	None	None	Yes	Acceleration normal to screen not successful due to damaged model.
5-2000 Hz	None	None	Yes	Acceleration parallel to screen was successful; good correlation with hydrostatic theory.
15-2000 Hz	None	None	Yes	Liquid side open to atmosphere. No significant difference between these results and closed system results.
5-2000 Hz	None	None	Yes	
1000, 700, 500, 300, 150, 100, 70, 40 Hz	None	None	Yes	Liquid side open to atmosphere. Bubble point measured as function of frequency.
5-2000 Hz	Shaker Input	Vertical	Yes	

2

B. TEST PROGRAM

A test summary is shown in Tables 3.2 and 3.3. Important parameters varied during the tests were: 1) pressure differential across the screen; 2) acceleration, both magnitude and direction; 3) frequency; and 4) hydrostatic head. The acceleration level was varied from 0.5 to 6.0 g at the levels indicated in Tables 3.2 and 3.3. Tests were run both with and without outflow. Those with outflow were restricted to random vibration tests. The frequency range investigated was from 5 to 2000 Hz. Both sine and random vibration tests were conducted. Greater emphasis was placed on the simpler nonoutflow tests because of the speed in which these tests can be conducted and also yield the required test data. The test matrix was structured to obtain data for the screen configuration in both hydrostatically stable and unstable conditions.

Random vibration was synthesized in the proportions indicated on the power spectral density curve of Figure 3.4. A second spectrum with a greater contribution from the low frequency range was used for a few of the later runs in the second test series. This second spectrum approached a uniform power density over the frequency range.

The random tests were conducted by vibrating the model at the specified input G-rms value for approximately 2 minutes. During this time period, the performance of the screen/plate configuration was monitored by visually noting the occurrence of gas ingestion into the controlled liquid volume.

The frequency sweep for the sinusoidal tests was started at 2000 Hz and completed at 5 or 15 Hz, as noted in Tables 3.2 and 3.3, with the input acceleration level fixed.

In a limited number of tests the model was vibrated in a horizontal direction. In these tests the acceleration vector was normal to the screen surface in all but one case, where it was parallel to the screen surface.

Various conditions of liquid level were tested as can be seen from Tables 3.2 and 3.3. A hydrostatic head of 39.6-cm (15.6-in.) corresponds to liquid on one side of the screen only. Lesser hydrostatic heads correspond to cases where the ullage side contained some liquid. The hydrostatic head entries in Tables 3.2 and 3.3 reflect the difference in liquid height across the screen. The test fluid was isopropanol for Tests 2.2, 2.4, 2.6, and 2.8 in which accelerometers were mounted on the screens and methanol for the remainder. The screen response was also measured without liquid on either side of the screen. These tests were run in the second test series and are identified in Table 3.3.

C. TEST RESULTS

A correlation between the observed performance of the screen/perforated plate and the performance predicted by hydrostatic theory was performed. The correlation involved checking the test data to determine if it satisfied the following relationships:

1) For no gas ingestion,

$$\frac{\Delta P_t}{BP} < 1.0$$

2) For gas ingestion,

$$\frac{\Delta P_t}{BP} \geq 1.0$$

where BP = differential pressure retention capability (bubble point) of screen,

ΔP_t = total differential pressure measured across top of screen.

For the nonflow conditions, the ΔP_t is expressed as

$$\Delta P_t = \Delta P_i + \rho g_t h$$

where ΔP_i = initial overpressure of ullage side of channel (pressure greater than amount needed to support hydrostatic head of exposed liquid)

ρ = liquid density

h = hydrostatic head

g_t = total acceleration = $g_o + g_i$ (rms)

g_o = acceleration due to earth's gravity

g_i(rms) = input vibration acceleration (root-mean-square value)

For the condition where there was liquid on both sides of the screen, ΔP_i must be zero.

1. Results From Random Vibration Tests

The results of the twenty random vibration tests performed in both the first and second series correlate well with hydrostatic theory, as presented in Figures 3.5 through 3.8, for both power spectral density curves used. Vertical random vibration results are shown in Figures 3.5 through 3.7. The data plotted in Figures 3.5, 3.6 and 3.8 is for cases where there was liquid on both sides of the screen. There was no liquid on the ullage side for data plotted in Figure 3.7.

Accelerometer data taken for selected random vibration tests in both the first and second series is tabulated in Table 3.4. The measured values show that the model experiences acceleration levels considerably higher than the input; however, the success of the hydrostatic theory correlation of the data indicates that the fluid senses only the input acceleration.

There are several anomalous points from the single layer screen vertical vibration tests; i.e., cases where breakdown occurred prematurely and where breakdown did not occur where predicted. Approximately the same number of each type are shown and it should be noted that they all occur in the nondimensionalized hydrostatic head range of .87 to 1.15. This may be due to the approximate level of input grms of the random vibration synthesis electronics. Table 3.4 lists some measured accelerations for two tests. Note that the measured input is up to 10% different from the programmed input listed in Table 3.2. Also, minor variations in the liquid temperature were possible which would affect the screen bubble point.

The serious failure of the 325 x 2300 double layer screen (Figure 3.7) can likely be attributed to dryout of the ullage

Table 3.4: Sample of Accelerometer Data for Random Vibration Tests

Input Acceleration g (rms)		Model Acceleration / Input Acceleration (g_x/g_{in})					
		Accelerometer #3		Accelerometer #4		Accelerometer #5	
Test 1b	Test 1e	Test 1b	Test 1e	Test 1b	Test 1e	Test 1b	Test 1e
0.6	0.67	2.1	1.8	2.1	1.65	4.7+	0.37*
1.1	1.0	1.9	1.7	1.8	1.6	3.6	0.30
1.55	1.5	1.9	1.67	1.9	1.53	4.1	0.33
2.05	1.95	2.0	1.74	1.85	1.66	3.8	0.31
2.5	2.47	1.9	1.72	1.9	1.62	4.8	0.32
3.18	2.8	2.0	1.7	1.7	1.65	4.0	0.31
3.4		2.0		1.85		4.35	
3.44		1.9		1.8		3.7	

NOTES: + Accelerometer oriented in vertical direction.

*Accelerometer oriented in horizontal direction.

Table 3.5: Sample of Accelerometer Data for Sinusoidal Tests

Input Acceleration g	Model Acceleration / Input Acceleration (g_x/g_{in}) at Resonance Frequency								
	Accelerometer Number								
	3				4				5
	Test Number								
	11a	11b	11c	11d	11a	11b	11c	11d	11a
0.5	4.0	3.4	3.3	3.2	5.2	4.3	3.0	3.0	14.1
1.0	5.0	4.7	3.9	4.0	4.7	5.3	3.5	3.8	17.8
1.5	4.6	4.6	4.2	4.5	5.6	5.3	3.8	4.3	20.0
2.0	4.3	4.3	4.2	4.5	5.3	5.3	3.8	4.5	22.4
2.5	4.5			4.3	5.3			4.2	22.4
3.0	4.5				5.3				22.4

side layer. This is supported by the fact that no breakdown points occur for a nondimensionalized hydrostatic head below .5, the bubble point of a single layer of screen.

The horizontal random test results are presented in Figure 3.8. Results are shown for vibration, both parallel and perpendicular to the screen. It appears that the hydrostatic theory prediction works fairly well in this case also, although there are again several anomalous points in the nondimensionalized hydrostatic head range of .87 to 1.04.

2. Results from Sinusoidal Vibration Tests

A summary of the accelerometer data for vertical sinusoidal tests 11a through 11c is presented in Table 3.5. At accelerometers 3 and 4, the ratio of model acceleration to input acceleration varied between 3.0 to 5.6 for the vertical direction. For accelerometer 5, located on a perforated plate inside the model, the ratio ranged from 14.1 to 22.4. The model resonance frequencies are in the range of 500 to 700 Hz. The maximum accelerometer amplification factors from the random vibration tests also occurred in this same frequency band.

The maximum observed resonant frequencies at the screen for tests 2-3 through 2-6 are plotted versus input acceleration in Figure 3.9. Data is shown both for cases with and without liquid in the channel. The vastly different response between these cases is apparent. The data plotted is for screen configuration number 4. Resonant frequencies for the other screen/plate configurations were not measured. Based on the observed destruction of capillary stability over a fairly narrow frequency interval for all screen samples, it is believed that the variance in the resonance frequency is not large.

Maximum amplification factors at the resonant frequencies obtained from the screen accelerometers during test 2-1 are plotted in Figure 3-10. Data shown are from modes 1 through 6. As would be expected, the data indicates an increase in the amplification factor at the center relative to the edge of the screen.

The ratio, dry case to liquid loaded case, of the observed dynamic amplification factors obtained from the screen mounted accelerometer data is plotted in Figures 3.11 and 3.12. Vertical acceleration data from tests 2-3 through 2-6 are shown in Figure 3.11.

The horizontal acceleration component from tests 2-7 and 2-8 is represented in Figure 3.12. In both figures the primary mode is shown along with two of the dominant upper modes; the second and sixth in Figure 3.11 and the third and fifth in Figure 3.12. The very large damping effect of the liquid is very apparent, particularly at the higher modes.

A summary of breakdown frequencies for the sinusoidal tests is given in Table 3.6. Several trends can be easily identified: frequencies at which the first breakdown and dropout occur rises with increased input g-level; and for all screen samples tested, the first breakdown does not occur above 1100 Hz. For a vast majority of tests, the initial breakdown is at a frequency of 400 Hz or less. Since screen displacement varies inversely with the square of frequency for a specified input g-level, the above results support the theory that destruction of the capillary interface stability must be influenced, at least to some degree, by the absolute displacement.

It should also be noted that dropout--loss of liquid from the controlled liquid volume--did not occur above 85 Hz, and was often initiated in the 45-70 Hz band determined as the resonant frequency range of the screen/perforated plate from accelerometer data. This dropout was quite large in some tests, up to 20% of the controlled liquid volume. The fact that this massive breakdown does occur near the resonant frequency of the screen/plate suggests that the amplified screen acceleration is a major contributing factor.

The limited pressure data obtained for the sinusoidal tests did correlate with the screen performance observed. Large pressure oscillations were observed at approximately the same frequencies where screen breakdown occurred.

Table 3.6: Summary of Sine Vibration Test Data

Test No.	G-Level	Screen Configuration	Breakdown Frequencies	Dropout Frequency	Comments
11a	.5	325 x 2300	50-5 Hz	None	39.6-cm Ullage
	1.0		400-300, 250-5		All pores not wicked
	1.5		1100, 700, 500, 200-100, 90-5	30 Hz	
	2.0		500, 400-5	35	
	2.5		600-5	40	
	3.0		600-5	45	
11b	.5	325 x 2300	100-5	None	39.6-cm Ullage
	1.0		40-5	25	
	1.5		600-200, 100-5	30	
	2.0		400-250, 150-5	35	
11c	.5	325 x 2300	100-5	None	39.6-cm Ullage
	1.0		150, 105-90, 50-5	30	
	1.5		150-5	30	
	2.0		400-330, 240-200, 150-5		
12	.5	325 x 2300	No Breakdown	None	30.5-cm Ullage
	1.0		No Breakdown	None	
	1.5		30-5	10	
	2.0		50-5	20	
	2.5		200-170, 150-5	30	
13	1.5	325 x 2300	900, 300, 150, 100-5	None	Double Layer Screen 39.6-cm Ullage
	2.0		1100, 900-500, 400-300, 240-150, 120-100, 50-5	20-10	
	2.5		150, 60-5	20	
	3.0		900-150, 60-5	25	
14	.5	325 x 2300	40-20	None	Double Layer Screen 39.6-cm Ullage
	1.0		60, 40-5		
	1.5		35-5	15	
	2.0		30.5	20	
15	.5	200 x 1400	No Breakdown	None	20.3-cm Ullage
	1.0		100-90	None	
	2.0		100-40, 30-5	70-40	
	2.5		500-400, 150-5	70	

Table 3.6 (continued)

Test No.	G-Level	Screen Configuration	Breakdown Frequencies	Dropout Frequency	Comments
16	1.5	200 x 1400	40-5	35	Double Layer Screen
	2.0		15	15	30.5-cm Ullage
	2.5		200-170, 35-5	15	
	3.0		200-170, 150-120, 40-5		
17	.5	80 x 700	No Breakdown	None	7.6-cm Ullage
	1.0		No Breakdown	None	
	2.0		200-5	50	
	2.5		300-150, 100-5	70-15	
22	3.0	80 x 700	45-5	40	Horizontal Vibration
	2.5		50-5	40	15.2-cm Ullage
			(Second Series)		
2-4	.5	200 x 1400	No Breakdown	None	Accelerometer
	1.0		No Data Record	No Data Record	Instrumented 39.6-cm Ullage
	1.5		430, 370, 190-170, 135-110, 105-5	60	
	2.0		500-430, 305-275, 230, 190-170, 100-5	40	Lower Frequency Limit Reset to 15 Hz
	2.5		500, 400-350, 300-15	No Data Record	
	3.0		450-250, 200-110, 90-15	No Data Record	
2-6	.5	200 x 1400	No Breakdown	None	Single Accelerometer
	1.0		30	30	Screen Instrumentation
	1.5		115-15	60	39.6 cm Ullage
	2.0		375-350, 150-125, 110-15	65	
	2.5		360-390, 200-130, 110-15	65	
	3.0		390-325, 130, 100-15	85	
2-8	.5	200 x 1400	100-80, 40-20	None	Cross Couple Accelerometers
	1.0		100-80, 40-15	30-20	
	1.5		105-70, 45-15	40-30	39.6-cm Ullage

Table 3.6 (continued)

Test No.	G-Level	Screen Configuration	Breakdown Frequencies	Dropout Frequency	Comments
2-8 Cont	2.0		270, 110-65, 50-15	50-25	
	2.5		400-270, 165-65, 50-15	50-25	
	3.0		110-60, 50-15	50-15	
2-10	.5	325 x 2300	35-15	None	39.6-cm Ullage
	1.0		30-15	25	
	1.5		80-15	30	
2-16	.5	325 x 2300	110-15	None	Liquid Side Open
	1.0		200-75, 50-15	None	39.6-cm Ullage
	2.0		100-15	20	

On test 2-18 with the input g-level fixed at 0.5 or 1.0 g the frequency was varied from 40 to 1000 Hz. At each frequency, the gas side pressure was increased (with the liquid side vented to the atmosphere) until breakdown was obtained. These results are plotted in Figure 3.13. The bubble point degradation when resonance is approached is quite evident.

D. SCREEN DYNAMICS

Vibration specifications are typically described in terms of acceleration spectral densities (ASD) for random spectra or simply as peak acceleration for sinusoidal vibrations. The vibrational effect on a screen system should be considered in terms of displacement or displacement spectral densities (DSD) because they may be more meaningfully interpreted in terms of screen performance. The conversion from ASD to DSD or from g to displacement shows that the significant frequency regime for screen performance is the low-frequency end of the spectrum for a typical random ASD or sine acceleration. The reason for this is that the maximum displacements and velocities tend to occur at the low frequencies. The physical significance of the displacement amplitudes is that, if a screen is not pulled tight, fluid particle displacements that are not sufficient to take up the slack in the screen cannot develop tension in the screen and it cannot, therefore, support a pressure load.

For sinusoidal vibration, the displacement amplitude for a given g-level is inversely related to the square of the frequency. The input, double amplitude displacement is given by

$$A = C \frac{(g/g_e)}{f^2}$$

where A is the input double amplitude

$C = 49.8\ cm/s^2$ $(19.6\ inch/s^2)$

f = frequency, Hz

g/ge = peak input sinusoidal acceleration ratioed to standard earth gravity.

In the vicinity of the screen resonance, approximately 60 Hz, the displacement obtained from the above equation is on the order of .013 cm per g (.005 inch per g). Applying an amplification factor obtained from the data plotted in Figure 3.12, a horizontal displacement at the center of the screen on the order of 0.2 cm per g (.08 inch per g) is obtained. For random vibration, the root mean square displacement is approximately

$$Xrms = \sqrt{\frac{\pi}{2}\ Q\ \frac{K}{f_n^3}\ ASD}$$

where:

Q is the system dynamic amplification factor

f_n is the resonant frequency of the system

$K = 617\ cm^2\ Hz^3$ $(95.6\ in^2\ Hz^3)$

ASD = acceleration spectral density in g^2/Hz

Using a Q of 2, a resonant frequency of 60 Hz, and ASD = .36 g^2/Hz leads to a root mean square horizontal displacement of .058 cm (.022 inch).

In addition to the simple hydrostatic considerations based on the vertical accelerations, a significant effect should be anticipated as a result of these large horizontal displacements. An indication of this second effect was provided by the fact that capillary breakdown never occurred at the very top of the screen where the rigid body effects are a maximum. Breakdown generally occurred approximately 5 cm down from the top of the screen. The position of the breakdown point relative to the

position which would be predicted from considerations of the vertical rigid body hydrostatic and screen dynamics effects leads to the conclusion that screen dynamics played a secondary role but was never-the-less present.

An analytical prediction of the screen/plate resonance was made. The test model is assumed to behave as a simply supported[1] thin, rectangular, perforated plate with 325 x 2300 screen attached and with liquid on one side. Considering the screen/perforated plate without liquid, the expression for the natural frequency of the first mode is (Ref. 3.1)

$$f = \frac{\pi}{2}\sqrt{\frac{D^*}{\rho_p t_p + \rho_s t_s}}\left[\frac{1}{a^2} + \frac{1}{b^2}\right]$$

where t_p = thickness of the perforated plate
t_s = thickness of the screen
a = width of the screen/plate
b = length of the screen plate
ρ_p = density of the plate
ρ_s = density of the screen
D^* = flexural rigidity of the perforated plate

The stainless steel perforated plate used in the test model was 0.0635-cm (0.025-in) thick with a width of 6.35-cm (2.5-in) and a length of 39.7-cm (15.63-in). The flexural rigidity of a solid thin plate is given as

$$D = \frac{E\,t^3}{12(1 - \nu^2)}$$

This expression can be corrected for perforations in the plate by the approach outlined in Ref. 3.2. When applied to the present case, the thick plate expressions in Ref. 3.2 will yield conservative results. For perforated plate, the expression is modified

[1]The screen specimens were clamped in rubber at their edges.

as

$$D^* = \frac{E^* t^3}{12(1 - \nu^{*2})}$$

where $E^* = 0.265\ E$

$\nu^* = 0.37\nu$

for perforated plate with 0.3175-cm (0.125-in.) diameter holes and ligaments of 0.1588-cm (0.0625-in.). With these adjustments, the natural frequency of the screen/perforated plate without liquid loading was calculated. To account for the isopropanol liquid mass and mass of the screen mounted accelerometers, the total effective point mass acting on the center of the screen/plate was assumed to be equal to the mass of the accelerometer located at the midpoint plus one-half the mass of the top accelerometer plus one fourth of the liquid mass. The one fourth factor on the liquid mass was obtained by consideration of an assumed mode shape along with a generalized mass expression of the form

$$\hat{m} = \Sigma m_i \phi^2 = \int m_i(X) \phi_i^2(X)\, dX$$

where m_i is the mass at the i^{th} point and ϕ_i is the modal deflection at the i^{th} point. ϕ_i is normalized to an arbitrary deflection at the center.

The natural frequency of the screen/plate without corrections for liquid mass and accelerometer mass was 240 Hz. Including the effective accelerometer and liquid masses, the natural frequencies of the system was calculated at 60 Hz which is in the observed resonant frequency range (58 to 75 Hz). In comparison, if the total liquid mass is assumed to be acting at the center of the screen, 36 Hz is computed for the resonant frequency.

E. CONCLUSIONS

The general conclusions that were obtained under the Task I effort were:

1) The performance of a capillary acquisition device can be predicted using hydrostatic theory for wide band random vibration spectra; i.e., gas ingestion will occur when the static plus dynamic pressure difference is in excess of the screen layer bubble point.

2) For sinusoidal vibration with frequencies well above the resonant point, the performance of a capillary system can be predicted by hydrostatic theory. For sinusoidal vibrations near the resonant frequency the screen breakdown results from a complete destruction of the capillary stability; i.e., liquid dropout from controlled liquid volume, as opposed to the less severe screen breakdown where gas bubbles are ingested into the liquid volume.

3) The degradation in screen retention at low frequencies from that predicted by hydrostatic theory is attributed to a combination of acceleration amplification near the resonant frequency of the acquisition system and the relatively large amplitude at low frequency for a specified input g-level. Conversion of the acceleration data to displacement data is desirable for analysis of low frequency effects.

4) The capillary breakdown is effected by screen dynamics. For rigid systems similar to the one tested here, however, this effect is of secondary importance.

F. DESIGN CRITERIA

In the design of capillary acquisition systems adequate allowance should be made for vibration effects by sizing the screen retention capability as follows:

$$BP \geq \rho g_t h$$

where g_t is the total acceleration level experienced by the device, including the grms level of random vibration; h is the exposed liquid head and ρ is the liquid density. This criterion is applicable to all Dutch-twill weave screens and any random vibration power spectral density which has a fairly even energy distribution over the majority of the included frequency range.

For operation in a sinusoidal vibration environment, the above applies as long as the vibrational frequency is well above the resonant frequency of the device, and, in any case, not less than 200 Hz.

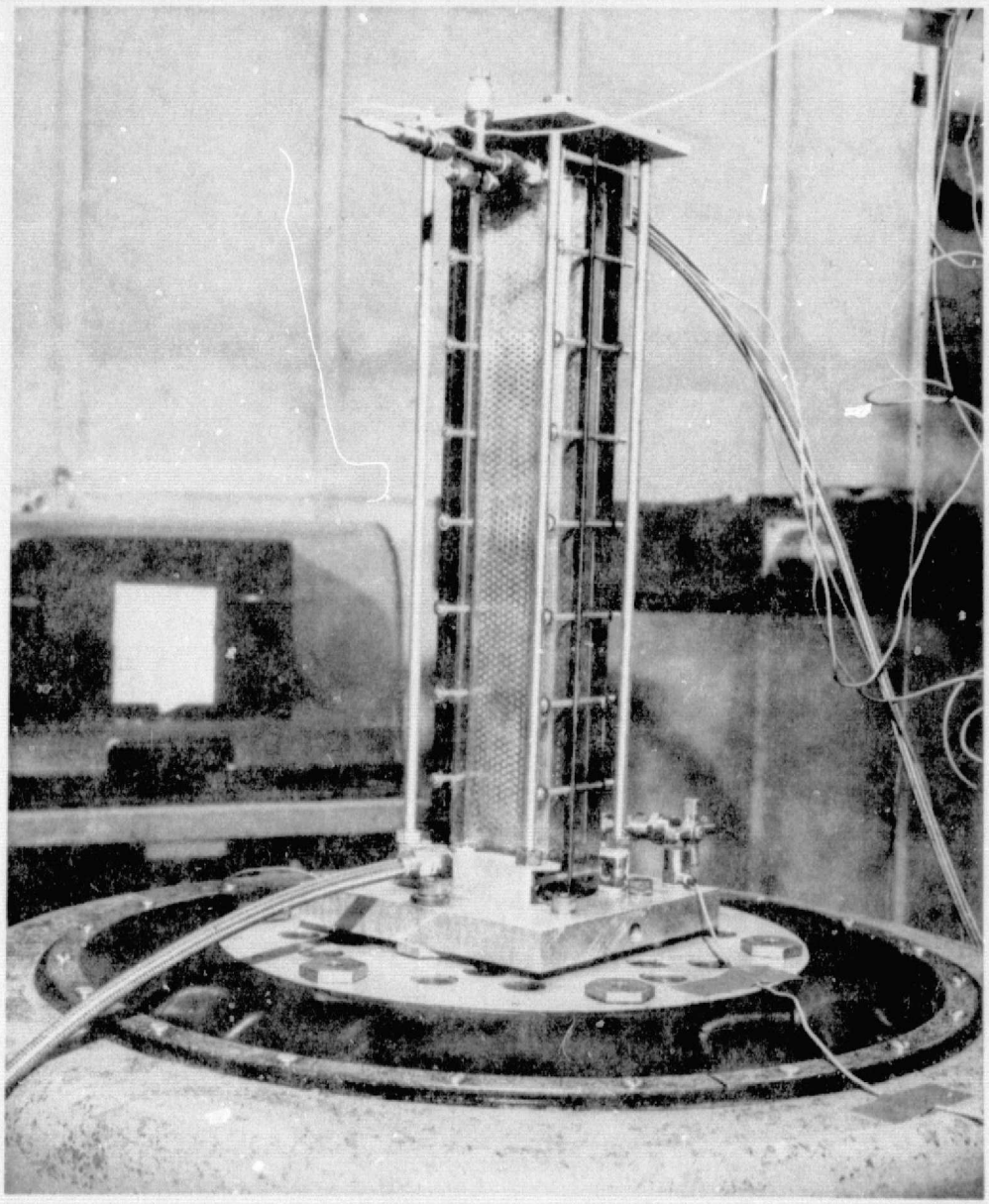

Figure 3.1: Test System Mounted on Shaker

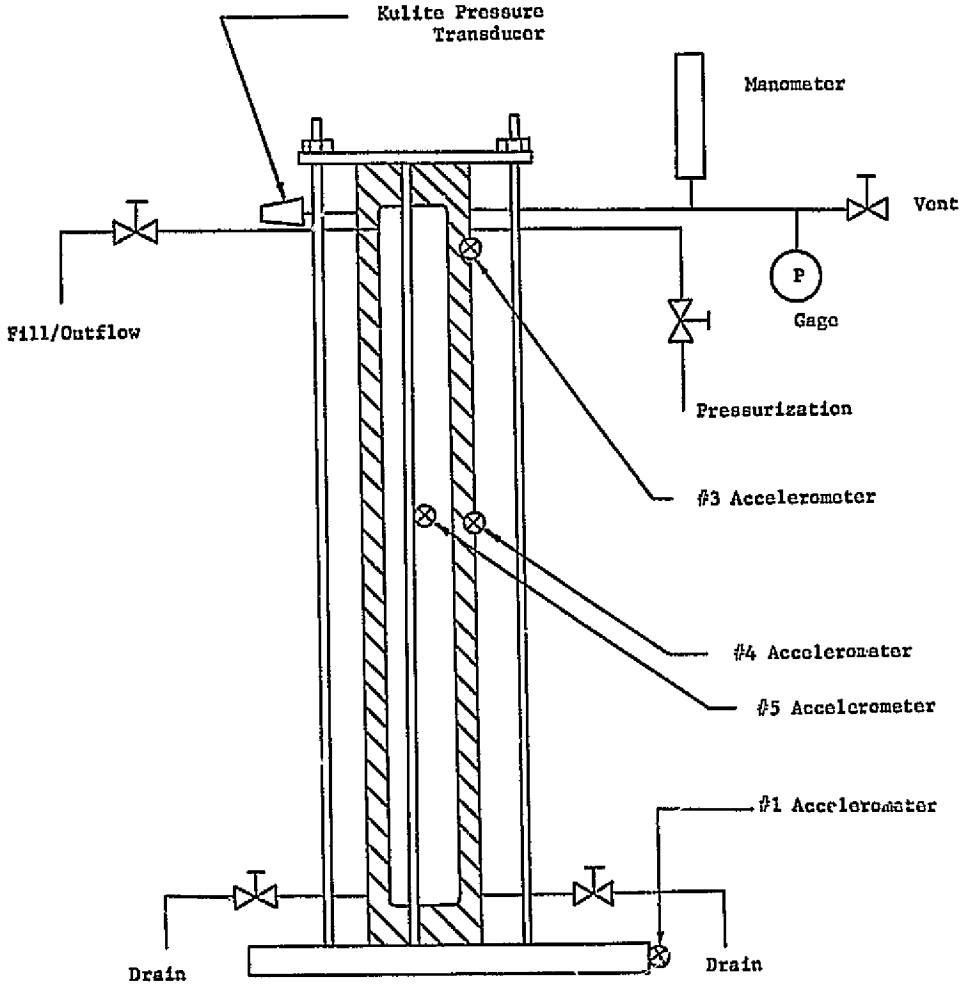

Figure 3.2: Test System Schematic

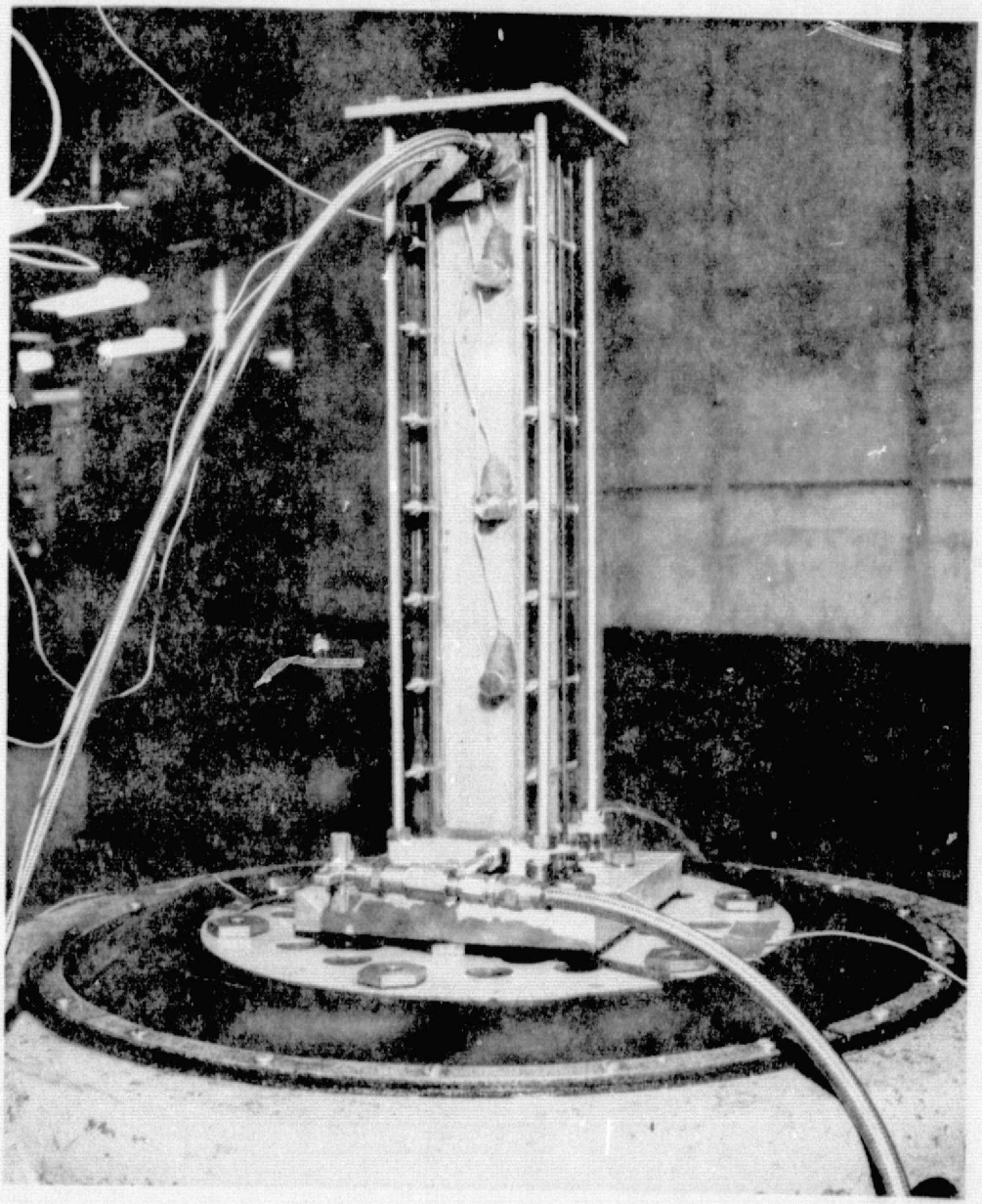

Figure 3.3: Instrwented Screen Test

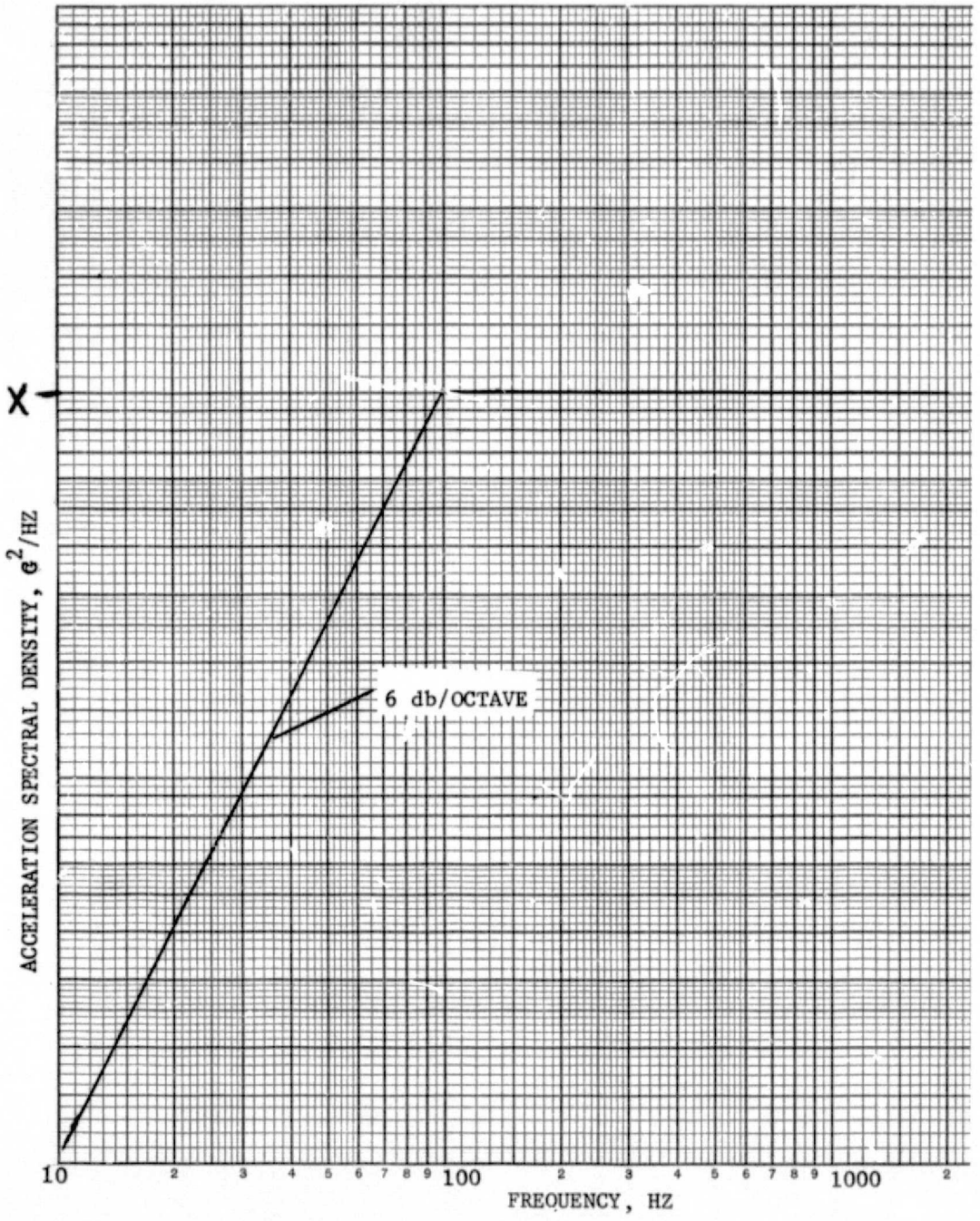

Figure 3.4: Random Vibration Power Spectral Density

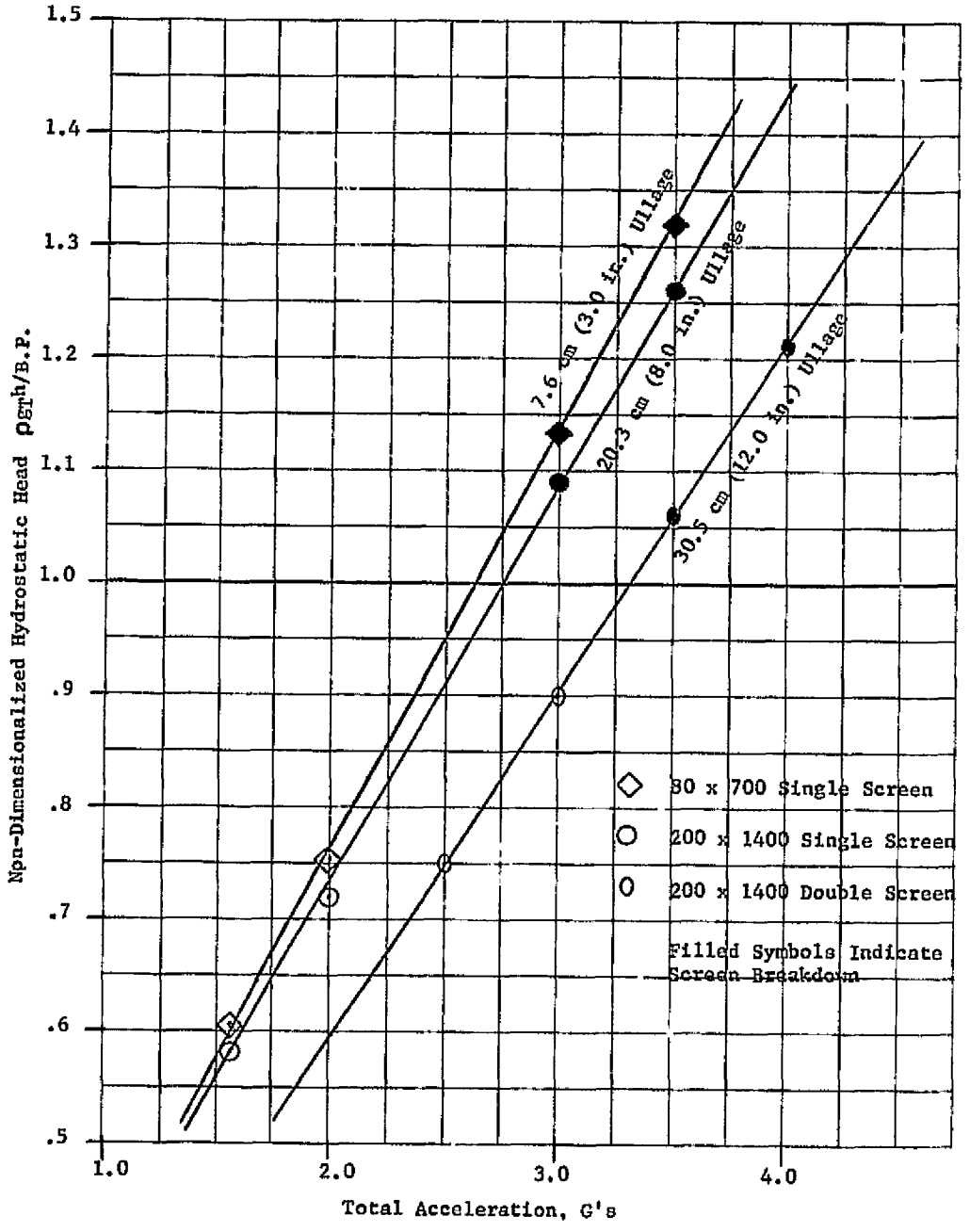

Figure 3.5: Correlation of Experimental and Analytical Screen Performance Data Under Random Vibration, Vertical Direction, for 200 x 1400 and 80 x 700 Screens

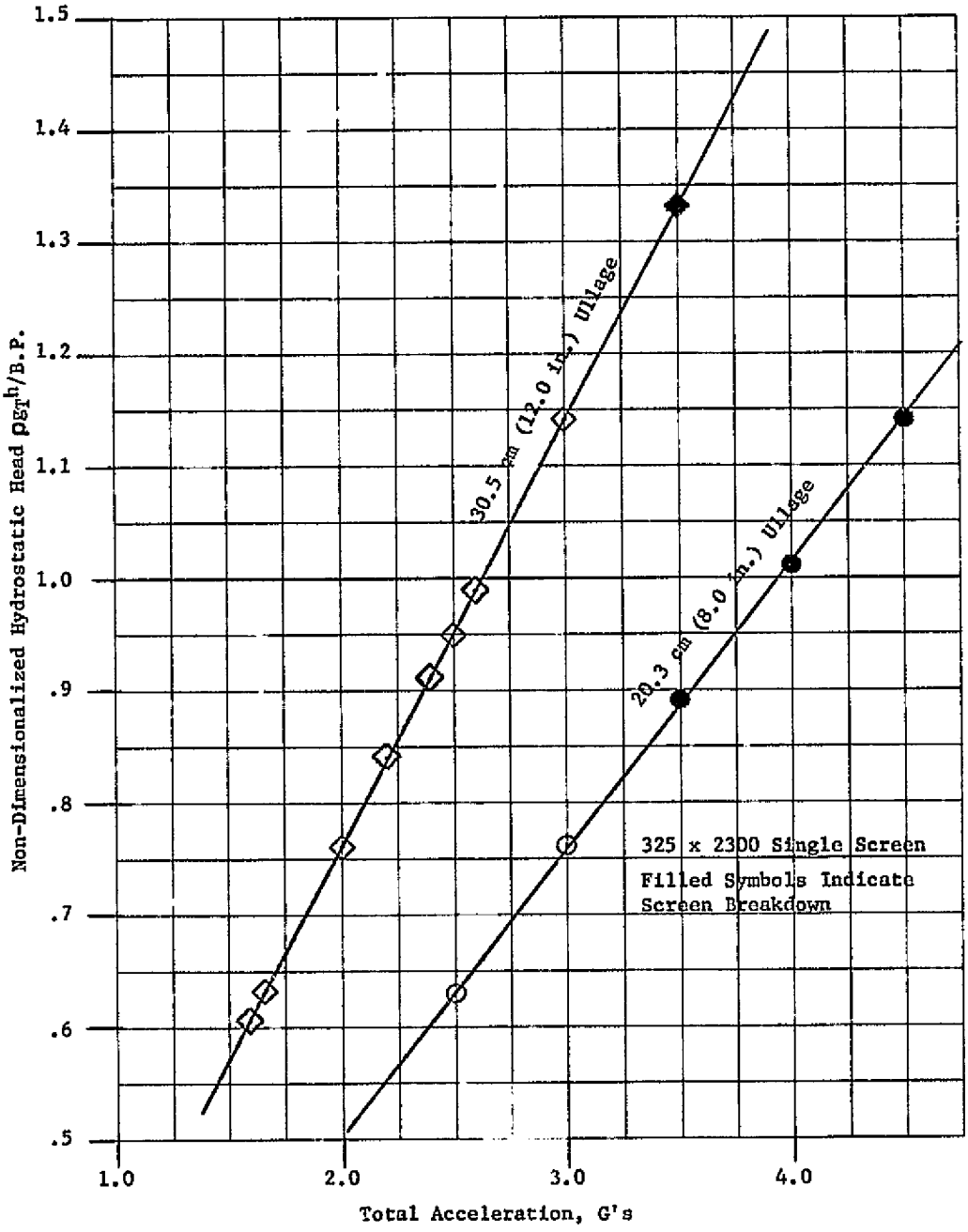

Figure 3.6: Correlation of Experimental and Analytical Screen Performance Data Under Random Vibration, Vertical Direction, for 325 x 2300 Single Screen

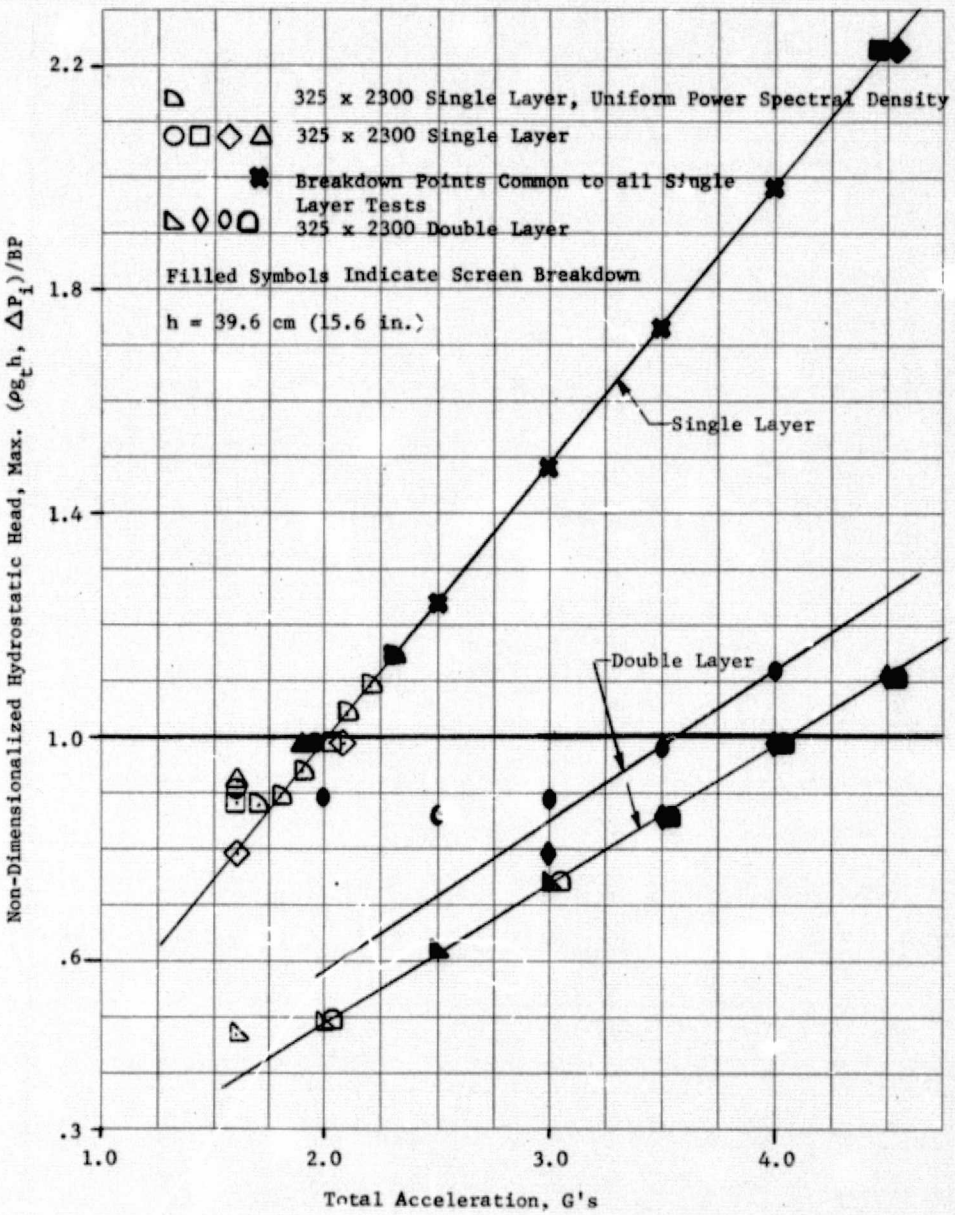

Figure 3.7: Correlation of Experimental and Analytical Screen Performance Data Under Random Vibration, Vertical Direction for 325 x 2300 Single and Double Layer Screens with Ullage Side of Screen Dry

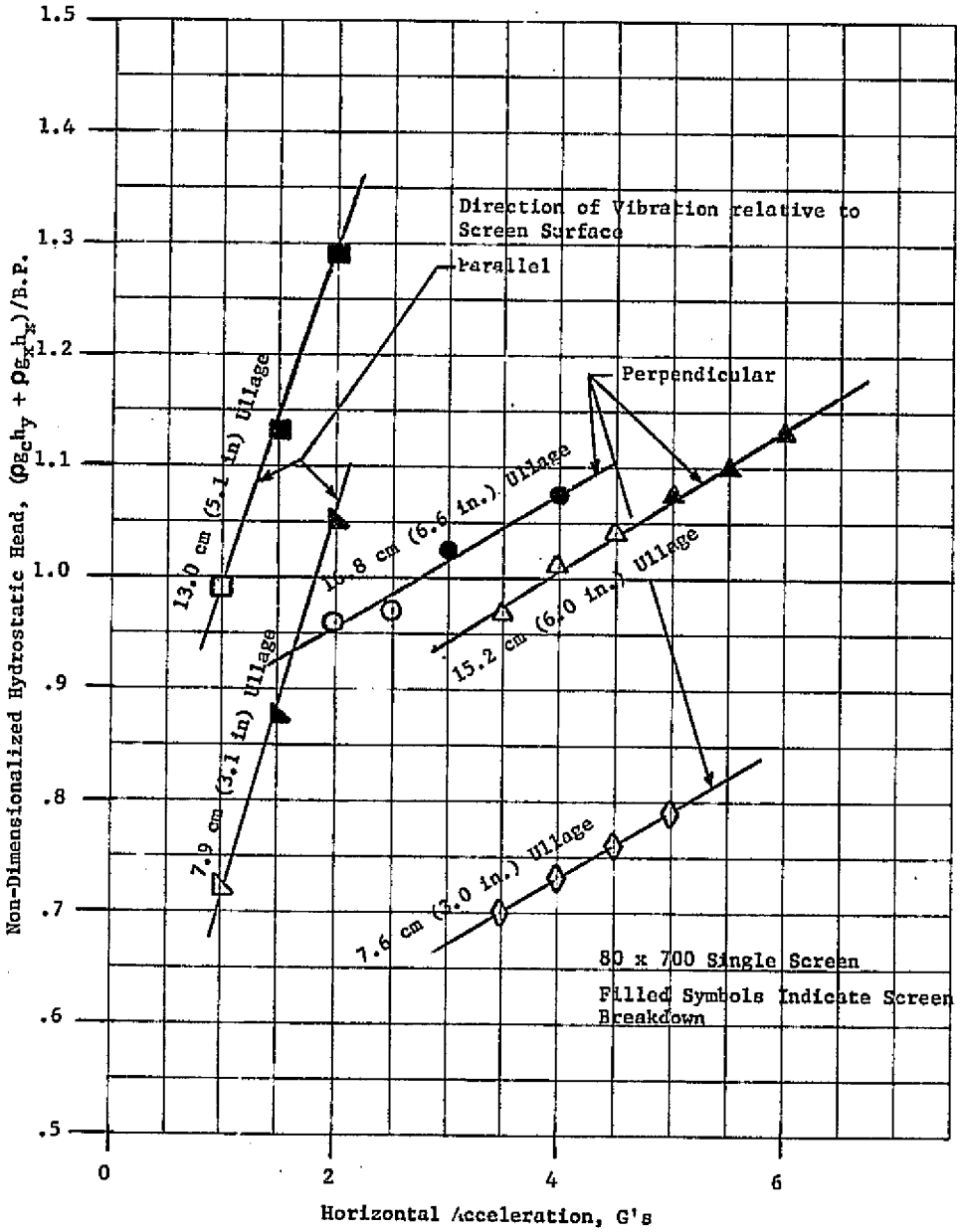

Figure 3.8: Correlation of Experimental and Analytical Screen Performance Data Under Random Vibration, Horizontal Direction, for 80 x 700 Single Screen

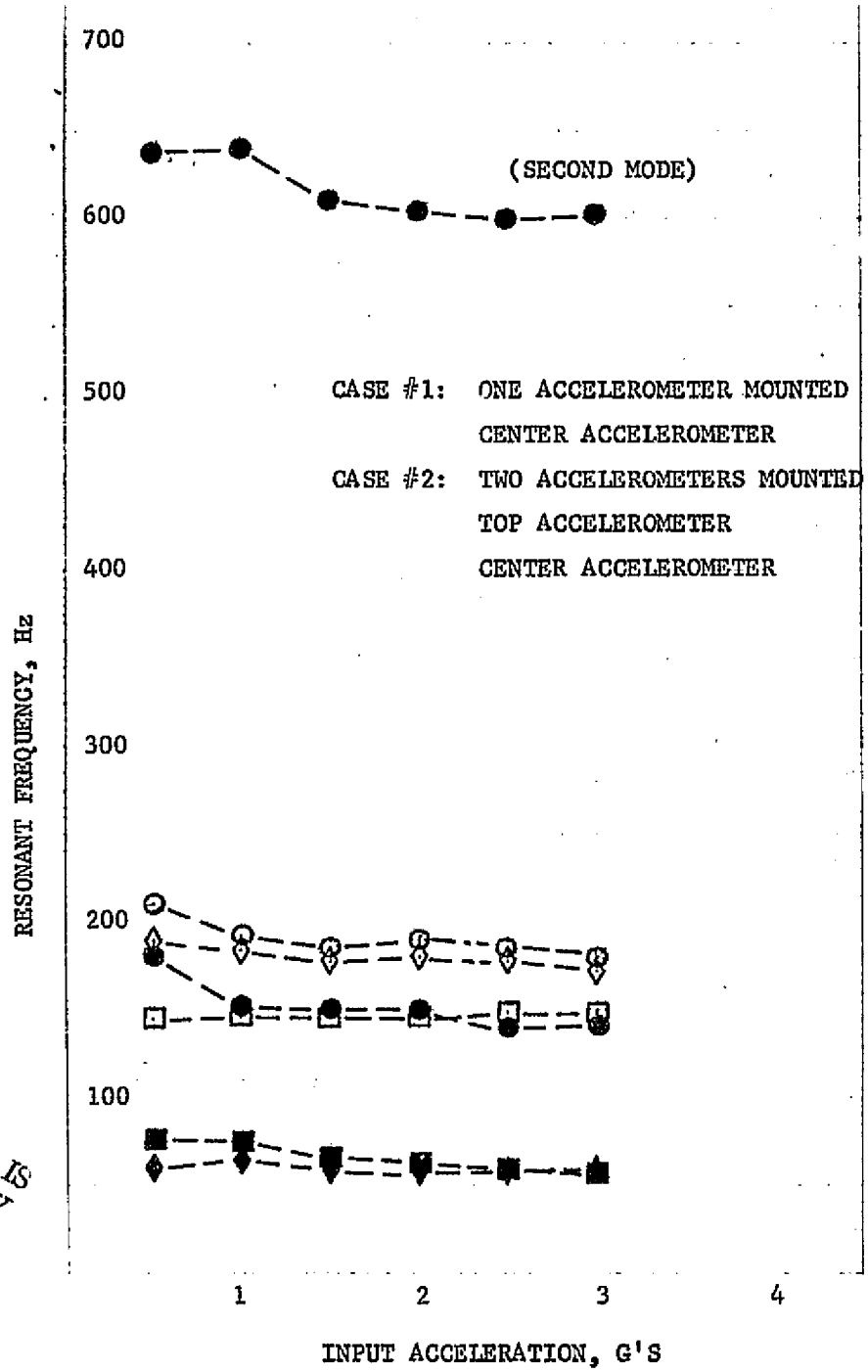

Figure 3.9: Resonant Frequency Versus Input Acceleration for Sinusoidal Vibration, Tests 2-3 through 2-6

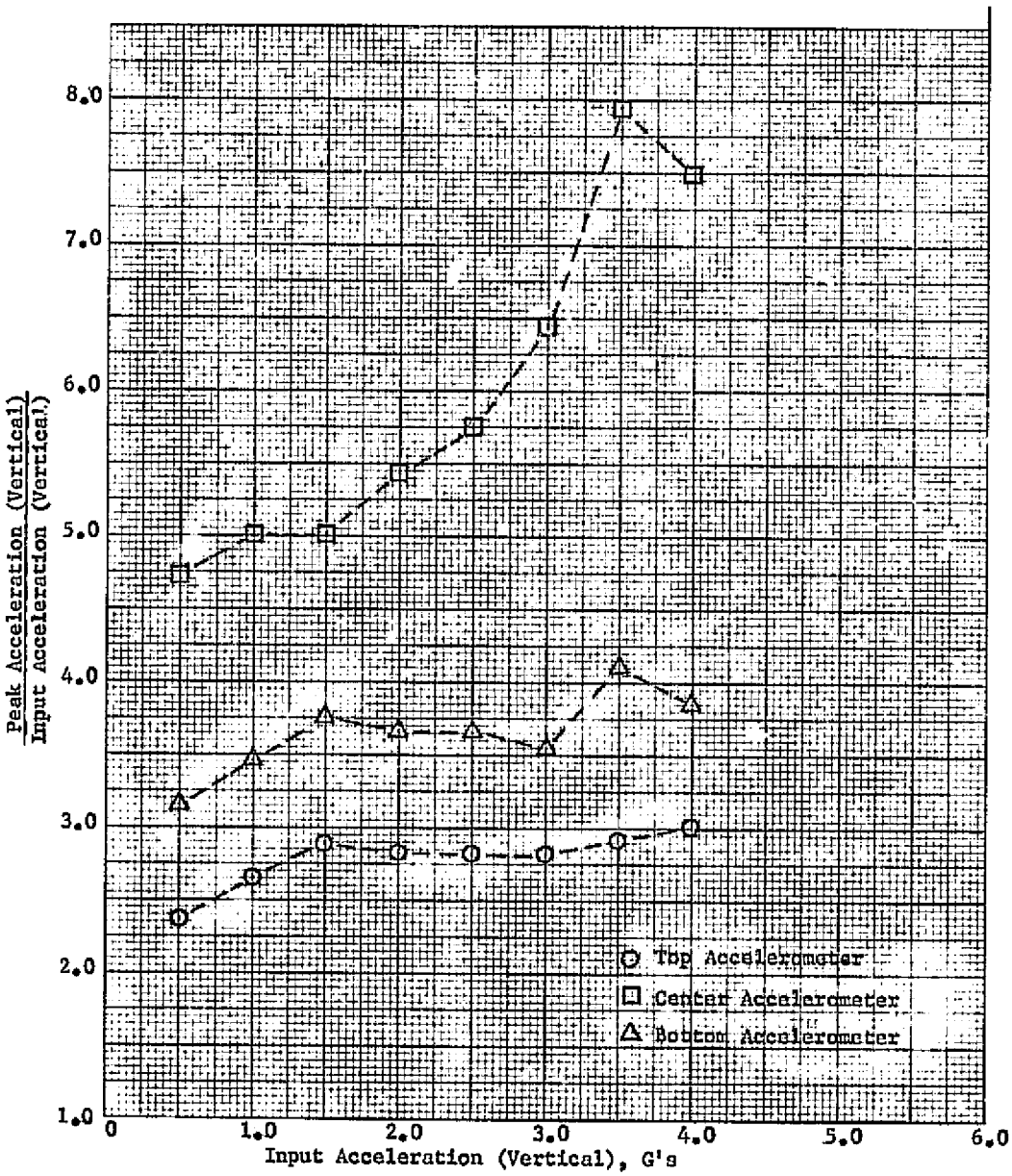

Figure 3.10: Amplification Factors Versus Input Acceleration for Sinusoidal Vibration, Test 2-1 (3 Accelerometers)

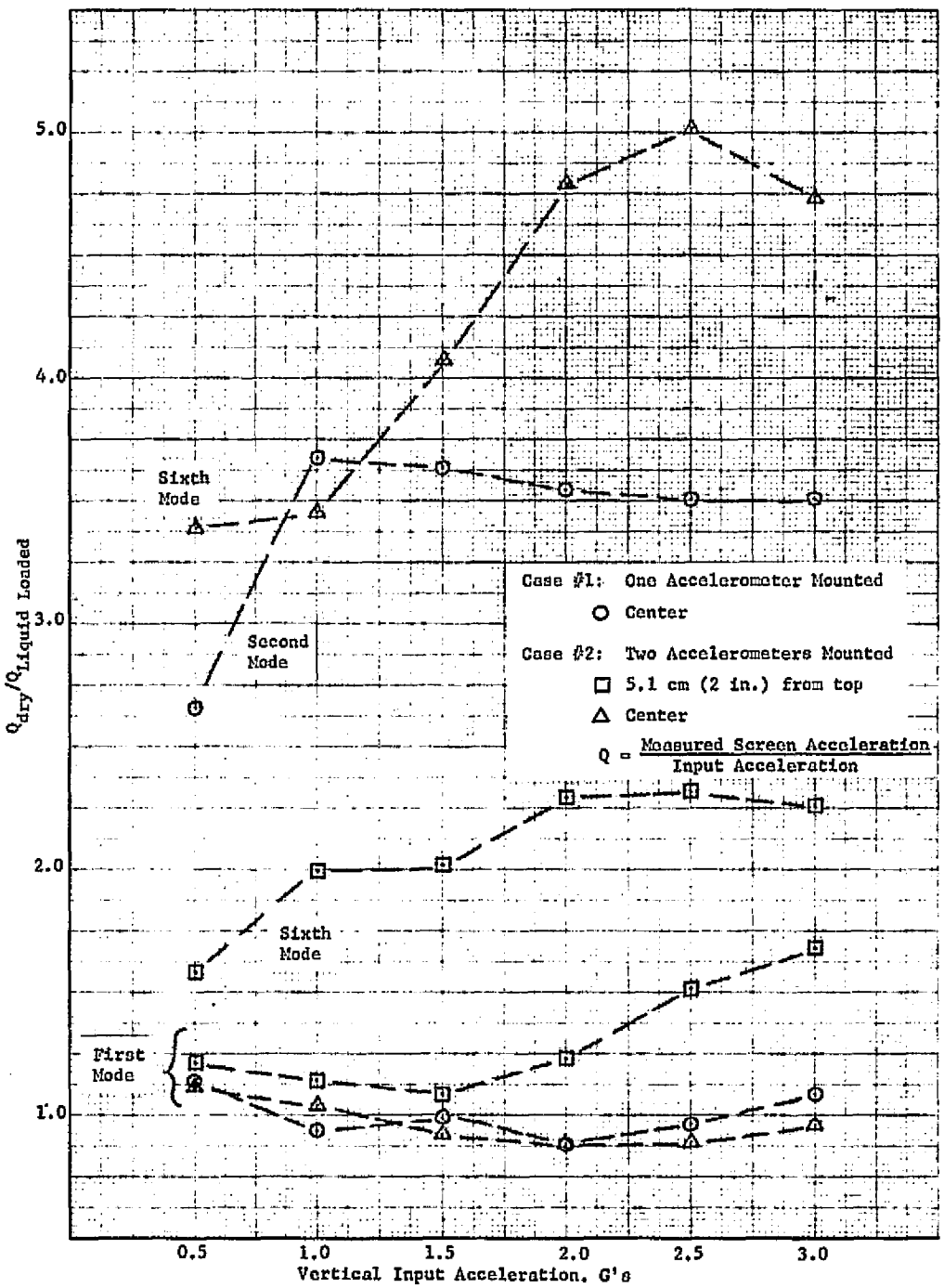

Figure 3.11: Amplification Factors Versus Input Acceleration for Tests 2-3 through 2-6

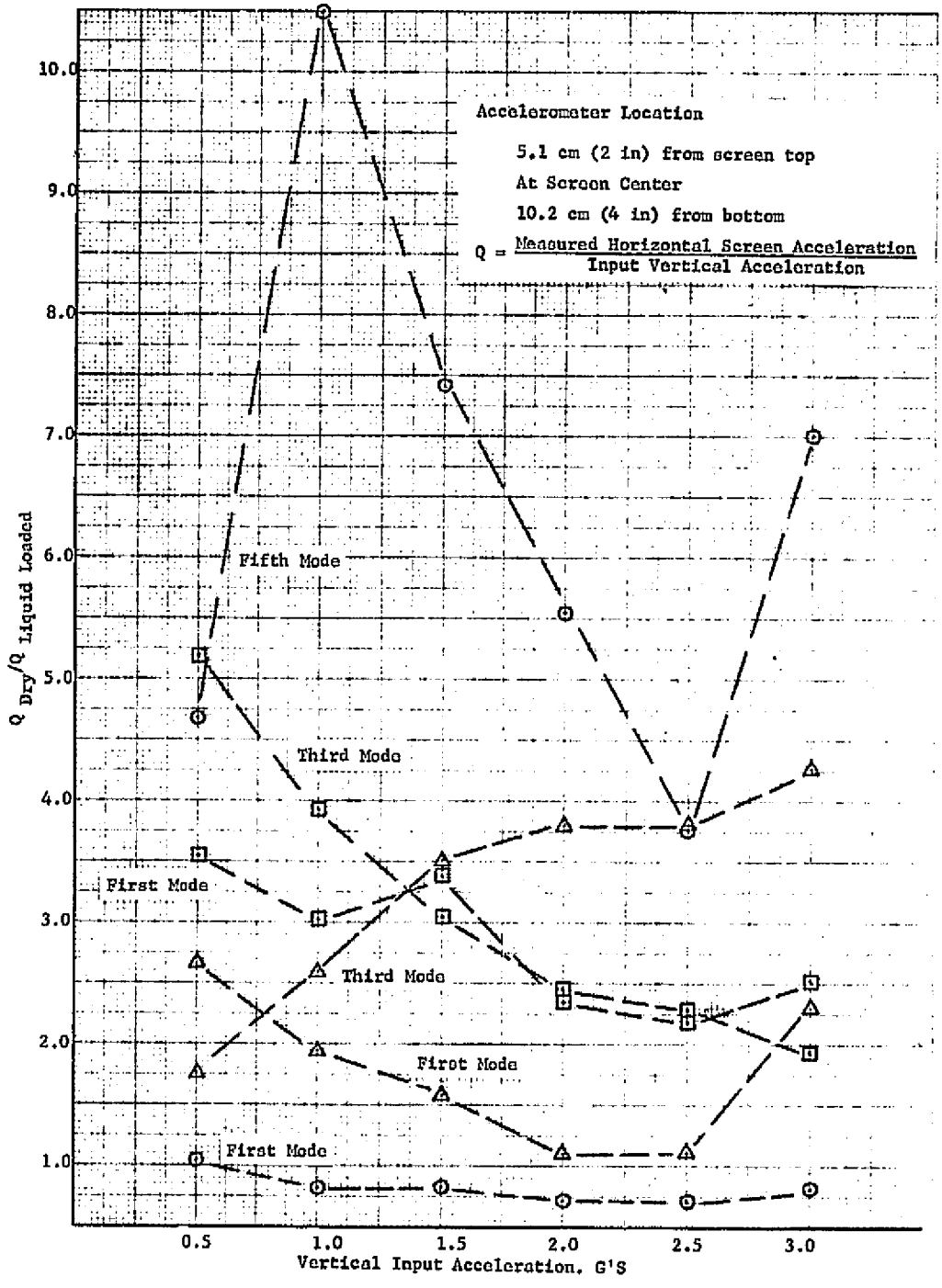

Figure 3-12: Amplification Factors Versus Input Acceleration for Tests 2-1 and 2-8

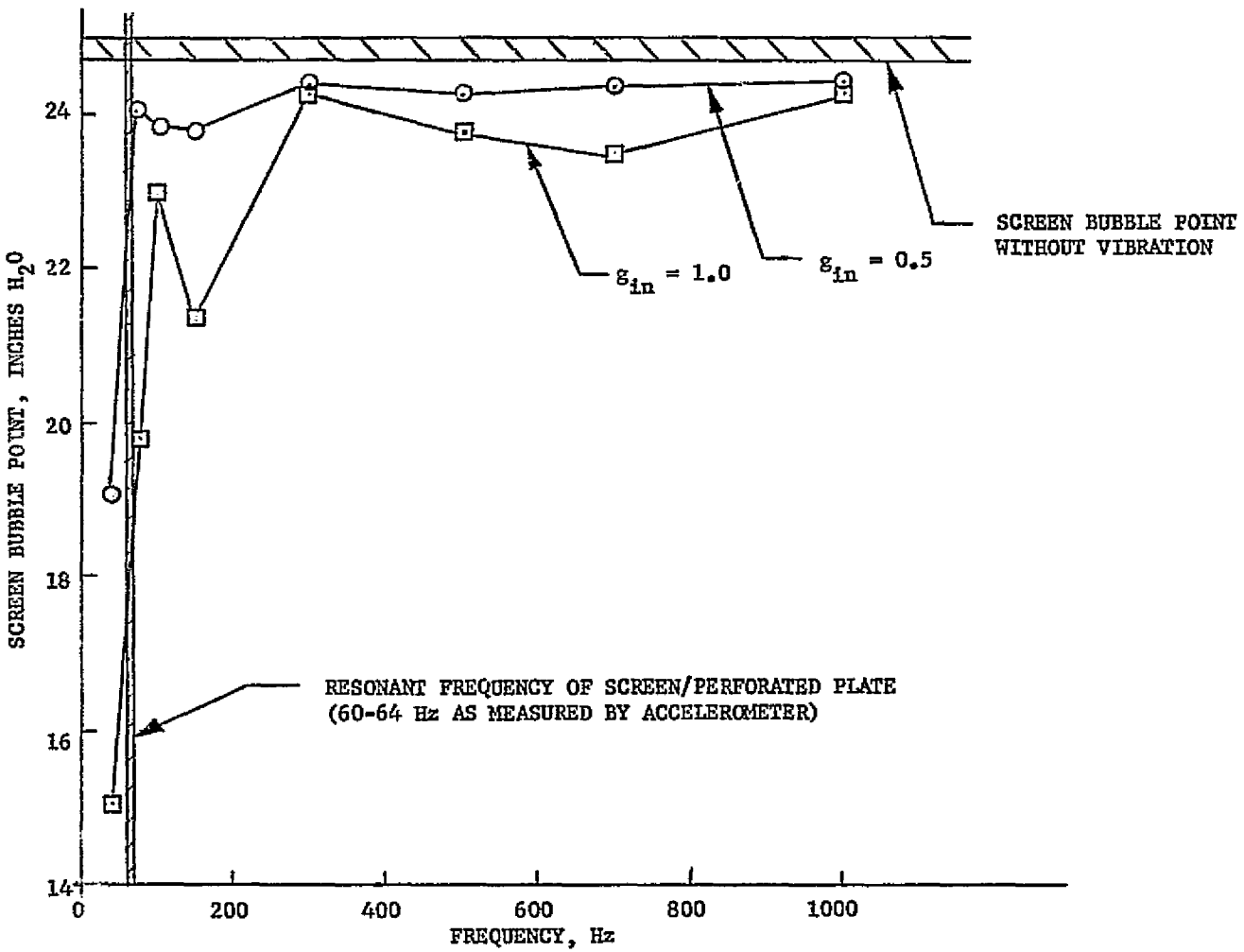

Figure 3.13: Vibration Degradation of Screen Bubble Point

IV. STARTUP/SHUTDOWN TRANSIENTS

A. DESCRIPTION OF TEST ARTICLE

A photograph of the test model is shown in Figure 4.1. There are four channels which are covered on the inner side with 325 x 2300 mesh stainless steel Dutch-twill screen. The four channels are manifolded together at both ends; one of which is connected to the outlet. Each channel has a 1.3-cm (.504-in.) x 5.1-cm (2.0-in.) cross-section, and is approximately 30.5-cm (12-in.) long. The device is installed in a 21.6-cm (8.5-in.) dia x 34.2-cm (13.5-in.) long stainless steel tank permitting ullage pressures to 103 N/cm^2 (150 psia). The measured bubble point of the screen channel was in a range of 62.5 to 64.0-cm H_2O (24.6 to 25.2-in. H_2O) which provides a safety factor of nearly three for the retention of methanol with an empty tank under one-g.

Two other screen device/tank combinations had originally been proposed for testing following testing of the above model. Inasmuch as these other models could not be subjected to the severe conditions to which the above model could be, and since breakdown was not obtained with the above model, testing was not conducted with these other models.

Five different line diameter-length combinations and two outflow valves were tested in conjunction with the four channel screen device. The outflow lines were:

Outflow Line No.	O.D.		I.D.		Length	
	cm	inch	cm	inch	m	ft
1	0.635	0.25	0.46	0.18	0.6	2.0
2	0.635	0.25	0.46	0.18	6.1	20.0
3	1.27	0.5	1.06	0.416	0.6	2.0
4	1.27	0.5	1.06	0.416	6.1	20.0
5	2.54	1.0	2.36	0.93	6.1	20.0

The two outflow valves employed:

Valve No. 1: Hoke - pneumatic operated - welded - bellows seal, teflon seat. Operating pressurant: helium at 100 N/cm^2 (145 psig). Opening or closing time: 1-5 ms.

Valve No. 2: Futurecraft electrically operated solenoid. Viton O-ring seal. Opening time: 15-25 ms.

B. TEST PROGRAM

A flow schematic is shown in Figure 4.2. A transparent section is included in the outflow line close to the tank in which to observe gas ingestion on startup. A liquid reservoir is included above the tank for the purpose of indicating gas ingestion on shutdown. Five Taber Instruments 0-69 N/cm^2 (0-100 psia) absolute pressure transducers with frequency response to 3000 Hz, were used to indicate pressure histories at discrete locations on the tank and outflow line. The pressure differential across the screen channels near the top outflow manifold was measured with a Statham $\pm$ 1.5 N/cm^2 ($\pm$ 2 psid) differential pressure transducer. Natural frequency on this unit is 1200 Hz. Two target type Ramapo flowmeters with ranges of 18.9-189 cm^3/S (0.3-3 gpm) and 63-630 cm^3/s (1-10 gpm) were used. The output was processed with a Dana signal conditioner and recorded on a Honeywell oscillograph.

A listing of the test conditions run is shown in Table 4.1. The test fluid for all runs was methanol. Tests were run both with the tank outlet up, minus-G orientation, and with the outlet down, plus-G orientation. For a given outflow line/valve combination, the run pressure, throttle valve setting and number of expulsions per depletion were varied.

In Table 4.1 runs are shown which appear to be otherwise identical but have different screen pressure differences and steady state flow rates. What is different between these is the throttle valve setting.

Since the test setup involves a number of fittings in the upstream end of the outflow line, a series of tests, numbers 34 through 37, were run with the 0.6-m (2.0-ft) outflow line in the vertical position which eliminates the elbow fitting at the tank. In all other tests the outflow line was in a horizontal position.

C. RESULTS AND DISCUSSION

In spite of the very severe conditions imposed, gas ingestion, either on startup or shutdown, was never observed. Measured pressure differentials across the screens, ullage minus outflow manifold pressure, are tabulated in Table 4.1. Note that these range up to nearly three times the screen bubble point. The differential pressure transducer was located at a height of 15.2-cm (6.0-in.) above the top of the channels. The differential pressure data shown has been corrected by subtracting out this amount of methanol head.

The largest pressure differentials obtained, both the time-wise pulse in the line and the difference across the screen device, were with the 2.54-cm (1.0-in.) line in conjunction with the fast acting Hoke valve. Time length of individual device manifold differential pressure spikes at pressures greater than the bubble point was up to 7 milliseconds. In general, the larger line diameters produced longer time durations of the pressure spike.

To reduce the flow impedance of the line, test series 27 through 33 were run without a flowmeter in the line. In tests

Table 4.1: Startup/Shutdown Test Summary

Test Series	Feed-line(1)	Valve No.(2)	Initial Tank Pressure N/cm^2 (psia)	Start Transient t_{max} ms	Start Transient t_{min} ms	Start Transient ΔP_{max} Head H_2O cm (inch)	Shutdown Transient t_{max} ms	Shutdown Transient t_{min} ms	Shutdown Transient ΔP_{max} Head H_2O cm (inch)	Steady State Flow Rate l/m (gpm)	No. of Expul-sions	Comments
1	2	1	60.0 (87.0)	85	40	24.7 (9.8)	335	60	83.9 (33.0)	6.1 (1.60)	10	
2	2	1	60.0 (87.0)	58	15	36.9 (14.5)	177	58	40.0 (15.7)	2.6 (0.70)	14	
3	2	1	25.5 (37.0)	98	20	30.3 (11.9)	63	36	39.7 (15.6)	3.2 (0.85)	17	
4	2	1	42.7 (62.0)	96	32	30.8 (12.1)	300	60	55.5 (21.9)	4.4 (1.15)	11	
5	2	1	60.0 (87.0)	102	33	34.6 (13.6)	370	62	51.9 (20.4)	5.9 (1.55)	13	
6	2	1	60.3 (87.5)	75	32	60.0 (23.6)	305	45	94.9 (37.4)	6.1 (1.60)	7	
7	2	1	60.0 (87.0)	106	75	34.6 (13.6)	295	50	38.7 (15.2)	6.1 (1.60)	3	
8	2	1	67.6 (98.0)	82	38	34.1 (13.4)	265	53	36.7 (14.4)	6.6 (1.75)	6	
9	2	2	60.0 (87.0)	80	41	30.6 (12.0)	318	56	25.0 (9.8)	6.2 (1.65)	6	
10	2	2	60.0 (87.0)	102	35	30.6 (12.0)	326	75	32.9 (13.0)	6.1 (1.60)	10	
11	2	2	66.9 (97.0)	66	56	-1.9 (-.75)	93	82	7.5 (3.0)	6.6 (1.75)	2	Differential not bled properly
12	3	1	60.3 (87.5)	75	48	82.6 (32.5)	318	150	68.9 (27.1)	5.3 (1.4)	8	
13	3	1	66.9 (97.0)	51	32	118.9 (46.8)	82	27	129.9 (51.1)	5.7 (1.5)	8	
14	3	1	66.9 (97.0)	46	27	95.9 (37.8)	26	24	114.9 (45.2)	23.8 (6.3)	3	

Table 4.1: (Continued)

Test Series	Feed-line[1]	Valve No.[2]	Initial Tank Pressure N/cm^2 (psia)	Start Transient t_{max} ms	Start Transient t_{min} ms	Start Transient ΔP_{max} Head H_2O cm (inch)	Shutdown Transient t_{max} ms	Shutdown Transient t_{min} ms	Shutdown Transient ΔP_{max} Head H_2O cm (inch)	Steady State Flow Rate l/m (gpm)	No. of Expul-sions	Comments
15	3	1	59.6 (86.5)	40	31	90.9 (35.8)	29	26	53.7 (21.1)	22.7 (6.0)	3	
16	3	1	39.3 (57.0)	38	29	56.2 (22.1)	39	27	64.6 (25.4)	18.2 (4.8)	4	
17	1	1	66.9 (97.0)	109	26	45.6 (18.0)	36	27	69.2 (27.2)	15.5 (4.1)	5	
18	1	1	60.0 (87.0)	46	23	49.4 (19.4)	36	23	79.1 (31.1)	14.8 (3.9)	6	
19	1	1	39.3 (57.0)	39	26	45.3 (17.8)	35	26	70.5 (27.8)	11.4 (3.0)	7	
20	1	2	39.6 (57.5)	53	28	32.4 (12.8)	85	41	28.0 (11.0)	11.4 (3.0)	6	
21	1	2	60.0 (87.0)	97	35	43.0 (16.9)	120	80	36.2 (14.3)	15.1 (4.0)	5	
22	1	2	67.2 (97.5)	58	28	51.4 (20.2)	128	76	41.2 (16.2)	15.1 (4.0)	5	
23	1	2	66.9 (97.0)	36	16	75.8 (29.8)	100	32	100.9 (39.7)	29.1 (7.7)	5	
24	3	1	67.9 (98.5)	20	13	77.8 (30.6)	34	22	85.9 (33.8)	25.0 (6.6)	13	Plus G
25	3	1	60.3 (87.5)	16	13	75.3 (29.6)	32	22	79.1 (31.1)	23.8 (6.3)	6	Plus G
26	3	1	40.0 (58.0)	19	13	37.7 (14.8)	26	21	93.6 (36.9)	18.9 (5.0)	5	Plus G
27	3	1	66.5 (96.5)			80.9 (31.9)	(3)				5	

Table 4.1 (continued)

Test Series	Feed-line (1)	Valve No. (2)	Initial Tank Pressure N/cm^2 (psia)	Start Transient t_{max} ms	Start Transient t_{min} ms	Start Transient ΔP_{max} Head H_2O cm (inch)	Shutdown Transient t_{max} ms	Shutdown Transient t_{min} ms	Shutdown Transient ΔP_{max} Head H_2O cm (inch)	Steady State Flow Rate l/m (gpm)	No. of Expul-sions	Comments
28	3	1	66.2 (96.0)			89.5 (35.2)	(3)				5	
29	4	1	66.2 (96.0)			44.3 (17.4)	(3)				5	
30	4	1	66.5 (96.5)			47.1 (18.5)	(3)				5	
31	5	1	57.6 (83.5)			112.5 (44.3)	(3)				9	
32	5	1	65.5 (95.0)			169.3 (66.7)	(3)				7	
33	5	1	76.5 (111.0)			152.2 (59.9)	(3)				10	
34	3	1	39.6 (57.5)			70.2 (27.6)	(3)				10	Vertical Feedline Orientation
35	3	1	59.6 (86.5)			91.5 (36.0)	(3)				8	↓
36	3	1	77.2 (112.0)			99.7 (39.3)	(3)				6	
37	3	1	77.2 (112.0)			90.0 (35.4)	(3)				6	Vertical Feedline Orientation

NOTE: t (max and min) - The maximum and minimum effective valve opening and closing times.

P_{max} - The maximum pressure differential across the channel manifold.

(1) See page

(2) 1 - Hoke Valve, 2 - Futurecraft Valve

(3) Flowmeter not installed, shutdown data not recorded.

using the 2.54-cm (1.0-in.) O.D. line, all instrumentation at the valve end of the feedline was removed to further increase flow rate and reduce attenuation of the start/shutdown transient pressure pulses in the feedline.

Differential pressures across the device manifold were found to be greater for the fast (Hoke) valve than when using the slower (Futurecraft) valve, except for the 0.635-cm x 0.6-m (0.25-in. x 2-ft) line configuration where no difference was noted. The plus-G orientation recorded lower pressure differentials at the device manifold than the minus-G orientation.

The pressure difference across the screen manifold under static conditions reflects the head difference between the top of the channels and the liquid level. For a 30.5-cm (12-in.) head difference (tank near empty), the static ΔP amounts to 24-cm H_2O (9.5-in.). With outflow there is a frictional pressure drop which also increases with decreasing liquid level and is additive to the static value. As the liquid level drops, therefore, the pressure difference across the screen should increase. This relation between pressure difference and liquid level has been observed in the present tests. In Figure 4.3, typical values of the pressure difference developed across the screen device are summarized. The initial value is represented by the darkened portion of the vertical bar while the total bar represents the value when the tank is drained.

A pressure drop approximately equal to the tank gage pressure was observed at the valve during the start transient. This pressure drop which moves as a wave up the line was found to be considerably attenuated in the line, ranging up to a 10:1 ratio for the 1/4-inch line. Typical values of the pressure drops at the valve end and feeder tank end of the line are shown

Table 4.2 Valve Opening Times and Acoustic Wave Transit Times for Martin Marietta Test System vs Rockwell International Test Systems

	Line Length	Fluid & Acoustic Velocity	Travel Time, Test Valve to Device	Travel Time, Test Valve to Test Valve (Reflected)	Valve Open Time
	m(ft)	m/sec (ft/sec)	milliseconds	milliseconds	
Martin Marietta	.61(2)	Methanol	.56	1.12	2.0 ms (Hoke)
	6.1(20)	1088(3570)	5.6	11.2	20-25 ms (Futurecraft)
Rockwell International	1.89(6.2)	Freon 11 800(2622)	2.4	4.8	
	5.33(17.5)		6.7	13.4	5 ms, 100 ms
	11.6(38)		14.5	29.0	

graphically in Figure 4.4. The total vertical bar represents the drop at the valve and the darkened portion represents the drop at the tank end of the line. It can be seen that the larger diameter lines are much less restrictive in terms of pressure pulse attenuation.

On startup, the flowmeter response would typically show the flow rate rising past the steady-state value, reaching a maximum and then decaying to the steady-state value. Tabulated in Table 4.1 is the range of times for a given test series, represented by t_{max} and t_{min} for the flowmeter trace to go from zero to the first crossing of the steady-state value. This is illustrated in Figure 4.5. On shutdown the flowmeter trace would decay in more or less a linear fashion. Tabulated in Table 4.1 is the range of times for the trace to go from the steady-state value to zero. Note that the flow transient period is far in excess of the value actuation time.

Analysis of a microswitch trace covering over 50 test runs gives a median Hoke valve opening time of 2.0 milliseconds, with a range of 1.5 to 4.5 ms. Closing time median was 3.5 ms with a range of 2.5 to 5.0 ms. When compared to the computed pressure pulse travel times shown in Table 4.2, it can be seen that the valve appears instantaneous (valve actuation time less than pulse travel time) for a 6.1-m (20-ft) line. Since the .61-m (2-ft) lines provided the more severe differential pressures for a given line diameter, the attentuation along the 6.1-m (20-ft) line apparently negates the effect of the relatively instantaneous valve opening.

Frequency analysis of the differential pressure traces gave the results presented in Table 4.3. All minus-G orientations, except the 2.54-cm (1.0-in.) diameter line case, have a frequency

Table 4.3: Comparison of Frequencies of ΔP Trace For Various Line Lengths, Valves & Orientation

Outflow Line Configuration		Valve No.	Average Frequency For Test Series	Orientation	Comments
Diam cm (in.)	Length m (ft)		Hz		
.635 (.25)	.61 (2)	1	205.8	Minus G	
.635 (.25)	.61 (2)	2	205.8		
.635 (.25)	6.1 (20)	2	193.2		
.635 (.25)	6.1 (20)	1	206.7		
1.27 (.5)	.61 (2)	1	205.3		
1.27 (.5)	.61 (2)	2	212.2		
1.27 (.5)	.61 (2)	1	214.6		No flowmeter
1.27 (.5)	6.1 (20)	1	233.5		No flowmeter
2.54 (1.0)	6.1 (20)	1	59.4	Minus G	No downstream instrumentation
1.27 (.5)	.61 (2)	1	56.8	Plus G	
1.27 (.5)	.61 (2)	1	62.6		
1.27 (.5)	.61 (2)	1	41.4	Plus G	
1.27 (.5)	.61 (2)	1	213.0	Minus G	Vertical outflow line
1.27 (.5)	.61 (2)	1	226.5		
1.27 (.5)	.61 (2)	1	227.0		
1.27 (.5)	.61 (2)	1	214.0	Minus G	Vertical outflow line

in a range of 205-230 Hz. In contrast, the plus-G and 2.54-cm line configurations' frequencies lie in the 40-60 Hz band. The reason for the frequency shift is not understood. This type of behavior is suggestive of a bubble in the system. The likelihood, however, of duplicating the plus G test frequencies in the minus G, one inch line tests when both test series were run with a gas bubble in the system seems quite remote. The effect of increasing the line diameter is to lower the resonant frequency and on this basis there is a sizable effect in going from the one-half to one inch line size. This trend is consistant with the experimental results. No such effect is seen in the data, however, when the one quarter and one half inch line sizes are compared.

Since screen breakdown has not been observed in the present tests, but was observed in the tests reported in Reference 4-1, which were conducted by Rockwell International, there is some interest in comparing the conditions for the two test series. This is done in Table 4.4. Significantly, both the liquid density and acquisition device velocity are nearly double in the Rockwell tests as compared to the present tests. In addition, because of the much larger screen area in the present tests, the energy in a pressure wave is more easily dissipated. This may explain the shorter time duration of the pressure spike above the bubble point in the present tests; 7-ms here versus 30-ms in the previous work.

The test fluid acoustic velocity and sonic transit times for the Rockwell tests are compared to those for the present tests in Table 4.2. Note that in the prior work that the valve actuation time is not relatively instantaneous compared to the transit time of an acoustic wave. The most severe conditions were obtained, however, with the shorter lines as was the case in the

Table 4.4: Test System Comparison

	RI (NAS7-200)	MMA (NAS8-30592)
Screen Meshes Tested	325 x 2300 200 x 1400 200 x 600	325 x 2300
Number of Channels in Device	1	4
Channel Cross-Section	1.9 x 1.9 cm (.75 x .75 in.)	1.28 x 5.08 cm (.504 x 2.0 in.)
Screen Flow Area	116.0 cm^2 constant (18.0 in^2)	666 cm^2 (103 in^2) max. 194 cm^2 (30 in^2) min. (Est.)
Flow Rates Tested	3.8 l/min. (1 gpm) 7.6 l/min. (2 gpm)	29.1 l/min. (7.7 gpm) max. 2.6 l/min. (.7 gpm) min.
Velocity in Channels Max. Flow Rate	.348 m/sec.	.187 m/sec.
Line Lengths	1.89 m (6.2 ft) 5.3 m (17.5 ft) 11.6 m (38 ft)	.6 m (2 ft) 6.1 m (20 ft)
Line Diameters	2.1 cm ID (1.0 in. OD)	.46 cm ID (.25 in. OD) 1.06 cm ID (.5 in. OD) 2.36 cm ID (1.0 in. OD)
Tank Run Pressures	14.5 N/cm^2 Gauge (21 psig) 9.7 N/cm^2 Gauge (14 psig) 4.8 N/cm^2 Gauge (7psig)	31.0 N/cm^2 Gauge (45 psig) 51.7 N/cm^2 Gauge (75 psig) 58.6 N/cm^2 Gauge (85 psig) 68.9 N/cm^2 Gauge (100 psig)
Accumulator Installed	Yes/No	No
Valve Opening Times	5 ms (fast open) 100-150 ms (fast close)	Hoke: 1-5 ms Futurecraft: 15-25 ms
Test Fluid	Freon 11	Methanol
Fluid Properties:		
Density	1.467 gm/cm^3 (92.1 lb/ft^3)	.79 gm/cm^3 (49.4 lb/ft^3)
Boiling Point	23.9°C (75°F)	65.0°C (149.0°F)
Viscosity	.42 cp at 25°C	.547 cp at 25°C
Surface Tension	18 Dynes/cm @ 24°C	22.6 Dynes/cm at 25°C
Acoustic Velocity	800 m/sec @ 24°C (2622 ft/sec)	1088 m/sec @ 30°C (3570 ft/sec)

present work.

As an extension of the present work, further startup/shutdown transient tests are currently planned to be run under a Martin Marietta IRAD program, D-02R. Under the proposed program, it will be possible to apply more severe pressure conditions to the screen model. A single channel transparent cast polyester model, Figure 4.6, was modified to provide start transient test capability utilizing an 80 x 700 Dutch-twill weave screen specimen. The outflow line has an internal diameter of 1.7-cm (0.68-in.) to provide the necessary high flow rate.

Some initial testing has been accomplished with this model. Tests were conducted at three ullage heights, approximately 1, 2, and 3 inches; and four pressures, 5, 10, 15, and 20 psig.

Breakdown was observed only at the 3-inch ullage level for 15 and 20 psig ullage pressures. The differential pressure drop at valve actuation exceeded 0.7 psi for all test conditions under which screen breakdown occurred. The bubble point for this specimen was 0.22 psi. The mode of breakdown observed consisted of a dryout of the screen along the top seam which was followed by dropout from the liquid side of the model. The liquid side connection to the differential pressure transducer was made at the top of the liquid side of the channel. This line was carefully purged of any gas prior to a test since any gas would greatly attenuate the pressure pulse seen at the transducer. With this design, the liquid coupling is lost when screen breakdown occurs. The pressure transducer indications on breakdown therefore, are probably not too precise. This has hampered attempts at data correlation.

1. Analytical Studies

The Martin Marietta Hydraulic Transient Computer Program (HYTRAN) was utilized to estimate the unsteady pressures which occur throughout the test system on startup and shutdown.

The basic HYTRAN model used for the pretest analysis was developed by F. M. Young under Contract NAS9-9313 (Ref. A.1). The computer program was developed to perform a one-dimensional method of characteristics solution to fluid transfer system transients. The basic model can be used to analyze a transfer system that may include tanks, orifices, accumulators, valves, transfer functions, integrator functions, cross connections, tee connections, series connections, and dead-end nodes. The model has been modified to include nodes that simulate fine-mesh screen components of an acquisition system as well as a plotting routine and pressure and velocity time histories. The derivation of the logic which describes a one-dimensional hydraulic transient between the bulk liquid and flow channel is described in Appendix A. Some results for the four channel model are shown in Figures 4.8 and 4.9. The peak excursions are of similar magnitude to those experienced in the test program. The model predicts much larger pressure excursions on shutdown than on startup, which is not, however, in agreement with the test data.

D. TEST RESULTS SUMMARY

The following observations have been drawn from an analysis of the data from the tests on the four channel model:

1. Start/shutdown, transient-initiated, breakdown was not observed. This includes the entire range of conditions tested.

2. Differential pressures across the device manifold that were greater than screen bubble point were measured during most

tests. The .635-cm x .6-m (.25-in. x 2-ft) line and some tests at low flow rates were exceptions to this. Time length of individual spikes at pressures greater than the bubble point was 1-7 milliseconds. In general, the larger the line diameter, the longer the pressure spike lasted.

3. Differential pressures across the device manifold were greater using the fast (Hoke) valve than when using the slow (Futurecraft) valve. There was essentially no difference in the pressure for the two valves during the .635-cm x .6-m (.25-in. x 2-ft) line tests.

4. Subsequent to valve actuation, the pressure immediately upstream of the valve fell to very close to the ambient pressure.

5. The pressure wave was considerably attenuated as it moved upstream, ranging up to a 10:1 ratio.

6. The plug-G configuration recorded lower pressure differentials across the device manifold than the minus-G configuration, except at the 31.0 N/cm^2 gage (45 psig) pressurization where little difference was noted.

7. A check of selected tests revealed that pressure transients at the valve were damped in about the same time period for start and shutdown; however, the differential pressure transients at the device manifold were damped at start in about one-half of the shutdown damping time.

E. DESIGN CRITERIA

An objective of this program is the development of guidelines which would preclude the ingestion of gas as a result of start/shutdown transients. Inasmuch as it was not possible in these tests to bracket the conditions leading to gas ingestion, the guidelines presented must be somewhat tentative and cannot

be definitive. Based on the present tests, in order to avoid gas ingestion, the capillary system designer is advised to adhere to the following criteria:

1. Screen material should have a bubble point in excess 50-cm (20-in.) of water.

2. Channel velocity should not exceed 0.2 m/s (0.66 ft/s).

3. Maximize screen-liquid contact area.

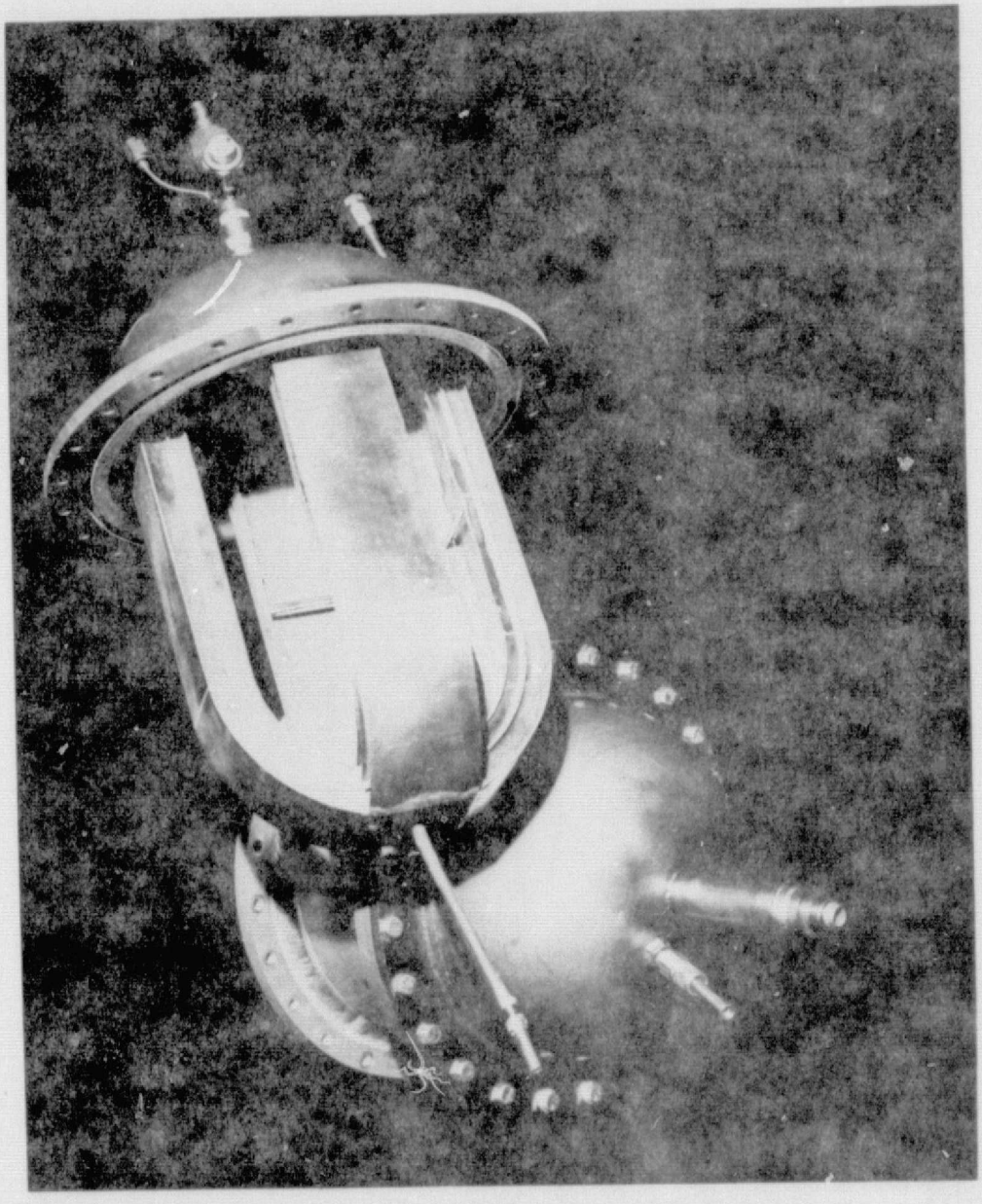

Figure 4.1: Start/Shutdown Test Four Channel Screen Device

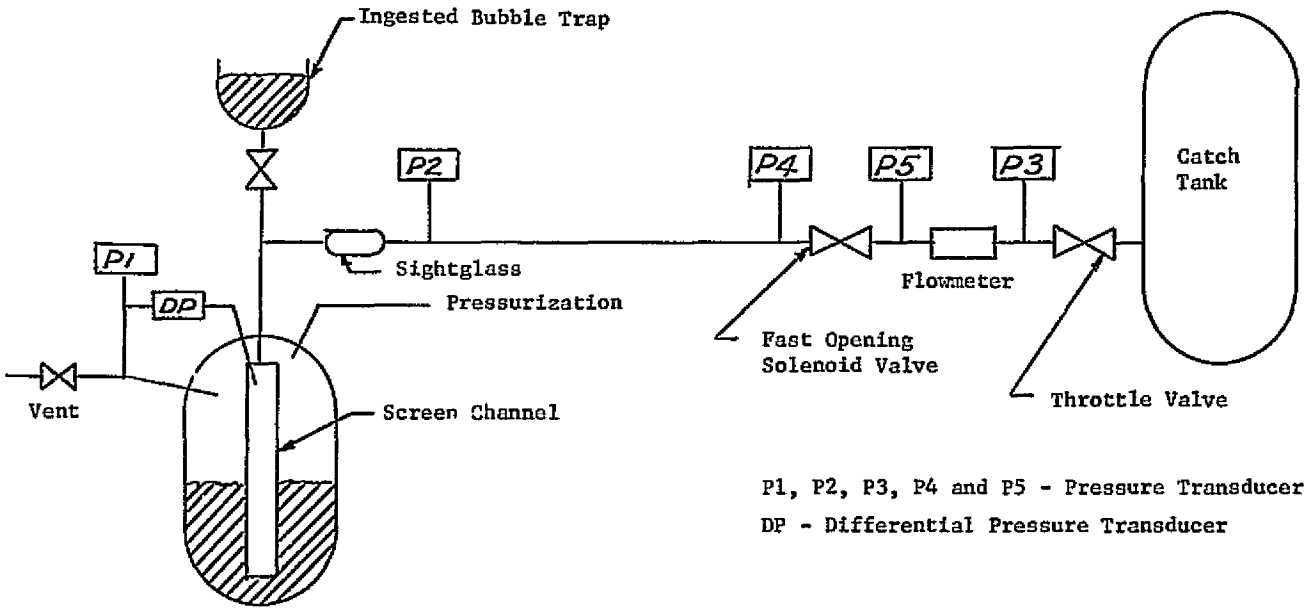

Figure 4.2: Flow Transient Test Schematic

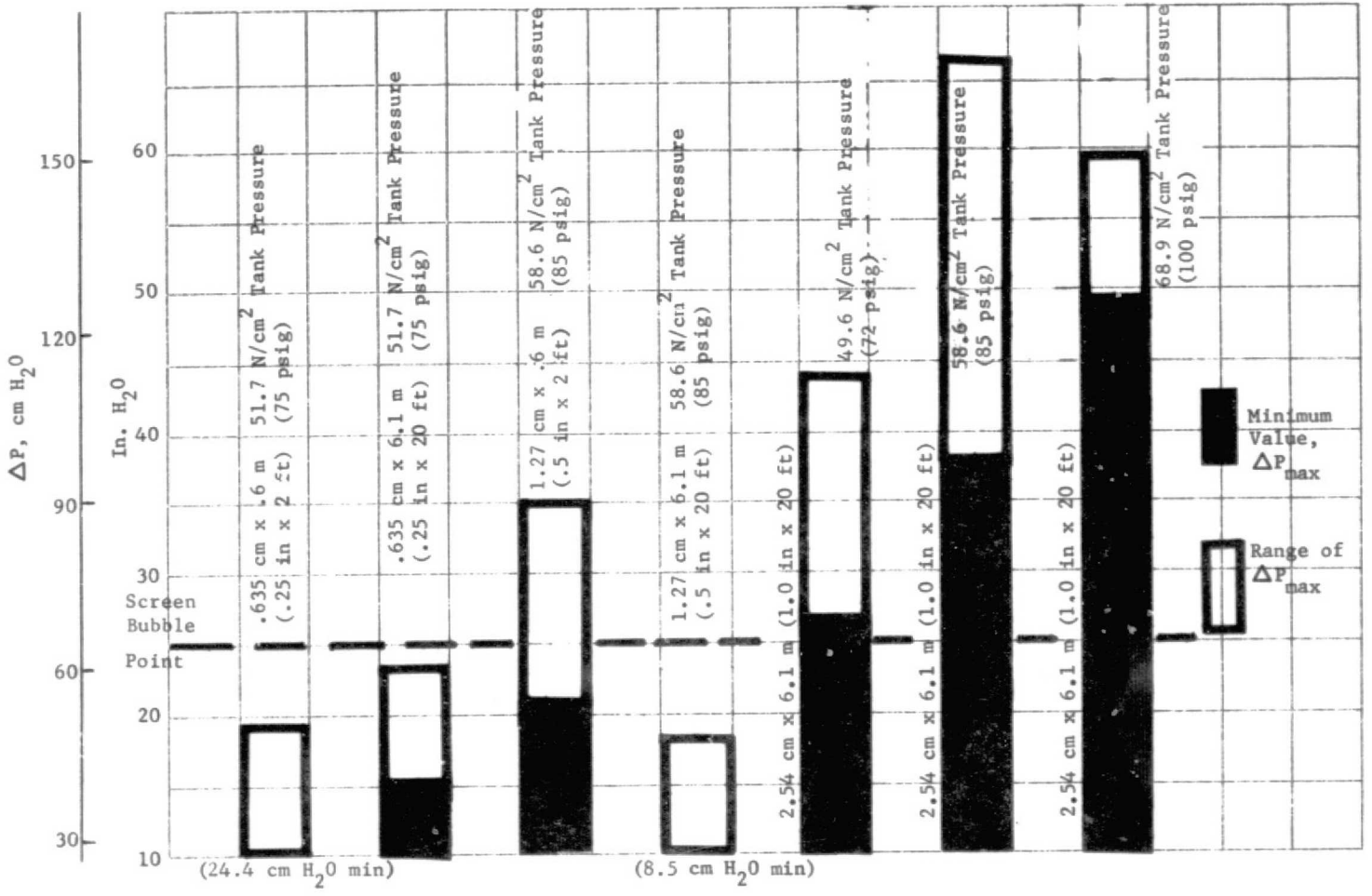

Figure 4.3: Typical Range of ΔP_{max} Across Screen Manifold for Various Test Configurations, Valve No. 1

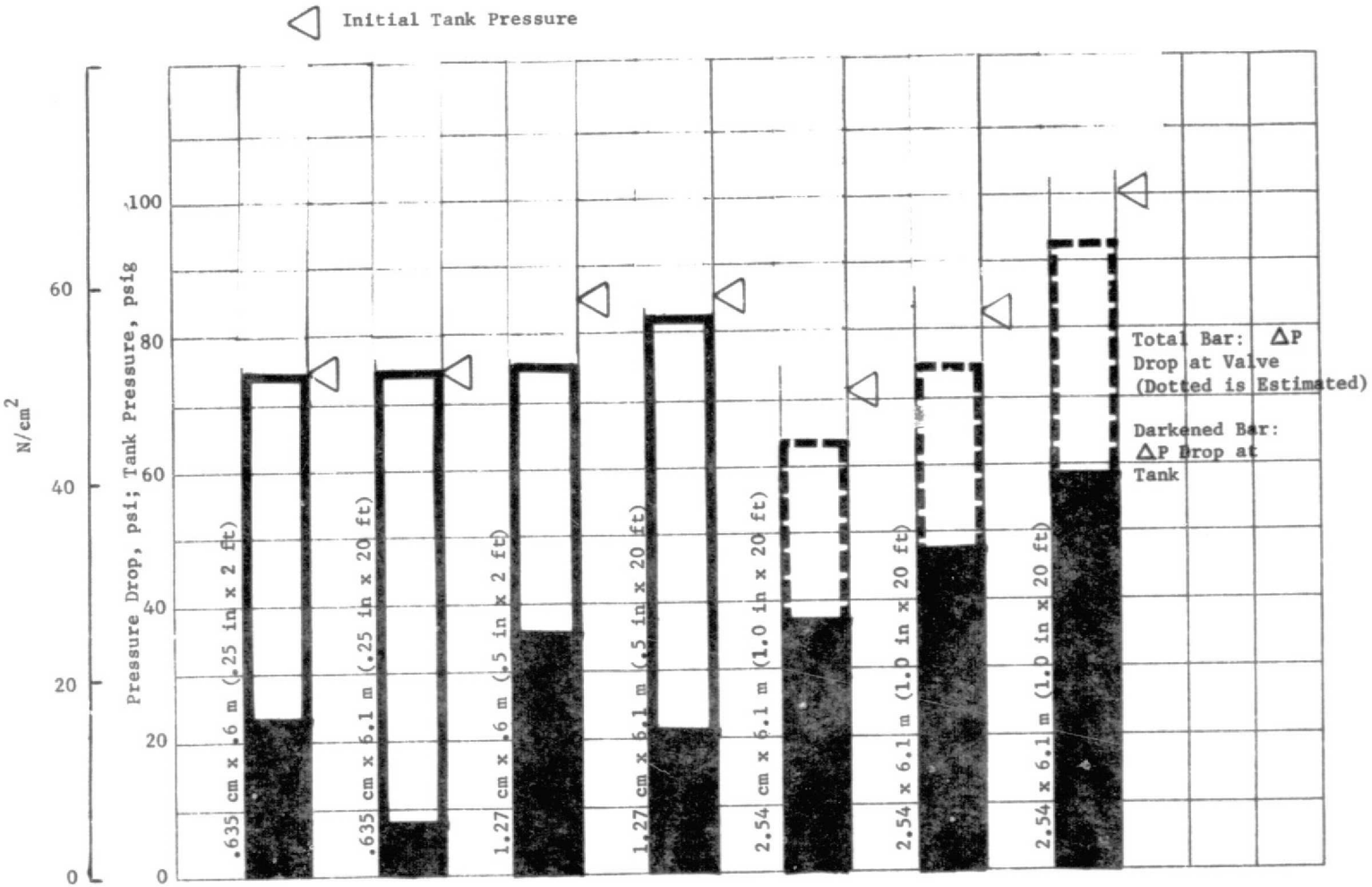

Figure 4.4: Start Transient Pressure Drop Attenuation, Valve No. 1

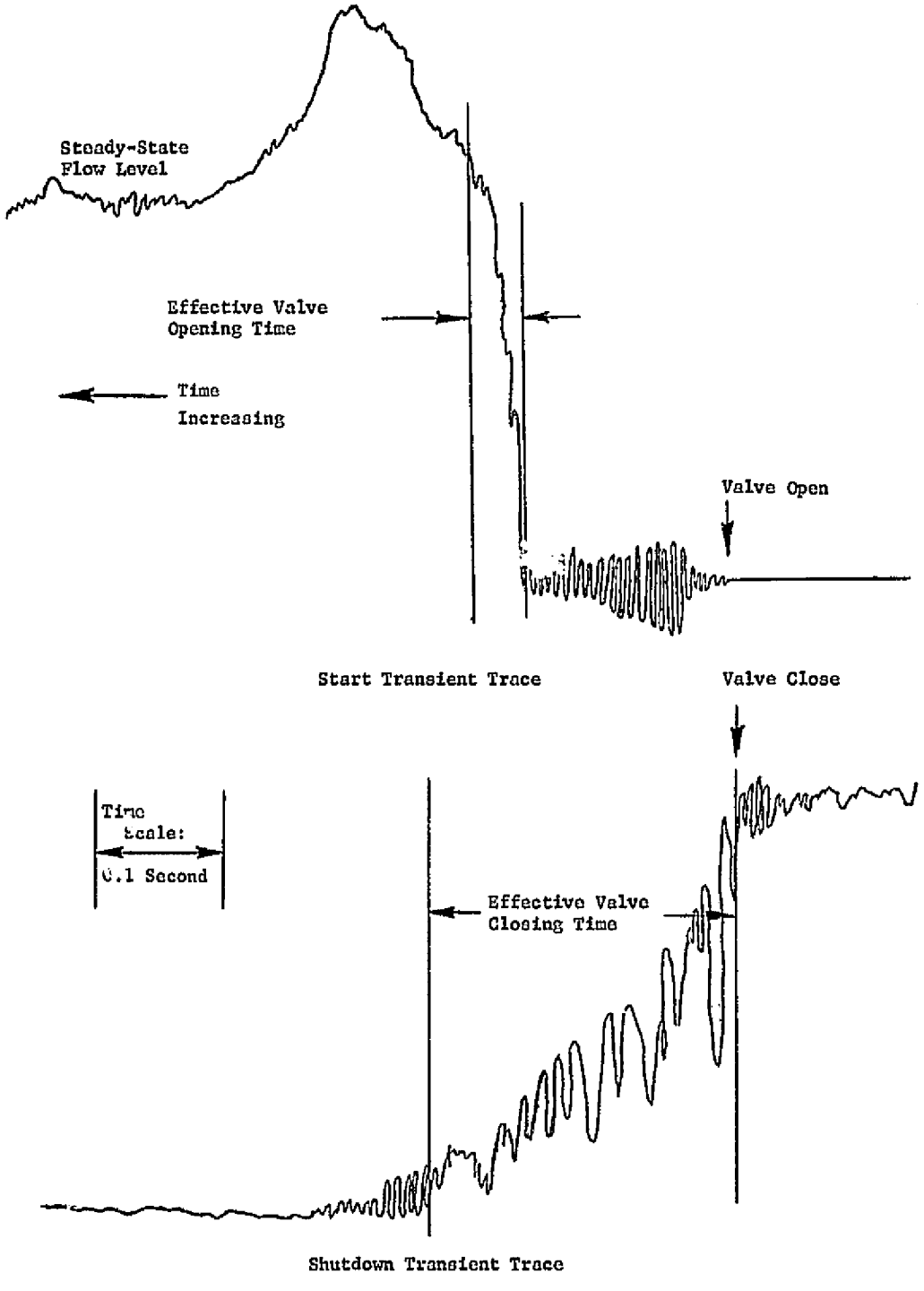

Figure 4.5: Sample Flowmeter Traces, Start/Shutdown Transients, Test 8-3

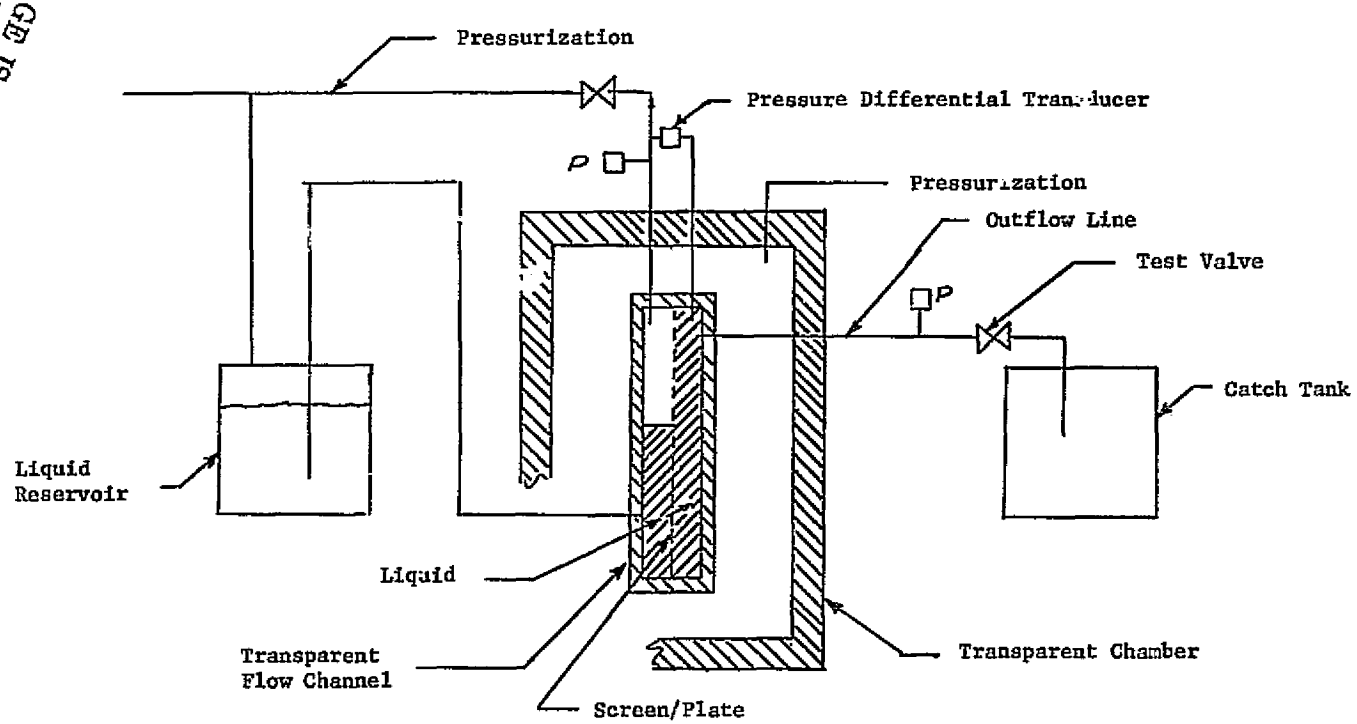

Figure 4.6 Outflow Test System for Independent Research Program

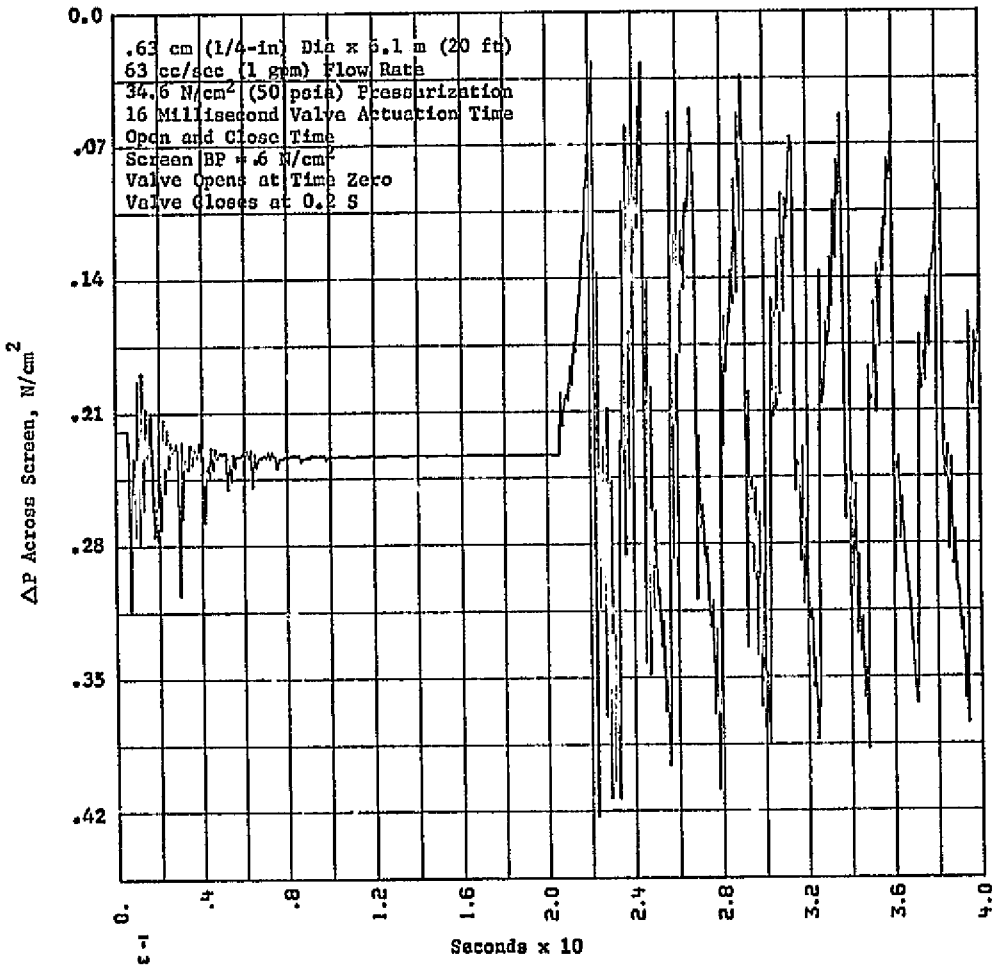

Figure 4.7: Calculated, Unsteady Pressure Differential Across Screen Manifold, Steady State Flow Rate 63 cm^3/s (1 gpm)

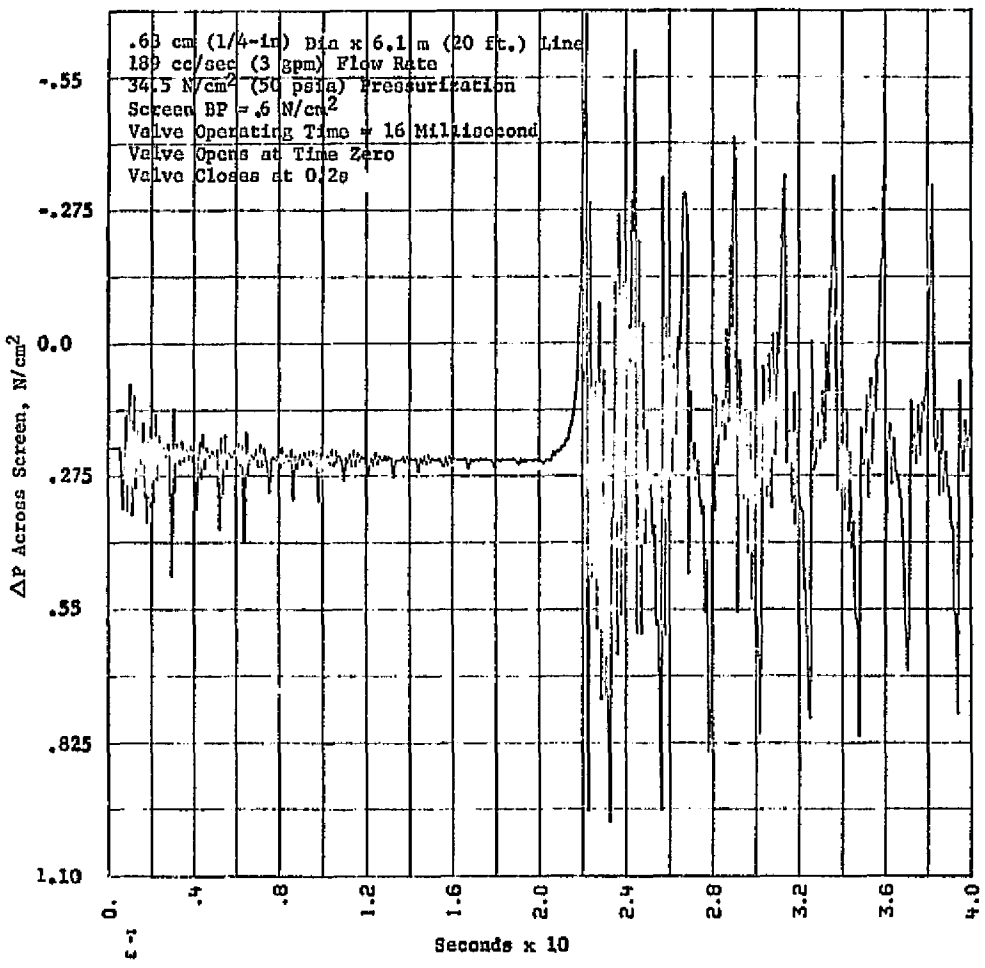

Figure 4.8: Calculated, Unsteady Pressure Differential Across Screen Manifold, Steady State Flow Rate 65 cm^3/s (3 gpm)

V. WARM ULLAGE EFFECTS

A. DESCRIPTION OF TEST ARTICLE

The test model which was employed for these tests is an eight-channel screen device within a 0.635 m (25-in.) diameter spherical tank. The singularly curved channels are assembled into an octo-spherical array and manifolded together at both poles. The outer surfaces of the screen channels are in contact with an octo-spherical screen liner which completely separates an outer vapor annulus from the inner or bulk region. An assembly drawing is shown in Figure 5.1. A cross-section of a screen channel is shown in Figure 5.2. The screens used are stainless steel Dutch-twill of 325 x 2300 mesh. Two layers are used on each side of the channels and an additional layer on the screen liner. Photographs of the capillary device are shown in Figures 5.3 and 5.4. Some of the more significant volumes and areas of the model are summarized in Table 5.1. Also, Table 5.2 lists a summary of some of the more pertinent model dimensions. Further detail can be obtained from Ref. 5.1.

The tank is both filled and outflowed from the line which communicates with the channel manifold. Pressurant can be introduced at either pole. With the outflow line down, pressurant is introduced by way of the cylindrical diffuser located at the upper pole. With the outlet line oriented up, pressurant was introduced through the one-quarter-inch open-ended tube which is located near the upper pole. This line was originally incorporated as a pressure sensing line and pressurant introduced through the bottom diffuser and bubbled up through the liquid.

An instrumentation schematic is shown in Figure 5.5. Nine platinum resistance thermometers are located inside the tank. Four are located in the bulk region along the centerline of the tank. The height of the thermometers corresponds to volumes of

Table 5.1: Test Article Areas and Volumes

Tank Volume	4.734 ft^3
Liner Volume	3.771 ft^3 79.5% of Tank Volume
Channel Volume	0.329 ft^3 8.7% of Liner Volume
Vapor Annulus Volume	0.970 ft^3 20.5% of Tank Volume
Liner Area	12.04 ft^2
Communication Screen Area	4.47 ft^2 37.1% of Liner Area

Table 5.2: Test Article Dimensions

	ension
Outer Liner and Feeder Channels	
Diameter, ft	1.92
Gas Annulus, in.	1.0
Communication Screen Mesh	325x2300
Channel Screen Mesh (2 layers)	325x2300
Perforated Plate, Percent of Open Area	30
Channel Depth (at Equator), in.	0.75
Channel Width (Equator & Manifold), in.	3.0
Communication Screen Width at Equator, in.	6.56
Number of Channels	8

20, 50, 80 and 99% of the bulk region volume*. One platinum thermometer is located in each of the flow channel manifolds, and another is installed inside one of the flow channels approximately at the equator. Platinum thermometers are also located in the outer annulus volume at each pole.

External tank temperatures are measured with thermocouples made from 24-gage Kapton-insulated chromel/constantan wire. For measuring tank wall temperature, five thermocouples are spot-welded on the outside of the tank. Two are installed at the poles and three are located about 1.3-cm (1/2-in.) from the tank support brackets. Five insulation thermocouples are installed under the first layer of insulation opposite the tank wall thermocouples. Three other thermocouples measure temperatures on the outflow valve body and coil, and on the outflow line approximately 10-cm (4-in.) from the tank.

The liquid level sensors are the hot-wire type made by United Control Corporation. The selection was based primarily on previous experience that proved this sensor to be very reliable with a fast response. The fast response is required as a result of the relatively short outflow periods. These sensors are also required to indicate gas ingestion into the liquid flow channels. A total of eight sensors is used. One is located in each of the two manifolds. One sensor is located in the outer annulus adjacent to the bottom manifold and can sense residual liquid in the outer annulus. The remaining five sensors are located in the bulk region along the centerline of the tank, at the 1, 20, 50, 80 and 99% liquid levels.

Two 0 to 50-psig strain-gage transducers measure the outer annulus and bulk region pressures. The differential pressure

*Minus G attitude.

between the outer annulus and bulk region is measured using a Rosemount Engineering transducer with a range of ± 0.1 psi and an accuracy of better than 1%*. A strain gage differential pressure transducer is used to measure differential pressure for the flowmeter in the outflow line. This meter is installed in the outflow line approximately 30-cm (12-in.) from the tank.

The flowmeter in the pressurization line utilizes an annular flow element. The flowmeter is installed as close to the vacuum penetration as is physically possible.

All the pressure, flowmeter and thermocouple temperature data are recorded on Bristol recorders. Data from the platinum temperature sensors and liquid level sensors are recorded on a Honeywell Visicorder oscillograph.

B. TEST PROGRAM

Outflow tests were conducted with the test article in both the minus-G attitude, that is, with the outflow line at the top of the tank; and in the plus-G attitude where the outflow line is at the bottom of the tank. Flow schematics for these two orientations are shown in Figures 5.6 and 5.7.

The solenoid actuated outflow valve in both the plus and minus G orientation is a 3/4-inch Valcor normally closed valve. The valve opens within 40 ms of application of the actuation voltage. The actual mechanical travel time is 20 to 30 ms.

Twenty seven tank depletions were run with the tank in the minus-G orientation. These include cases in which the tank was depleted in a single continuous expulsion and those in which the tank was depleted in several segmented expulsions. Four multiple expulsion tests were conducted with the tank in the plus-G orientation; two with warm helium pressurant and two with warm hydrogen

*This pressure transducer failed during the course of testing.

pressurant.

Pressurization sources included warm gas (K-bottle) storage of H_2 and He and H_2 dewar vent gas. The pressurant gas was thermally conditioned in a tubular heat exchanger which was immersed in warm water for the higher temperature tests, in liquid nitrogen for the intermediate temperature tests and in liquid nitrogen followed by liquid hydrogen for the lowest temperature tests. Two tests were run with dewar vent gas with no further preconditioning.

The test conditions are summarized in Tables 5.3 and 5.4. The pressurant temperatures were varied in the range of about 311 K (560 R) down to about 39 K (70 R) for the helium and to 28 K (50 R) for the hydrogen pressurant. These temperatures are measured in the pressurization line external to the vacuum chamber as shown in the schematic. As is indicated in Table 5.3, for the first seven tests, the pressurant inlet temperature varied considerably over the length of the run. The pressurant line was cold prior to initiating the outflow since it is also used as a vent line and as a result, had a cooling effect on the pressurant gas. This was corrected by adding a bypass line as is shown in Figure 5.6 (valve SV7). The pressurant line could then be thermally conditioned prior to initiating outflow.

C. TEST RESULTS

1. Minus-G Orientation

With only a few exceptions the tank was successfully outflowed for the range of test conditions shown in Table 5.3. The primary indication of a successful outflow was provided by the liquid sensor, OMLS, which resides in the outflow manifold. Typically, when beginning the expulsion, the outflow manifold would

Table 5.3: Warm Gas Pressurization Test Matrix, Minus-G Orientation

Test No.	Single/ Multiple Expulsion*	Press- urant	Pressurant Conditioning (**)	Pressurant Temperature Range K (R)	Tank Pressure Range N/cm^2 (psia)	
1	S	He	2	122-217 (220-390)	20.8-13.1 (30.1-19.0)	Temperature data inaccurate as a result of temperature sensor location and uninsulated pressurant line for first 7 tests. Low pressurization regulator setting resulted in substantial autopressurization for first 7 tests.
2	M (4)	He	2	158-256 (285-460)	21.8-9.8 (31.6-14.2)	
3	S	H_2	2	189-231 (340-415)	26.1-15.2 (37.8-22.0)	
4	M (3)	H_2	2	194-239 (350-430)	22.9-9.1 (33.2-13.2)	
5	M (4)	H_2	2	194-236 (350-425)	2[illegible].2-12.1 (33.6-17.6)	
6	M (4)	He	1	194-278 (350-500)	27.7-8.9 (40.2-12.9)	
7	S	He	1	244-278 (440-500)	30.4-12.1 (44.1-17.5)	
8	S	He	1	293-291 (527-524)	25.0-8.7 (36.2-12.6)	
9	S	H_2	1	291-290 (524-522)	28.8-8.8 (41.8-12.8)	
10	M (2)	H_2	1	306-298 (550-537)	32.7-9.2 (47.4-13.4)	
11	M (3)	H_2	1	306-294 (550-530)	35.5-9.4 (50.0-13.7)	New pressurant reg. installed.
12	M (3)	H_2	1	>311-302(>560-543)	20.5-8.7 (29.8-12.6)	
13	S	H_2	1	323-314 (582-565)	33.9-8.5 (49.2-12.3)	New range on thermocouples.
14	S	He	1	311-306 (559-551)	26.6-8.8 (38.6-12.7)	Dome loader regulator.
15	S	He	1	300-294 (540-530)	21.0-9.9 (30.4-14.4)	Reg. pressure manually increased during run, different reg. installed.
16	M (3)	He	1	298-296 (537-532)	31.[illegible]-8.8 (45.0-12.7)	
17	M (4)	H_2	4	107-94 (192-170)	34.3-9.2 (49.7-13.4)	Dewar ullage is pressurant supply.
18	S	H_2	4	96-86 (172-155)	34.3-10.8 (49.8-15.7)	Dewar ullage is pressurant supply.
19	S	He	3	89-64 (160-115)	34.8-9.6 (50.5-13.9)	
20	M (4)	He	3	81-54 (145-98)	35.3-9.3 (51.2-13.5)	
21	S	He	3	64-47 (115-85)	35.6-9.7 (51.7-14.1)	
22	M (4)	H_2	3	39-28 (70-50)	30.5-10.1 (44.3-14.7)	Dewar ullage is pressurant supply.
23	S	H_2	3	31-29 (55-53)	27.3-10.3 (39.6-14.9)	Dewar ullage is pressurant supply.
24	M (3)	H_2	3	42-32 (75-57)	33.3-10.5 (48.3-15.3)	Dewar ullage pressurant; flowmeter removed to reduce flow impedance.
25	M (4)	He	3	64-39 (115-70)	33.1-9.4 (48.0-13.7)	Pressurant flowmeter removed.
26	M (4)	He	2	119-108 (215-195)	>37-9.4 (>53-13.6)	Pressurant flowmeter removed.
27	M (5)	He	2	133-106 (240-190)	37+-9.2 (53+-13.3)	Pressurant flowmeter removed.

*Figure in parentheses indicates [illegible] number of expulsions per fill.

**Pressurant Conditioning: 1 - Wa[illegible] Water Bath, 2 - LN_2 Bath, 3 - LN_2 + LH_2 Baths, 4 - Pressurant Gas from Dewar Ullage

Table 5.4 Plus One-G Test Matrix

Test No.	Single/ Multiple Expulsion*	Press-urant	Pressurant Conditioning (**)	Pressurant Temperature Range K (R)	Tank Pressure Range N/cm^2 (psia)	Comments
+G-1	M(4)	H_2	1	(No Temp Data)	28.0-12.4 (40.6-18.0)	All External Pressurant Lines Increased to 1.27 cm (.5 in.) OD for +G Tests
+G-2	M(4)	He	1	283-282 (509-507)	21.4-14.0 (31.0-20.3)	
+G-3	M(4)	He	1	284-281 (511-505)	35.3-14.1 (51.2-20.4)	
+G-4	M(4)	H_2	1	294-284 (529-511)	36.3-19.8 (52.6-28.7)	

*Figure in parentheses indicates the number of expulsions per fill.
**Pressurant Conditioning: 1 - Warm Water Bath.

be gas-filled. On all but four occasions the outflow manifold refilled with liquid when the outflow valve opened and with some qualifications, remained liquid-filled until the outflow terminated. On a number of the runs, a start transient effect was noted. On these runs subsequent to the opening of the outflow valve, the outflow sensor would indicate some two-phase flow. The actual quantity of gas is not large. The gas indications appear as sharp spikes with a time duration typically on the order of a tenth of a second on the data tape. Figure 5.8 shows some representative traces for the outflow manifold liquid/gas sensor. The top trace is typical of the expulsion which exhibits the small amount of gas flow in the outflow manifold on startup.

A typical trace for an expulsion to tank depletion is depicted in the middle of Figure 5.8. This trace would occur following the uncovering of the liquid/gas sensor at the 1% level. Here, note that larger and larger amounts of gas are indicated until finally the sensor is completely dry.

Shown at the bottom of Figure 5.8 is a trace which typifies the four cases where the outflow manifold could not be refilled with liquid. The cases where this occurred were all with hydrogen pressurant gas; two at an inlet temperature of 300 K (540 R) (tests 11 and 12), and one at about 217 K (390 R) (test 4), and one at about 100 K (180 R) (test 17). This inability to refill the outflow manifold was not actually repeatable. Three multiple expulsions were performed with about 300 K (540 R) pressurant and two at an inlet temperature of about 217 K (390 R). Of these five multiple expulsion tests, only on three occasions did screen dryout occur to the degree that the outflow manifold could not be refilled. In all cases where this occurred, the liquid level

was approximately 20% or less. A screen dryout summary is shown in Table 5.5. The cases in which dryout occurred are listed along with otherwise similar cases where dryout did not occur. Also tabulated are the length of the pressurization and vent periods between outflows. It should be noted that the breakdown generally occurred following the longer times. At the beginning of the second expulsion under test 12 the screens appeared to be very close to being in a dried-out condition. Two-phase flow persisted for twelve seconds before the outflow manifold filled with liquid.

The dryout phenomena never occurred with helium pressurant. The longest pressurized hold period with warm helium pressurant was prior to the second expulsion on test 16. The pressurant temperature was about 295 K (530 R). On startup there was a light indication of gas in the outflow manifold.

For summary purposes, gas indication at OMLS subsequent to the start of outflow was tabulated in three categories, as shown in Table 5.6. These were Light, Medium and Heavy, represented by 1 to 4, 5 to 9, and 10 or more gas indications or "shifts" (see Figure 5.8) of the sensor output, respectively. The tabulation shows that for hydrogen, this gas indication had a slightly higher incidence of occurrence and tended toward heavier indications than for helium.

As was noted previously, the pressurization line was originally incorporated as a pressure sensing line and was inadequate to maintain a steady pressure within the tank during outflow. As a result, the tank pressure, in many cases, dropped to the saturation line with subsequent boiling within the tank. The start transients noted above may simply be the result of boiling within the outflow channels as opposed to gas ingestion across the screens. Both would result in a similar response at the outflow manifold

Table 5.5: Screen Dryout Summary

Hydrogen Pressurant

Test No.	Press. Temp. K(R)	Pressure psia	Liquid Level[1]	Vent Between Outflows	Length of Vents min:sec	Press Period Min:sec	Dryout
10-1	300 (540)	35.0/31.2	2		----	:45[2]	No
10-2		47.4/13.4	3	No	----	1:05[2]	No
11-1	295 (532)	34.6/27.1	2			1:15	No
11-2	300 (540)	33.3/22.9	3	No		:35	No
11-3	304 (548)	50.0/	4	Bulk Only	3:00	3:05	Yes
12-1	304 (547)	29.8/24.8	2			:30	No[4]
12-2	310 (558)	28.3/18.4	2	Bulk Only	1:40	:45	No
12-3	311 (560)	27.2/	3	Bulk Only	2:00	:30	Yes
4-1	217 (390)[3]	33.2/24.0	1			:30	No
4-2		27.8/20.3	2	Bulk Only	2:30	:30	No
4-3		25.3/13.7	3	Bulk Only	6:00	1:00	Yes
5-1	215 (386)[3]	33.6/21.8	1	Bulk Only			No
5-2		29.6/21.8	2	Bulk Only	1:27	1:10	No
5-3		28.0/21.5	3	Bulk Only	1:05[2]	1:00	No
5-4		27.2/17.6	4	Bulk Only	1:18[2]	1:00	No
17-1	95.5(172)	49.4/31.3	3	No		1:45[2]	No
17-2	99.0(178)	45.3/36.6	3	No		1:46[2]	No
17-3	96.7(174)	48.8/24.7	4	No		1:1[2]	No
17-4	106 (191)	49.7/13.4	4	No		2:16[2]	Yes

(1) 1 - 80 to 90%, 2 - 50 to 80%, 3 - 20 to 50%, 4 - 1 to 20%

(2) Total time between expulsions

(3) Averaged

(4) Extensive gas indication on startup lasts for 12 seconds before outflow manifold filled.

Table 5.6: Start Transient Data Summary

Temperature K (R)	Pressurant	Liquid Level*	Total Runs	Observations of Start Transient Gas Indication		
				Light	Moderate	Heavy
300 (540)	He	1	2	1		
		2	2			
		3	2	1	1	
		4	3	1		
300 (540)	H_2	1	1			
		2	5	4		1
		3	3	1	1	
		4	1			
217 (390)	H_2	1	4	2		
		2	2	1	1	
		3	2		1	
211 (380)	He	1	1	1		
		3	2		2	
		4	1			1
172 (310)	He	1	1		1	
117 (210)	He	1	1			
		2	3	1		
		3	1			
		4	2			
97 (175)	H_2	3	2	1		1
		4	3			
89 (160)	H_2	2	1			1
78 (140)	He	3	1	1		
67 (120)	He	2	1			
		3	1			
		4	2	1		
56 (100)	He	2	1			
47 (85)	He	2	2	1		
		3	1			
		4	1			
33 (60)	H_2	1	2		2	
		2	4			
		3	2			
Totals			63	18	9	4
	H_2		32	9	5	3
	He		31	9	4	1

*1: 80-99%
2: 50-80%
3: 20-50%
4: 0-20%

liquid sensor. Some pressure histories are shown in Figures 5.9, 5.10, and 5.11. On each figure are shown cases which exhibited large amounts of gas on startup as well as cases which exhibited none. Also shown in several cases is the saturation pressure corresponding to the liquid temperature sensor closest to the interface. Note, for instance, that for the single expulsion of test 18, Figure 5.9, for which there was a heavy gas indication, that the tank pressure was initially at saturation and fell immediately below saturation. Note further that on the third expulsion of test 17 (same figure), a case for which there was no initial gas indication, that the pressure is initially well above the saturation line. The initial pressure for the first expulsion on test 17, which had a heavy gas indication subsequent to the outflow valve opening, was much closer to saturation than for the third expulsion. This same pattern is repeated in Figure 5.10 where the heavy gas indication on startup occurs when the initial pressure is close to saturation and a light indication occurs where there is greater subcooling. Two pressure traces are shown in Figure 5.11 for expulsion with helium pressurant gas. One of these runs (test 2, fourth expulsion) which exhibited a heavy gas indication on startup, has a much lesser slope in the pressure-time curve than does the other pressure-time history plotted (test 6, third expulsion) which exhibited only a light gas indication on startup. The implication here is that the smaller pressure decay rate is indicative of gas generation resulting from boiling.

Generally, during the expulsions, the liquid sensors in the bulk region, particularly those at the 20 and 50% levels, indicated a two-phase mixture. This would tend to substantiate the conclusion drawn from the pressure traces that boiling should be occurring. The screen channels are apparently functioning

here as bubble strainers since the outflow sensor has only rarely indicated gas during the outflow.

As mentioned above, dryout of the outflow manifold generally occurred within a few seconds of outflow termination. With very cold hydrogen pressurant (tests 22 and 24), the outflow manifold did not dry out for an appreciable time following outflow termination. Following the first outflow on test 22, the manifold liquid sensor indicated liquid for about 37 seconds. Liquid was indicated in the manifold for the entire time between the second and third outflows; about 97 seconds. Similar results were obtained on test 24. On one occasion the outflow manifold refilled with liquid prior to opening the outflow valve. This occurred on test 21 when helium pressurant gas at a temperature of about 56 K (100 R) was introduced. The liquid level was between 50 and 80%.

It is interesting to speculate as to the mechanism which causes the immediate dryout of the outflow manifold following introduction of the warm pressurant gas, but not following the cold pressurant. Inasmuch as the warm pressurant is directed onto the top manifold coverplate (see Figure 5.1), it is quite possible that during the outflow period this plate is heated significantly above the saturation temperature thus forming a vapor layer on the inside surface which is not detected by the liquid sensor. This vapor layer is held aginst the wall by the momentum of the outflow. When the outflow is terminated, the vapor blanket is free to move in and envelop the liquid sensor. Also, the tank wall in the outlet region is likely to have been heated well above saturation. On outflow termination this enthalpy excess in the manifold coverplate and tank wall (relative to the saturation temperature) is immediately absorbed by vaporization of the propellant in the outflow manifold.

a. Temperatures - Some representative temperatures from selected runs are plotted in Figures 5.12 to 5.18. The cyclic nature of the temperature profiles is evident for the multiple outflow tests. The decay of the liquid temperature which is particularly evident in the single expulsions is suggestive of boiling and pressure decay within the tank.

2. Plus One-G Tests

Temperature histories for several selected sensors are shown in Figures 5.19 through 5.22. The interesting feature that was repeated in all of the plus-G runs was the immediate temperature rise of the temperature sensor in the stagnant end of the outflow channels (top of outflow channel for the plus-G orientation). It was not possible in these tests to maintain the flow channels full of liquid prior to, or during the fill; however the level sensor located in the top of the channels would indicate liquid subsequent to the attainment of a liquid level of about eighty percent in the bulk region. As soon as the fill was terminated the sensor would again indicate gas. Inasmuch as the channels had been full, or close to full, during the fill, the screens may have been wicked at the beginning of the initial pressurization. In any event, the channels are dry at their upper end very shortly after the introduction of pressurant gas, which is verified by the response of the channel top temperature sensor. (See Figures 5.19 to 5.22.) Further evidence that the screens are dry is provided by the channel midpoint temperature sensor. The indication here is that the liquid levels are equal in the bulk region and outflow channels. The channel temperature sensor for tests +G-1, -2, and -4 responds simultaneously with the uncovering of the 50% level. This is contrasted to the minus-G tests where the channels were full and the channel midpoint temperature sensor

always indicated liquid temperature prior to tank depletion. In the helium pressurant test +G-3, the channel midpoint temperature sensor does not show a response as the 50% bulk level sensor is uncovered--but, neither does the similarly situated sensor in the bulk region. Both of these sensors did respond with the 50% level sensor in the other plus-G helium pressurant test, +G-2. In addition, the response of the upper annulus temperature sensor in these two tests is considerably different. In test +G-2 the upper annulus temperature reaches 30 K (54 R) in 13 seconds, whereas in +G-3, 97 seconds are required. Several differences between the two tests can be enumerated. The initial liquid level was above 50% for +G-2 and below 50% for +G-3. The liquid temperature was somewhat higher and there appears to be significant thermal stratification in +G-2. These differences would tend to produce the conditions observed. However, the pressure for +G-3 was higher than for +G-2, 50 vs 30 psia, which by virtue of a higher heating rate should have enhanced dryout in +G-3 relative to +G-2. From the temperature data it does appear that the channels did dry out in both +G-2 and -3; however, the dryout was almost immediate in +G-2 and somewhat delayed in +G-3. The time at which dryout occurred in +G-3 is not clear since there is a strong evaporative cooling effect associated with the helium pressurization which tends to restrain the temperature rise of the sensor subsequent to its uncovering by the liquid.

The temperature sensors are, however, very accurate indicators of the passing of the liquid level in runs +G-1, -2, and -4. The very sharp drop of the sensor temperatures as the liquid level passes is very evident in Figures 5.19, 5.20 and 5.21. This same effect shows up during the second expulsion of minus-G test 16, Figure 5.16. In spite of the fact that in the minus-G orientation the temperature sensor is physically located slightly below the level sensor, it responds in advance of the

level sensor. The delayed response of the level sensor does not, however, show up in the plus-G runs. The level sensor which is now below the temperature sensor responds generally within two seconds of the temperature sensor.

D. ESTIMATE OF HEAT FLUX TO CAPILLARY SCREENS

An estimate of the heat flux from the pressurant gas to the screen device has been made based on the annular heat transfer models of Reference 5.2. The position of interest is the point of maximum heating which occurs at the screen location nearest to the pressurant inlet. For the minus-G orientation, this point also corresponds to the location of minimum pressure in the outflow channel. Breakdown should, therefore, be anticipated at this location. Referring to Figure 5.1, the screen portion of the channels begins about 10.2-cm (4-in.) from the pressurant inlet. For the plus-G orientation, the stagnant end of the flow channel is adjacent to the pressurant inlet; the screen beginning at about 15.2-cm (6-in.) from the inlet. Again, it is anticipated that dryout, if it occurred, would begin at this location. The heat transfer model used was developed for axial flow in a cylindrical annulus and, therefore, is only approximate for the present case of a spherical annulus. The flow areas used were 177-cm^2 (0.19-ft^2) for the minus-G orientation and 232-cm^2 (0.25-ft^2) for the plus-G case. Measured pressurant flow rates and temperatures were used in the calculations. Minus-G results are shown in Figures 5.24 and 5.25. Note, for example, that for a ΔT of 11 K (20 R) that the estimated heat flux with hydrogen pressurant was on the order of 40 to 65 w/m^2 for pressures in the range of 20.7 to 34.5 N/m^2 (30 to 50 psia), and with the helium pressurant the estimate is on the order of 60 to 80 w/m^2. The calculations for the hydrogen pressurant do not include any mass transfer

which occurs at the interface. With hydrogen, condensation was very likely occurring which represents an additional heat load. Plus-G results were similar. Estimates for the heat flux prior to screen dryout for the plus-G helium pressurant tests ranged from 56 to 72 w/m^2 over the range of test conditions. This was based on a ΔT of 11 K (20 R) (see Figures 5.20 and 5.21). The heat flux estimate for the plus-G hydrogen pressurant test number +G-4 was 71 w/m^2 (pressurant flow data was not available for the other +G hydrogen pressurant test no. +G-1). Again, this does not include any contribution due to condensation, which was very likely occurring.

E. CONCLUSIONS

1. With the proper operating procedures, a capillary screen device with either warm hydrogen or helium pressurant can be utilized to provide gas-free liquid outflow when there are no stagnant liquid regions within the acquisition device. This includes operation in adverse acceleration environments up to one-g Further testing is required to define the operating procedures which would allow operation with stagnant liquid regions.

2. There is less tendency for the device to dry out with warm helium pressurant than with warm hydrogen pressurant.

3. The tendency for the device to dry out increases with increasing pressurant temperature and exposure time to the warm pressurant prior to initiation of outflow.

4. The capillary device functions as a bubble strainer. Gas generated as a result of boiling within the bulk liquid is not ingested into the device. The results obtained indicate that a screened acquisition device may be feasible in a self-pressurized tank.

F. DESIGN CRITERIA

An objective of this program is the development of guidelines which would preclude the ingestion of gas as a result of warm gas pressurization. On the basis the data obtained any such guidelines must be quite tentative. For successful operation, the following should be adhered to:

1. Minimize the pressurization period prior to outflow. This period should not be longer than about one to two minutes.

2. The pressurant gas used for prepressurization should be close to the liquid temperature. Following initiation of outflow, pressurization may be accomplished with warm gas. Temperatures up to 300 K (540 R) for liquid hydrogen pressurization are satisfactory.

3. Prepressurization by bubbling helium pressurant gas through the liquid should be considered if significant thermal stratification is anticipated.

4. If the operation of the device requires that a partial outflow occur when the body forces are such as to cause a stagnant region of the device to be in the ullage area, it must be recognized that this area may ingest gas.

5. For liquid hydrogen service the capillary device should be covered with at least the equivalent of two well spaced layers of 325 x 2300 Dutch-twill screen.

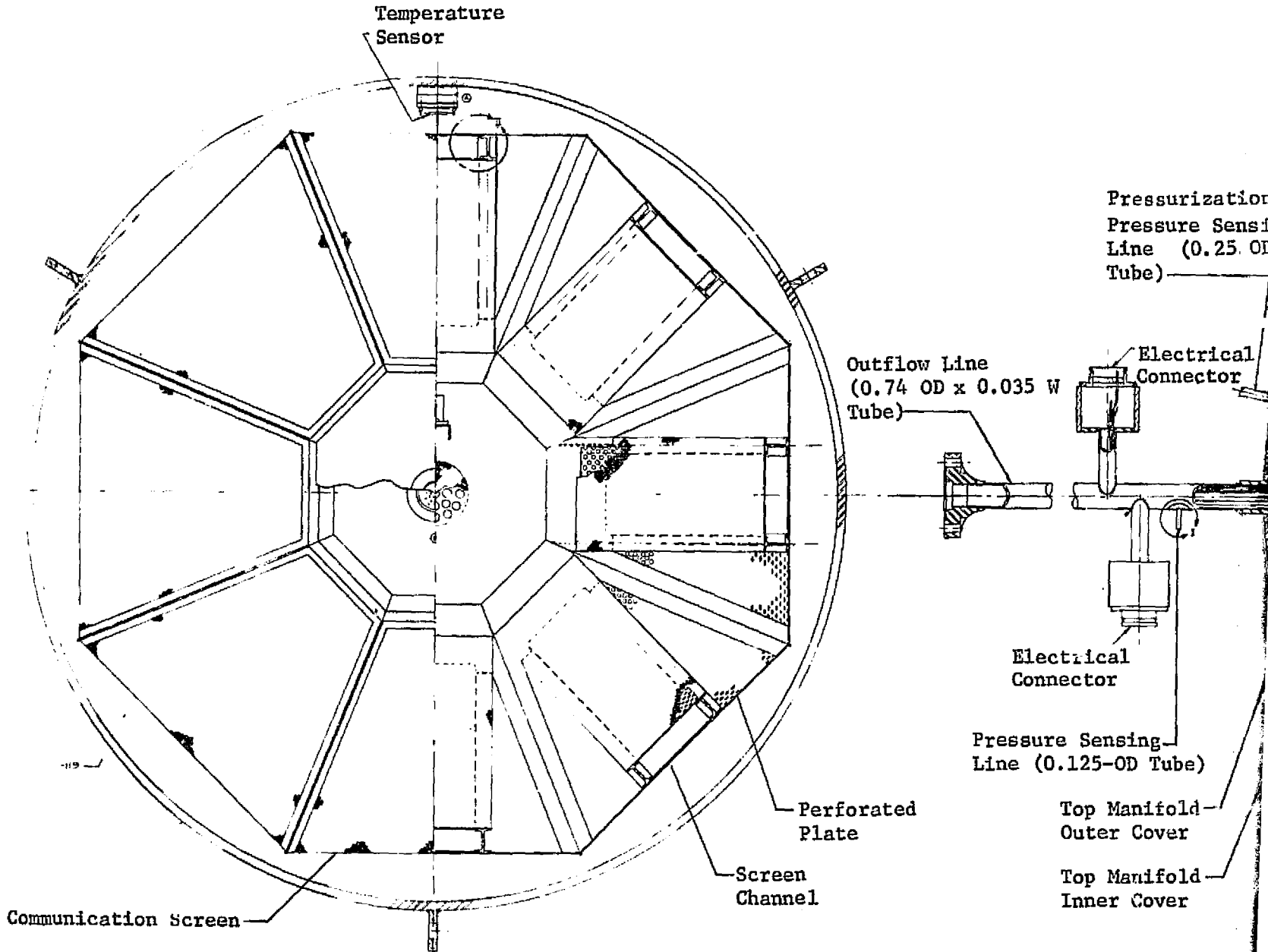

PLAN VIEW

FOLDOUT FRAME

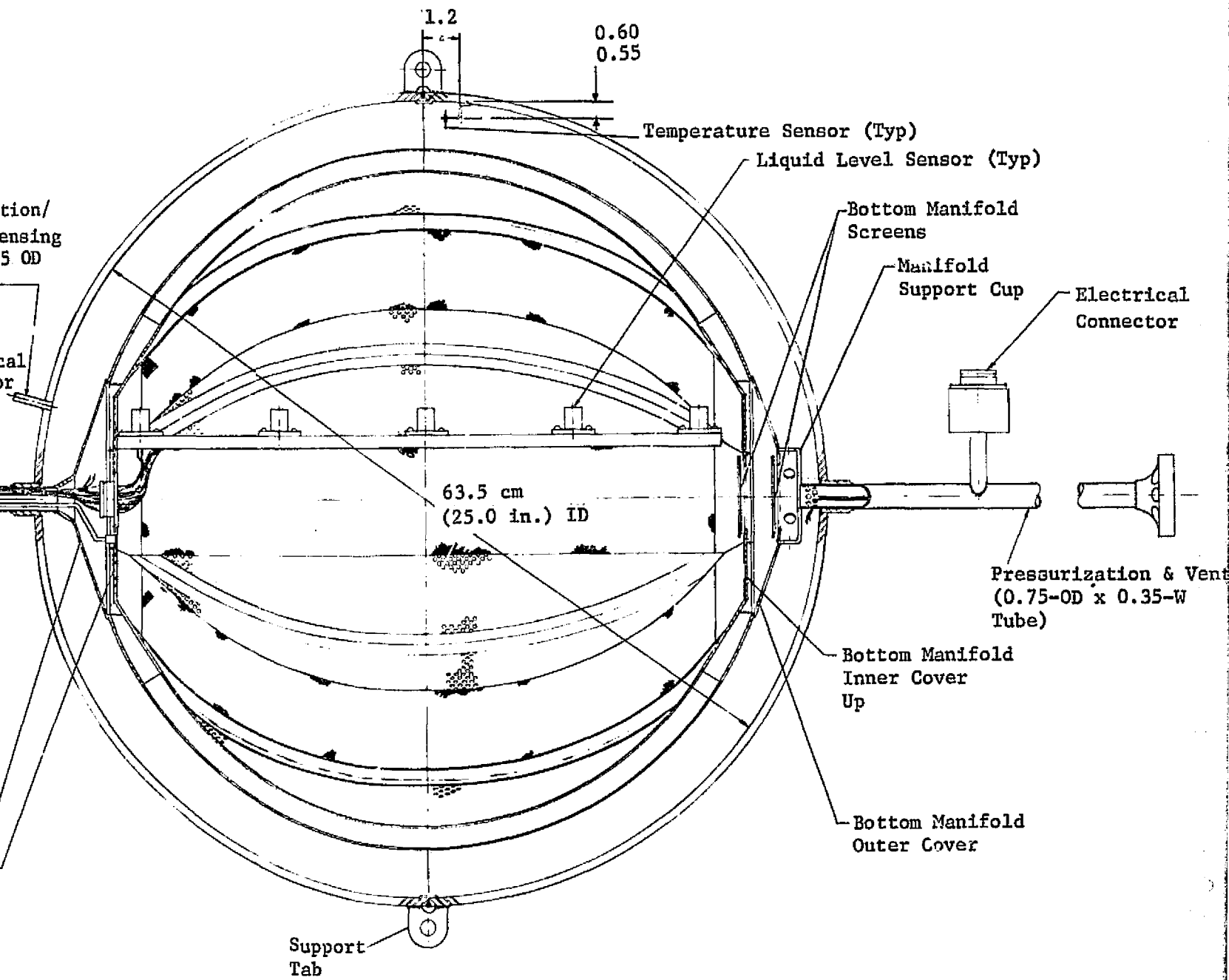

FOLDOUT FRAME

Figure 5.1 Test Article Assembly Drawing

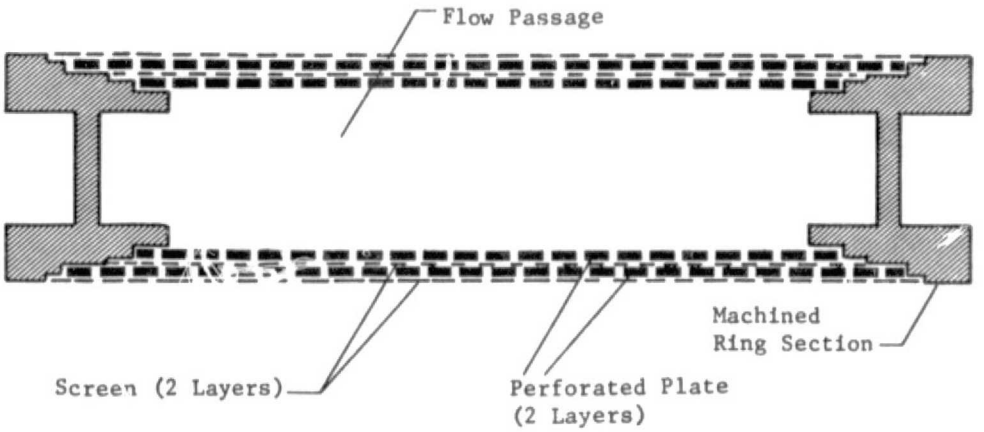

Figure 5.2 Screen Channel Cross Section

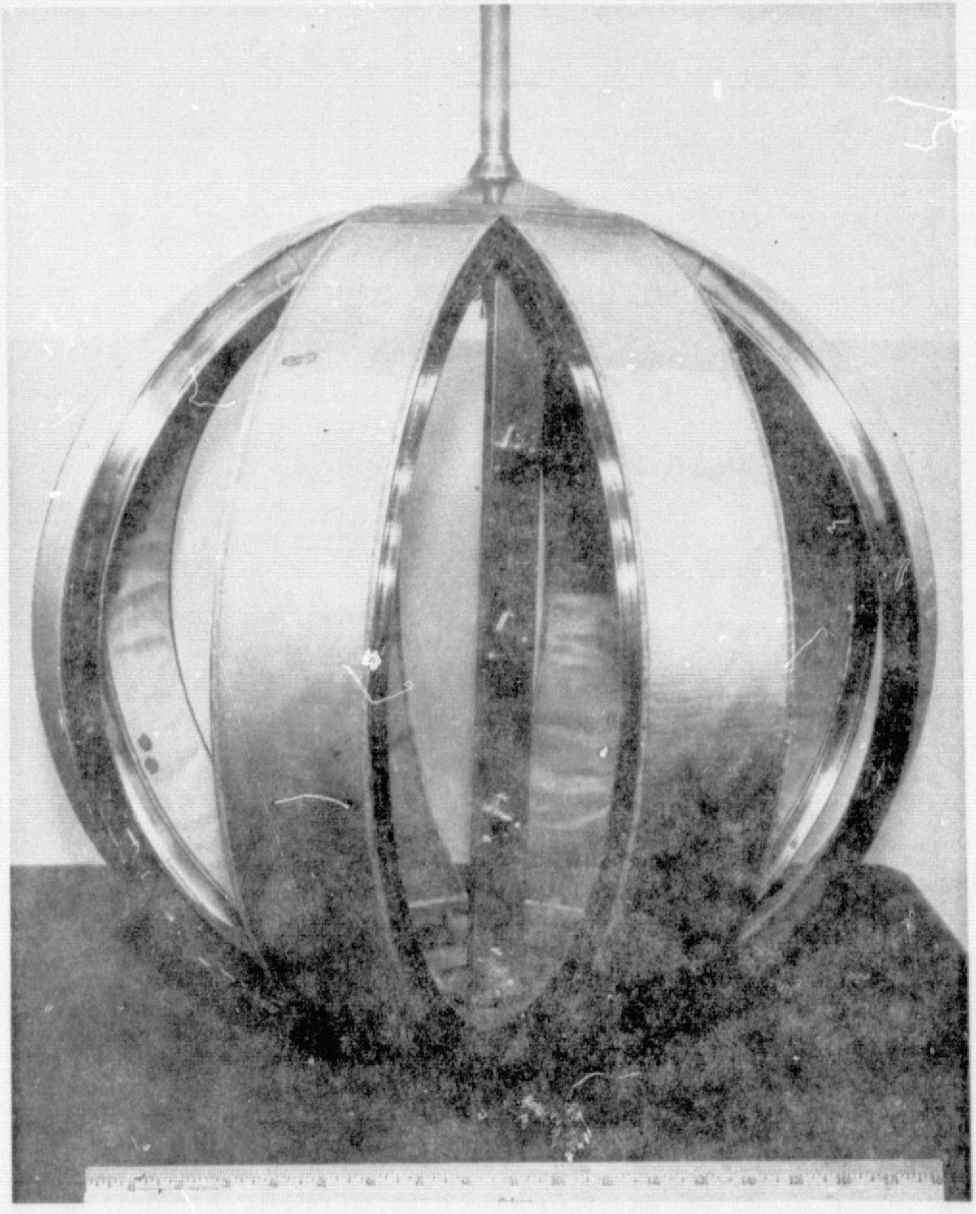

Figure 5.3: Screen Channels and Instrumentation Rate

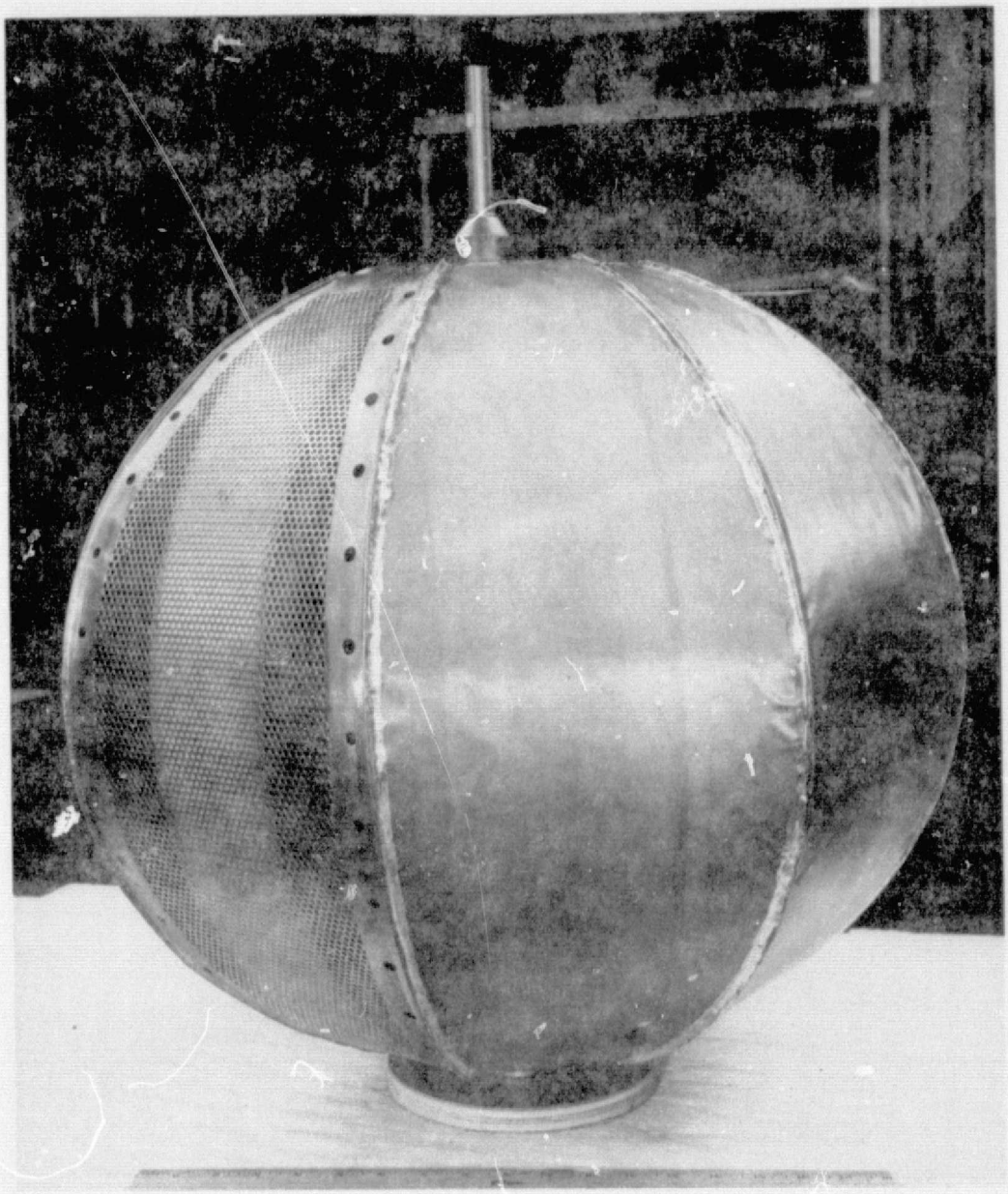

Figure 5.4: Partially Completed Screen Liner Assembly

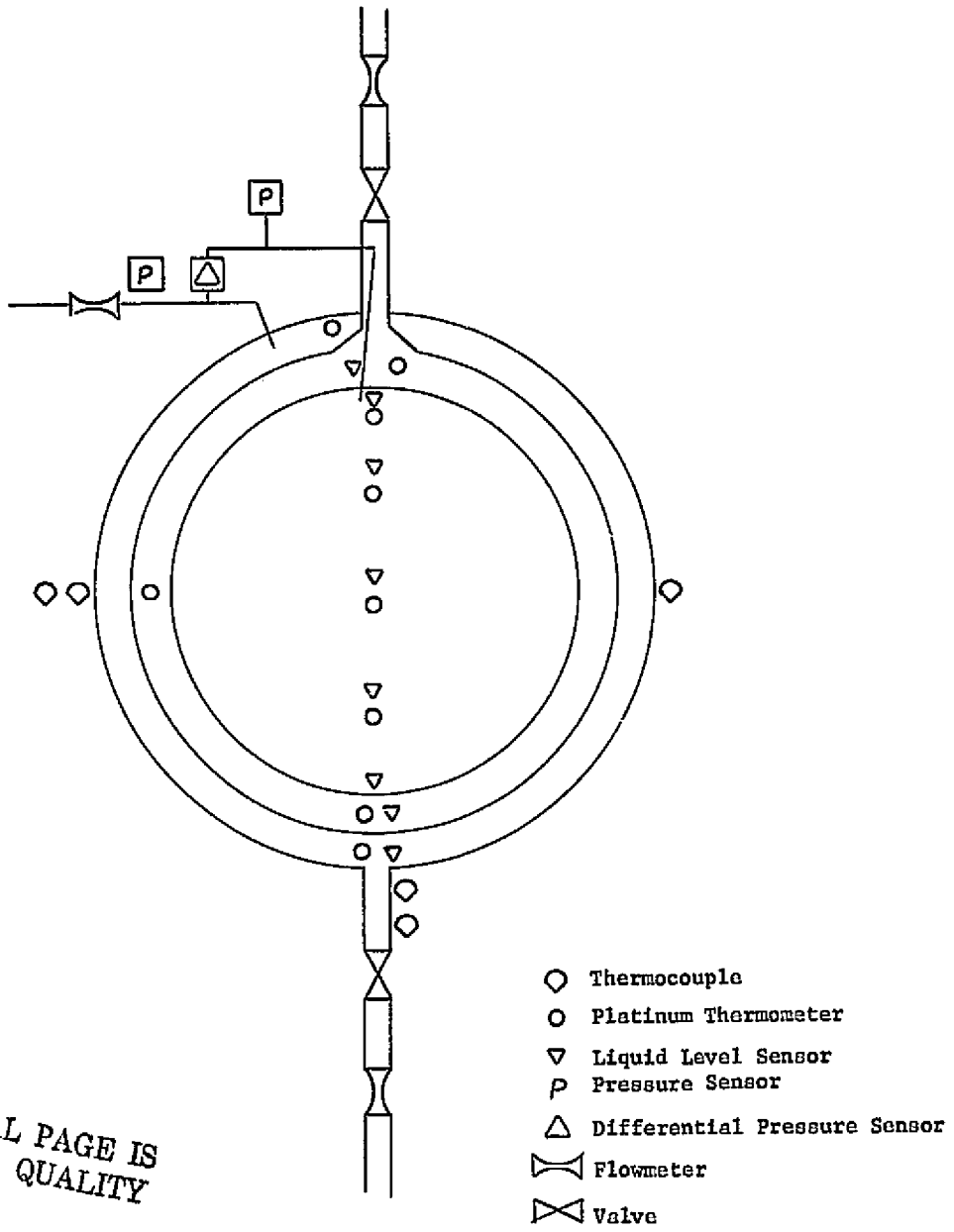

Figure 5.5 Instrumentation Schematic

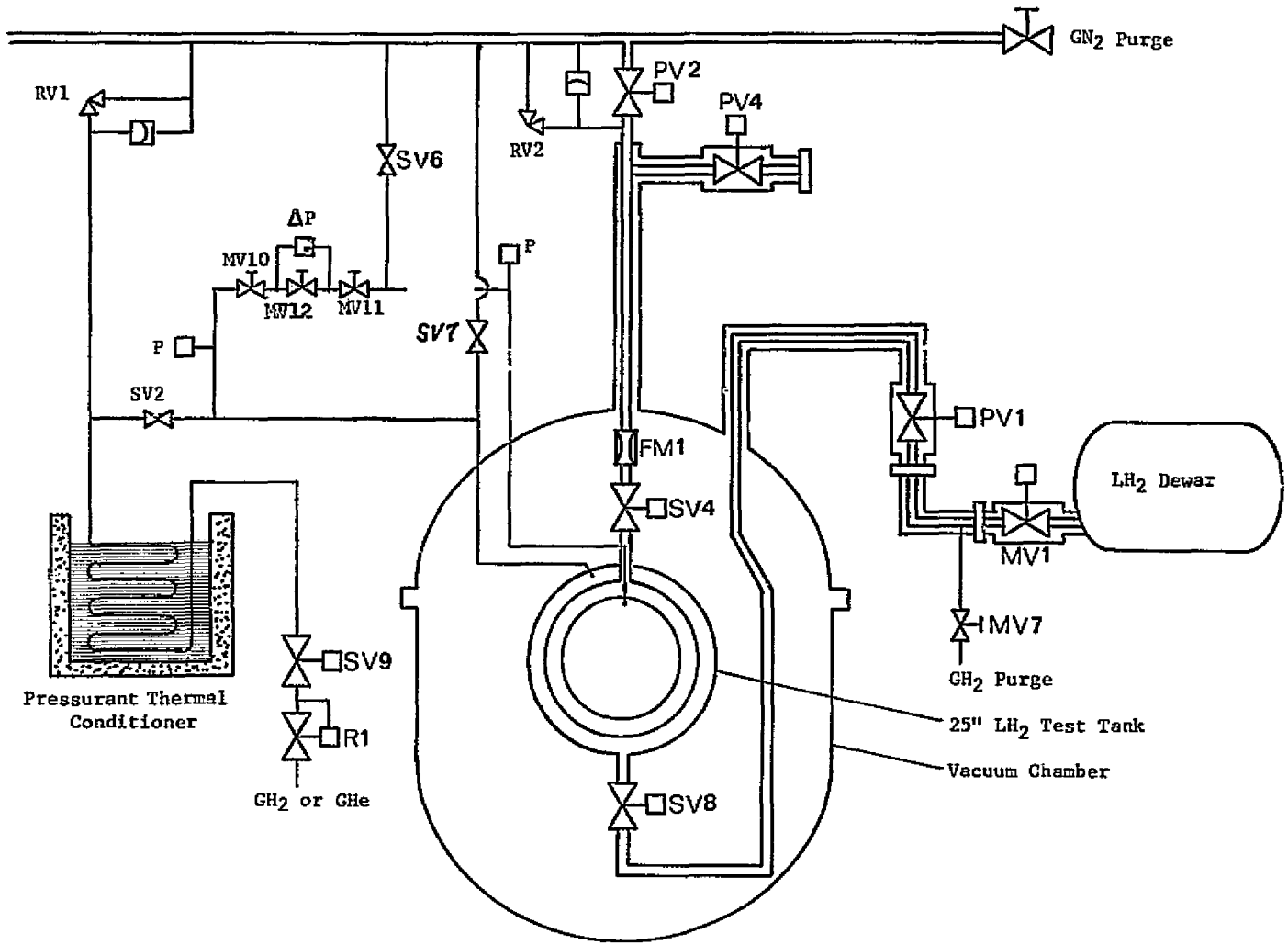

Figure 5.6: Flow Schematic - Minus-Z Attitude

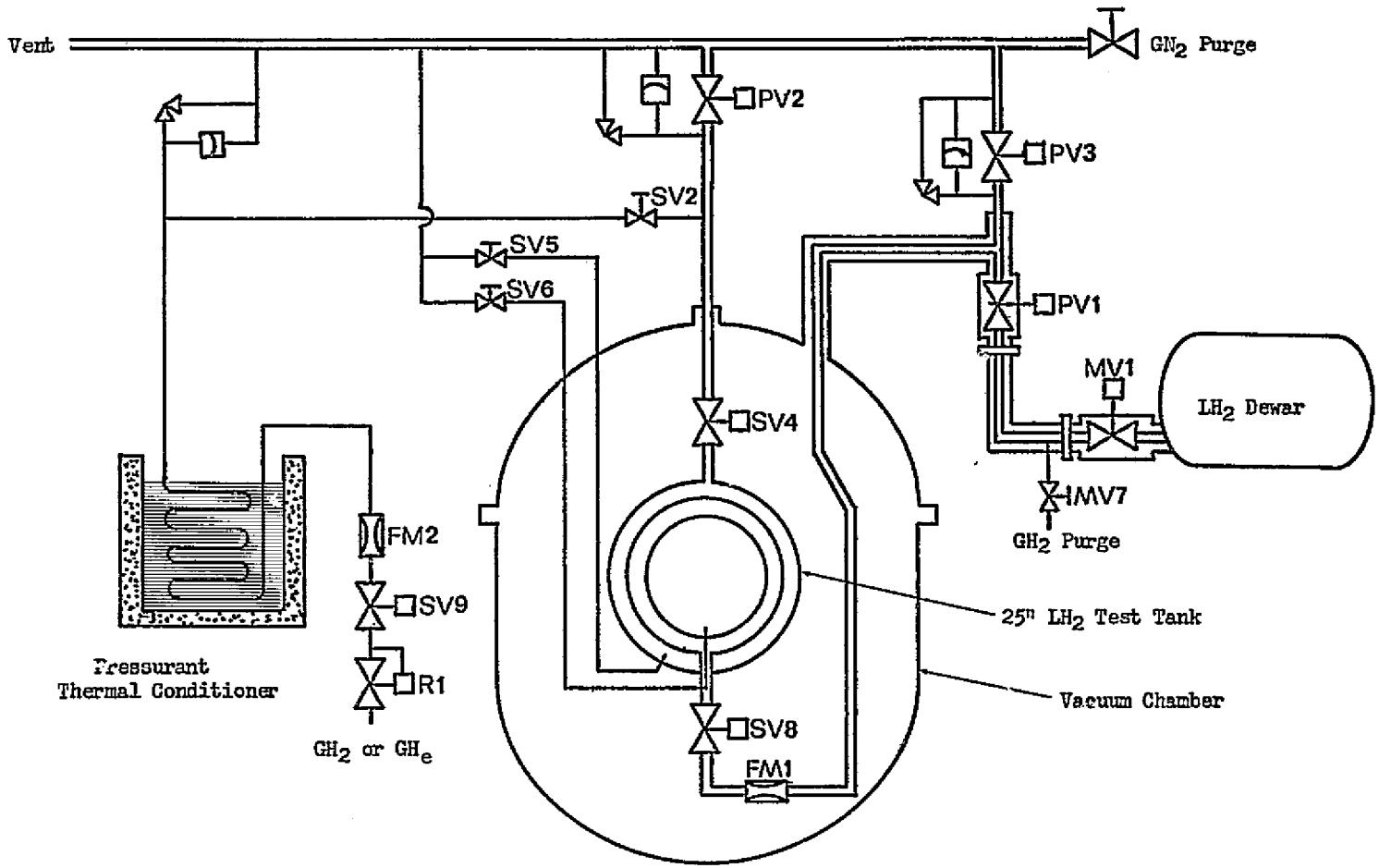

Figure 5.7: Flow Schematic - Plus-G Attitude

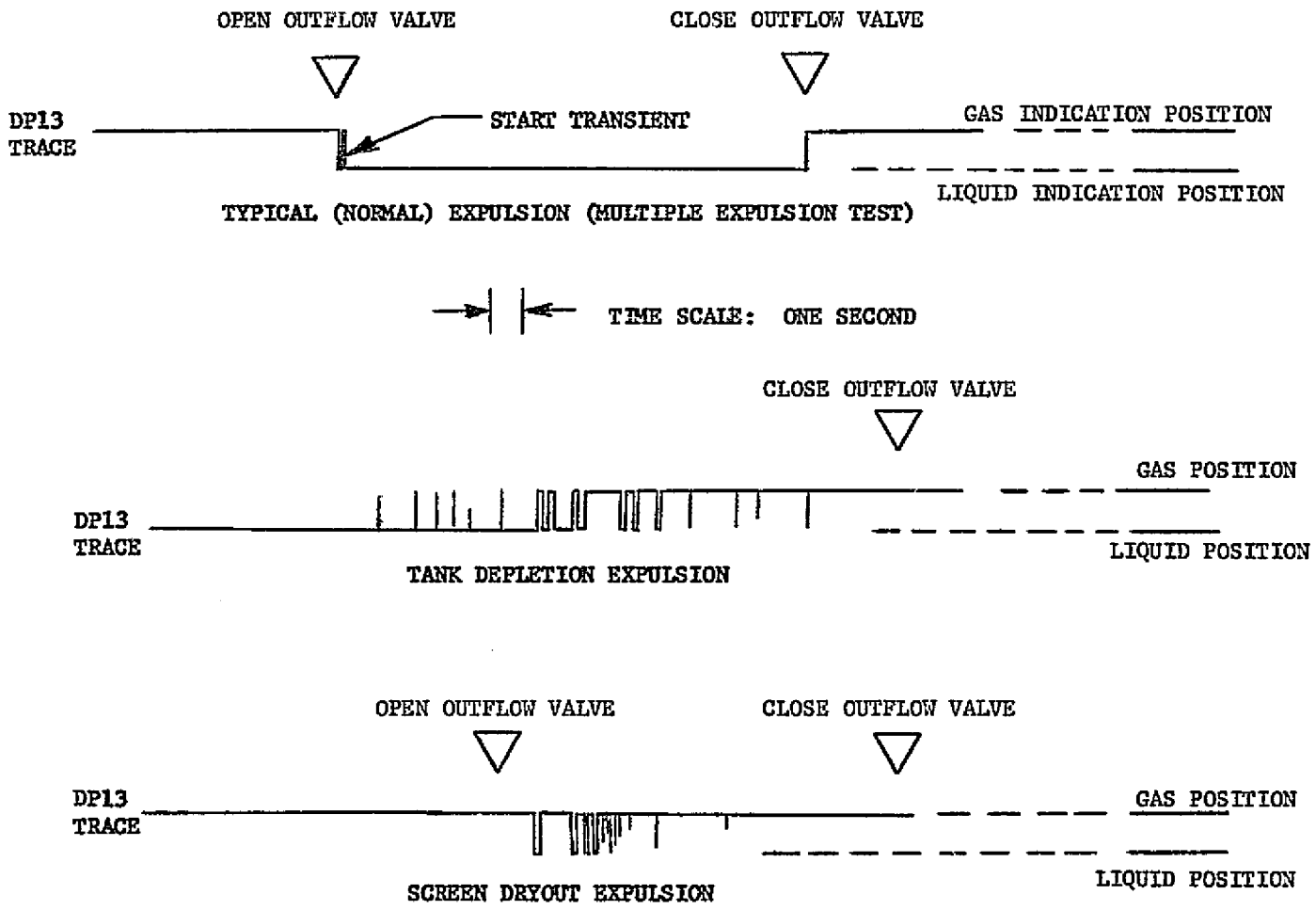

Figure 5.8: Warm Gas Pressurization Test, Typical Outlet Level Sensor Data

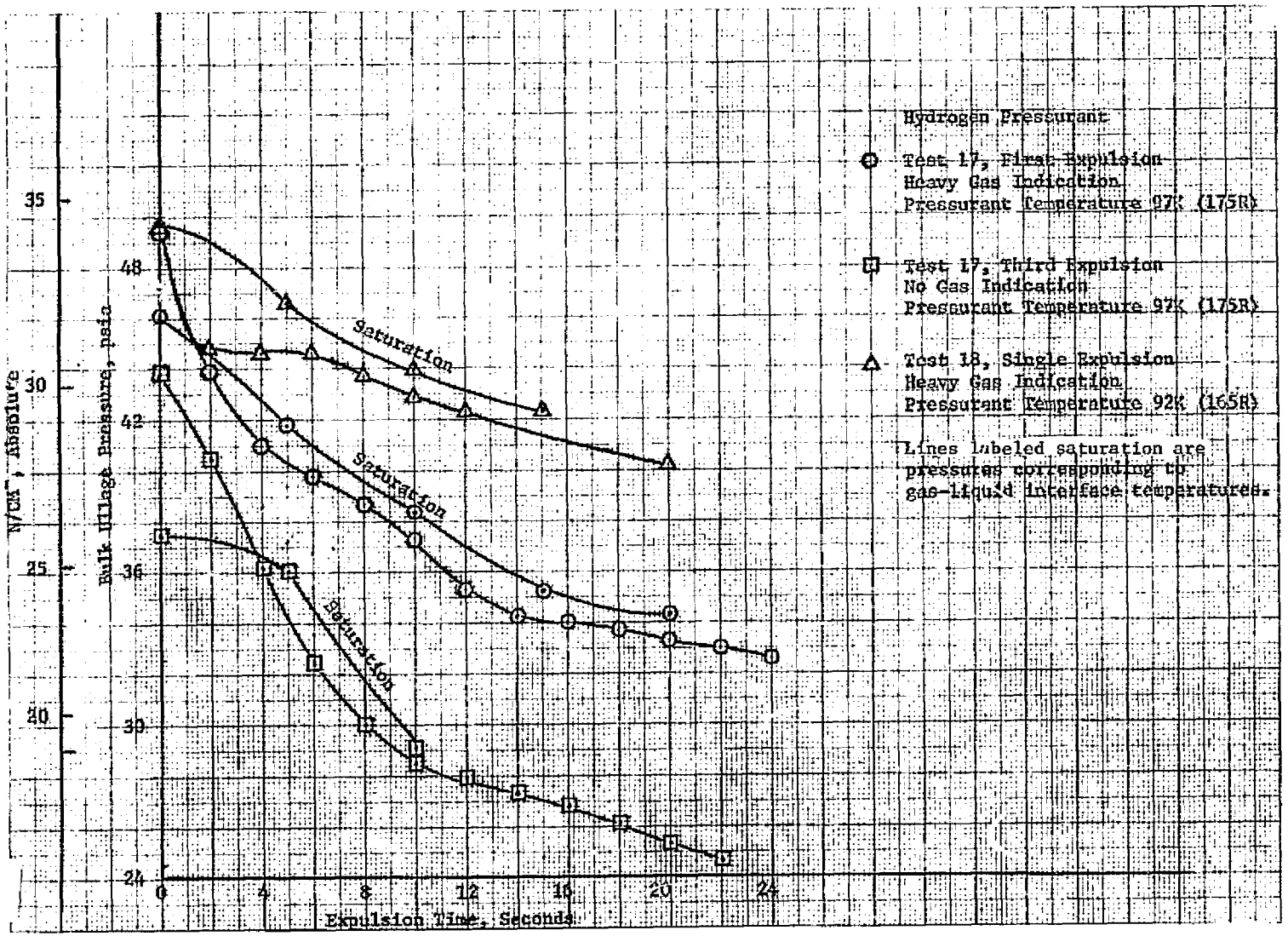

Figure 5.9: Pressure Histories for Several Expulsions with Low Temperature Hydrogen Pressurant

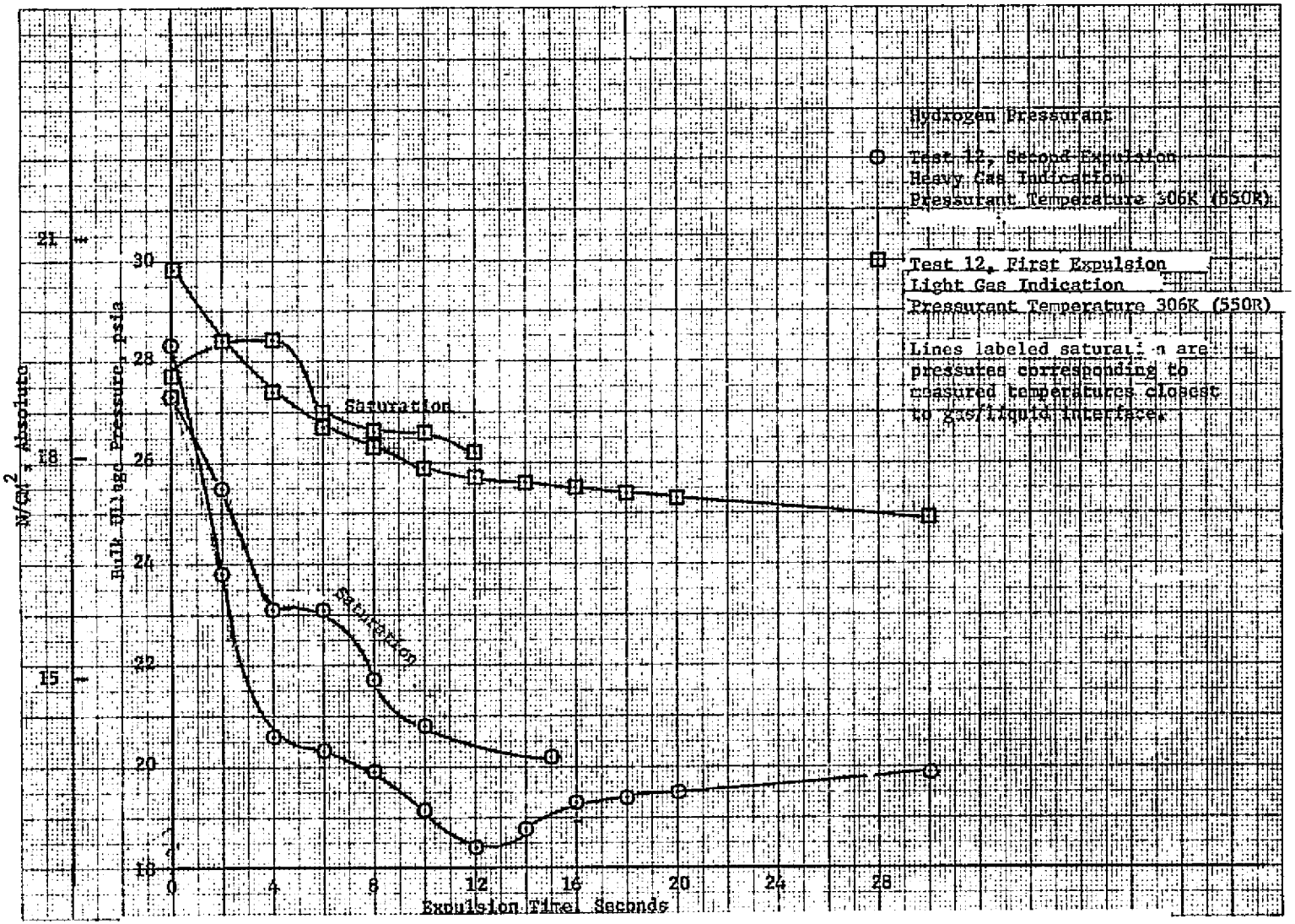

Figure 5.10: Pressure Histories for Two Expulsions with Warm Hydrogen Pressurant

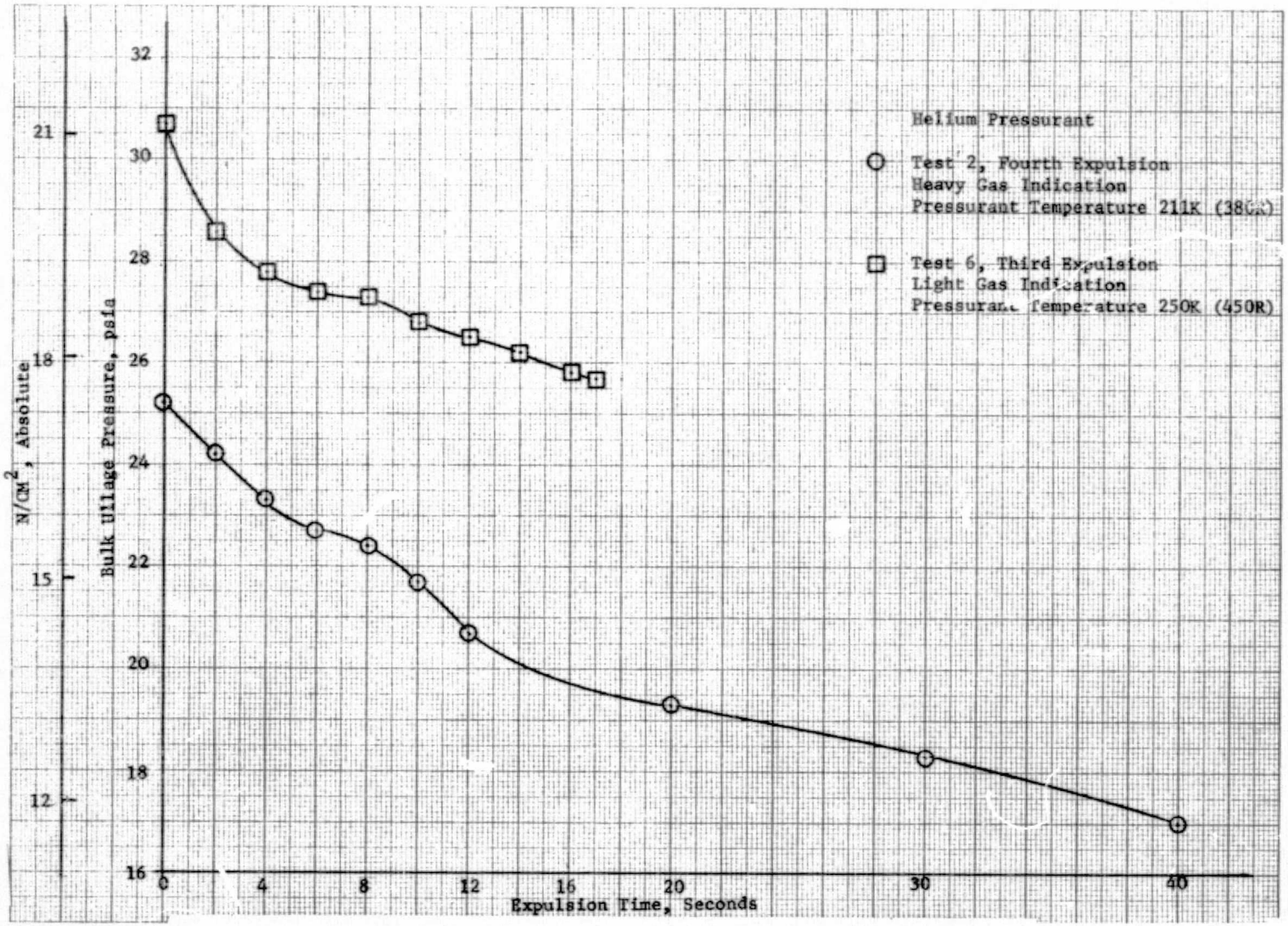

Figure 5.11: Pressure Histories for Two Expulsions with Helium Pressurant

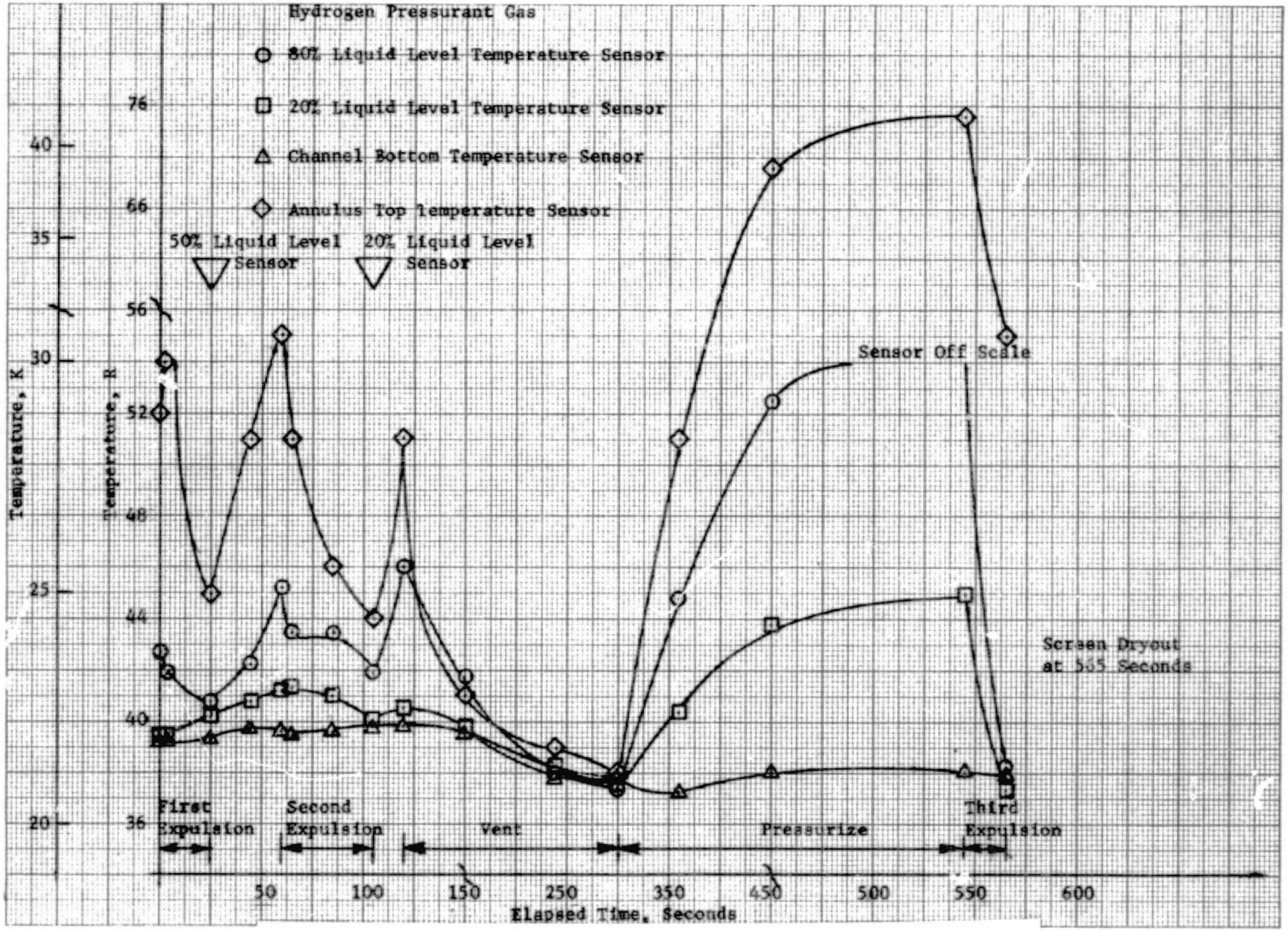

Figure 5.12: Temperature History, Test 11, Multiple Expulsion

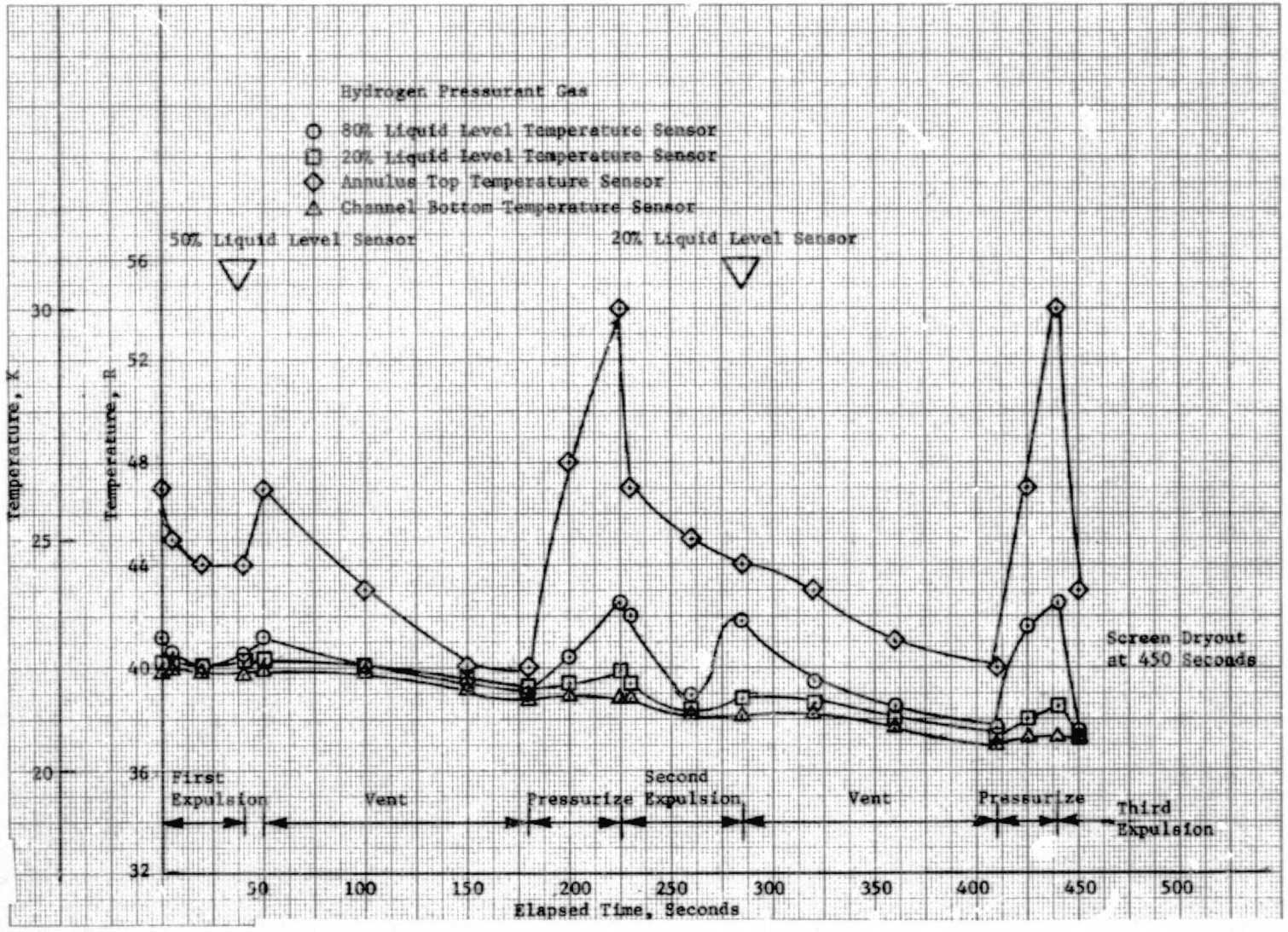

Figure 5.13: Temperature History, Test 12, Multiple Expulsion

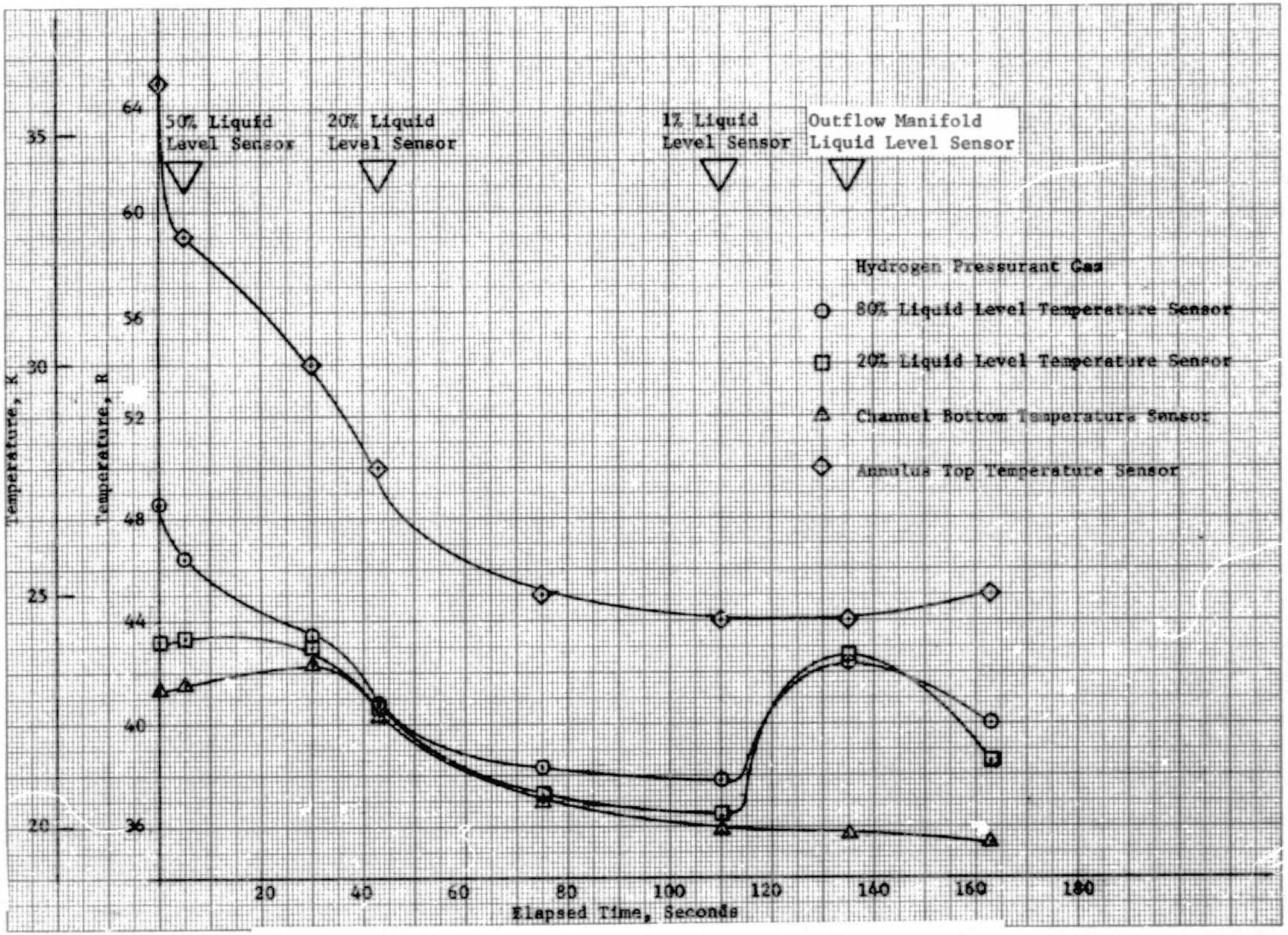

Figure 5.14: Temperature History, Test 13, Single Expulsion

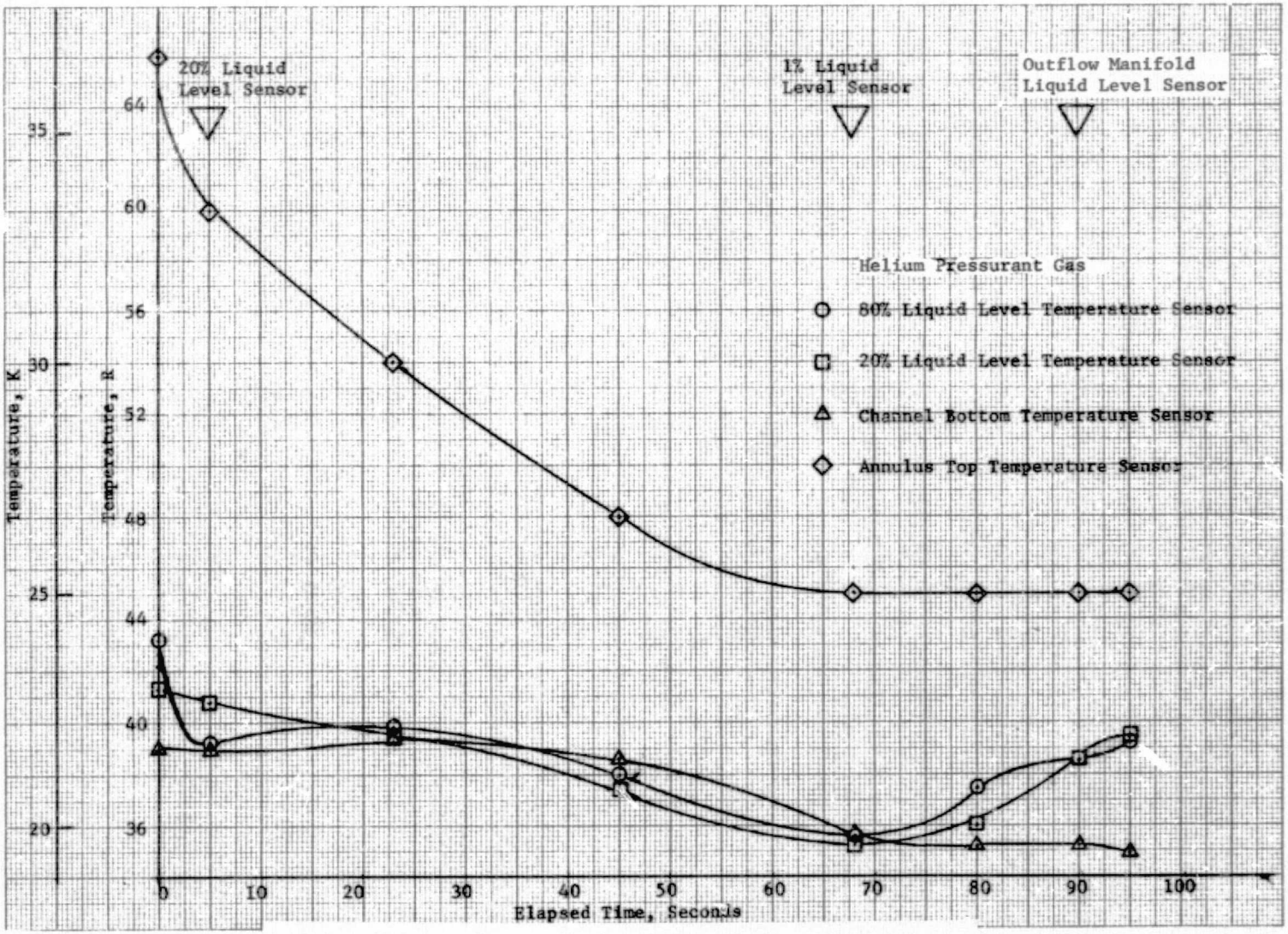

Figure 5.15: Temperature History, Test 14, Single Expulsion

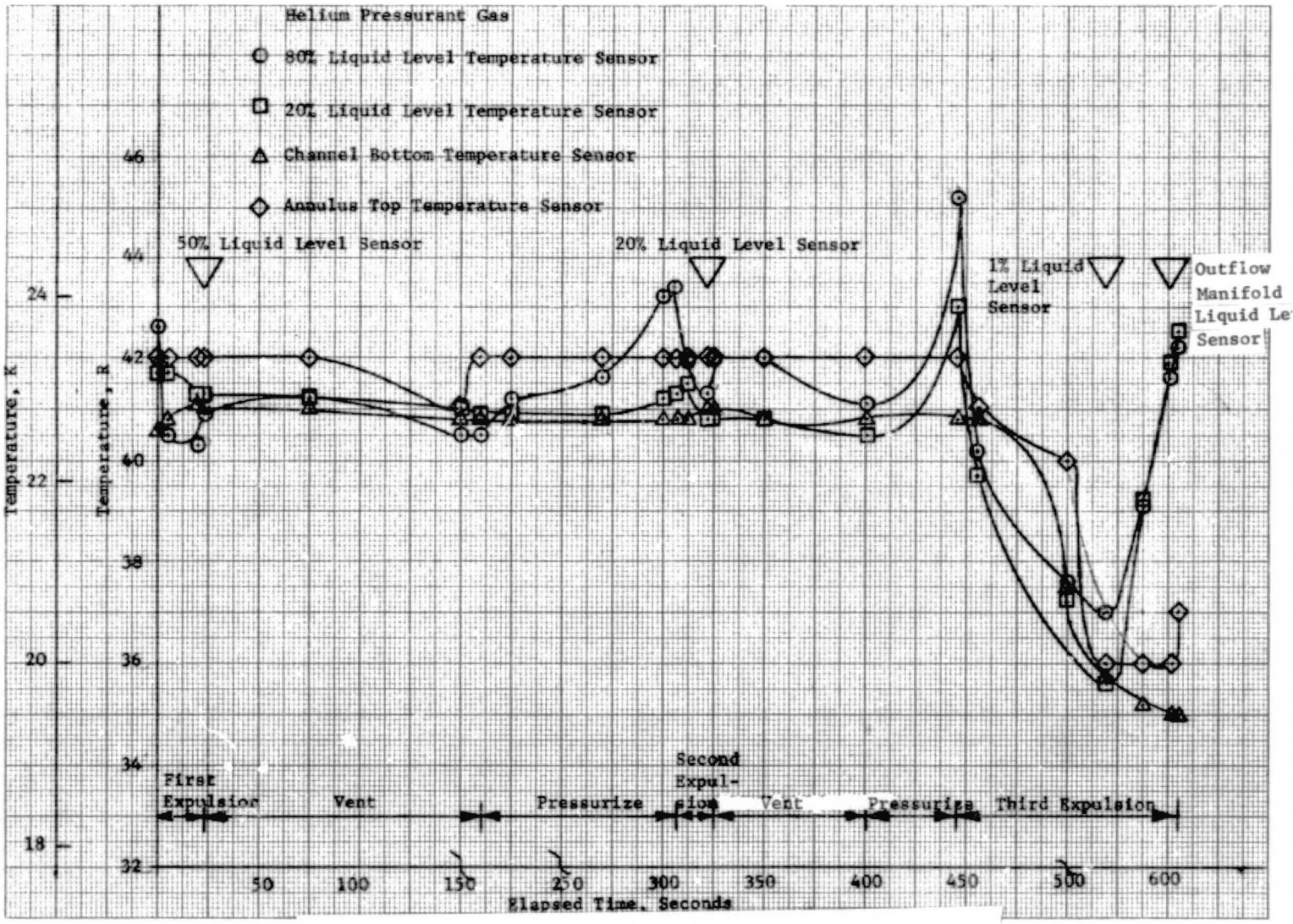

Figure 5.16: Temperature History, Test 16, Multiple Expulsion

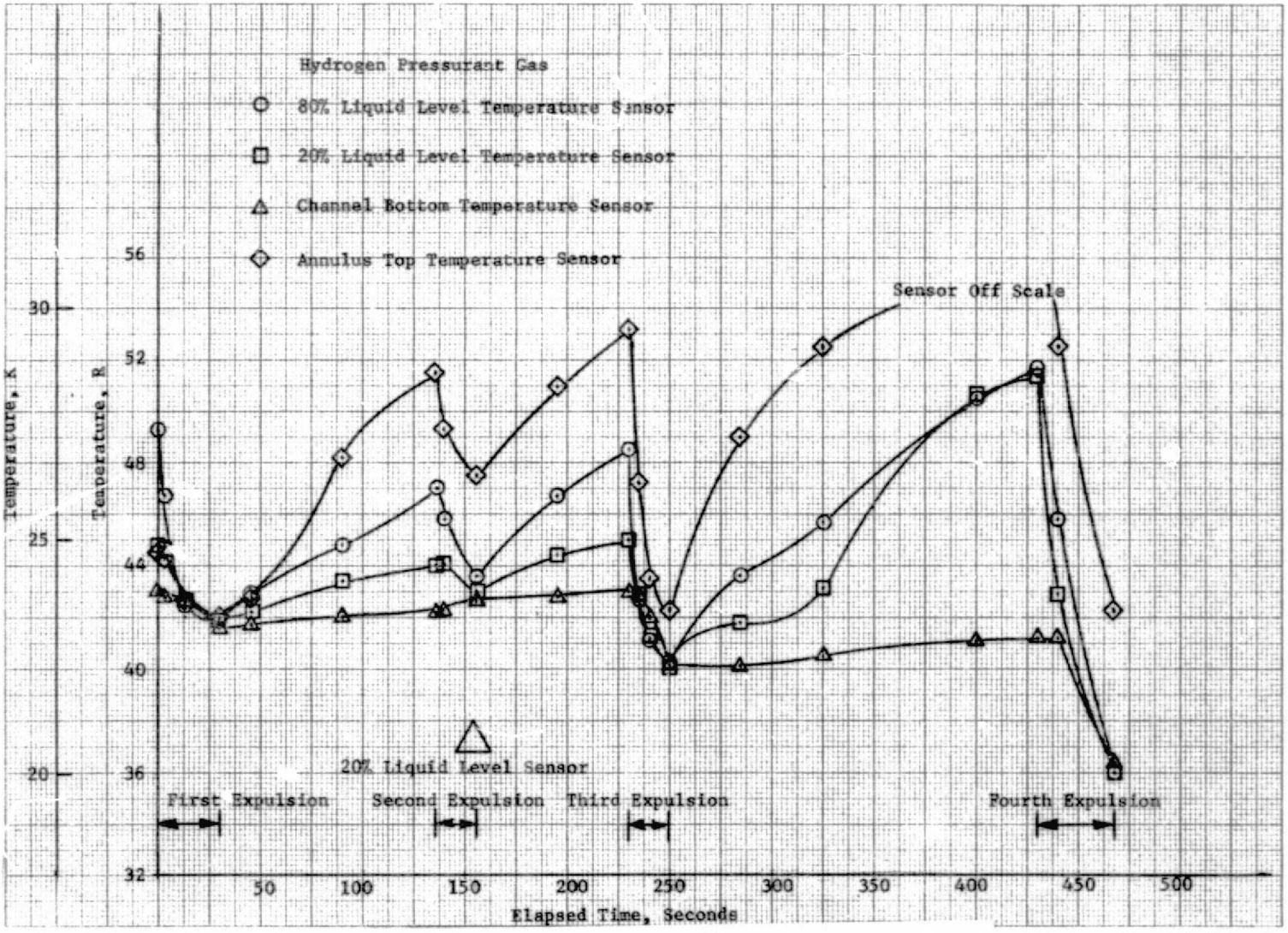

Figure 5.17 Temperature History, Test 17, Multiple Expulsion

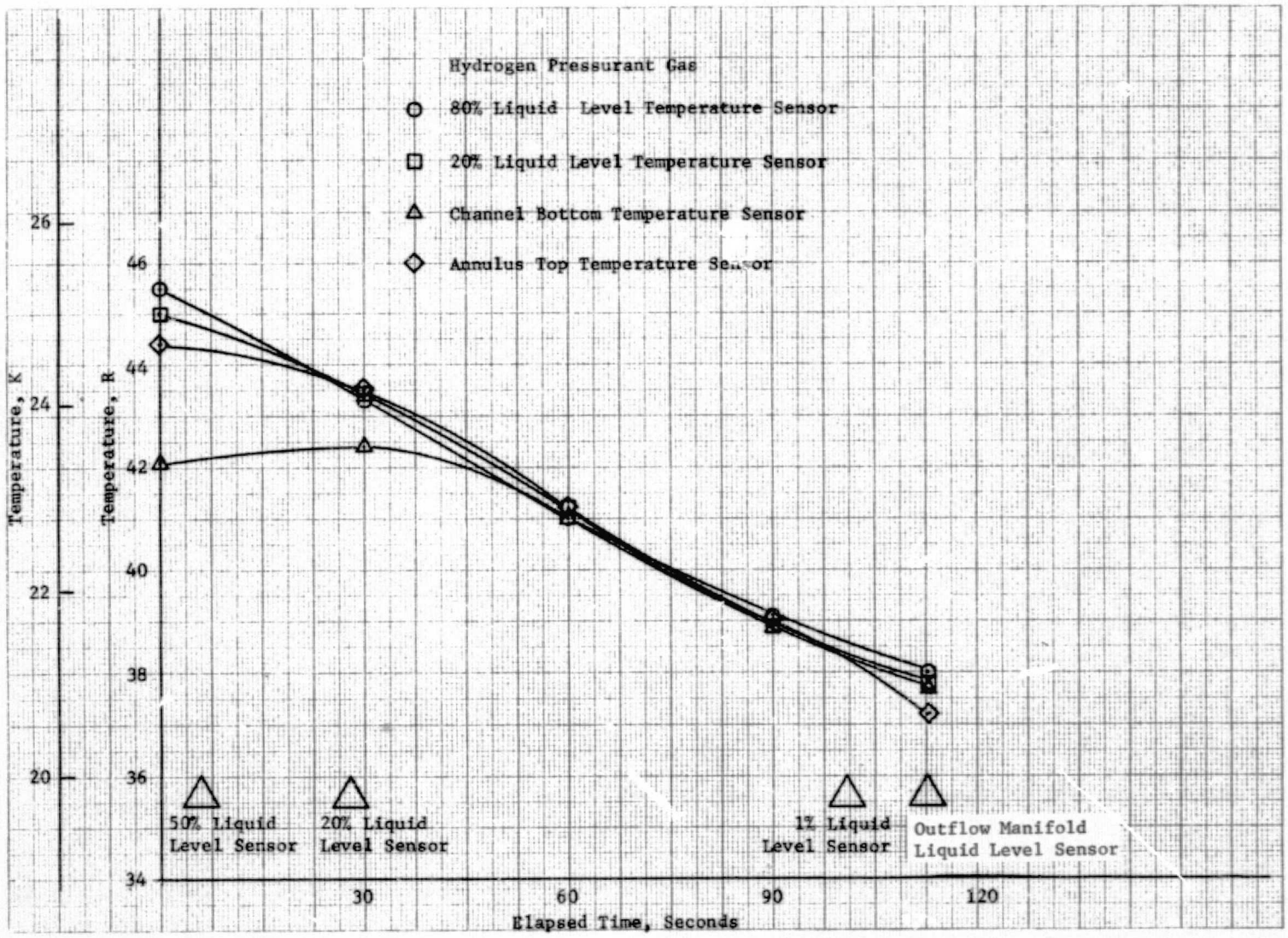

Figure 5.18: Temperature History, Test 18, Single Expulsion

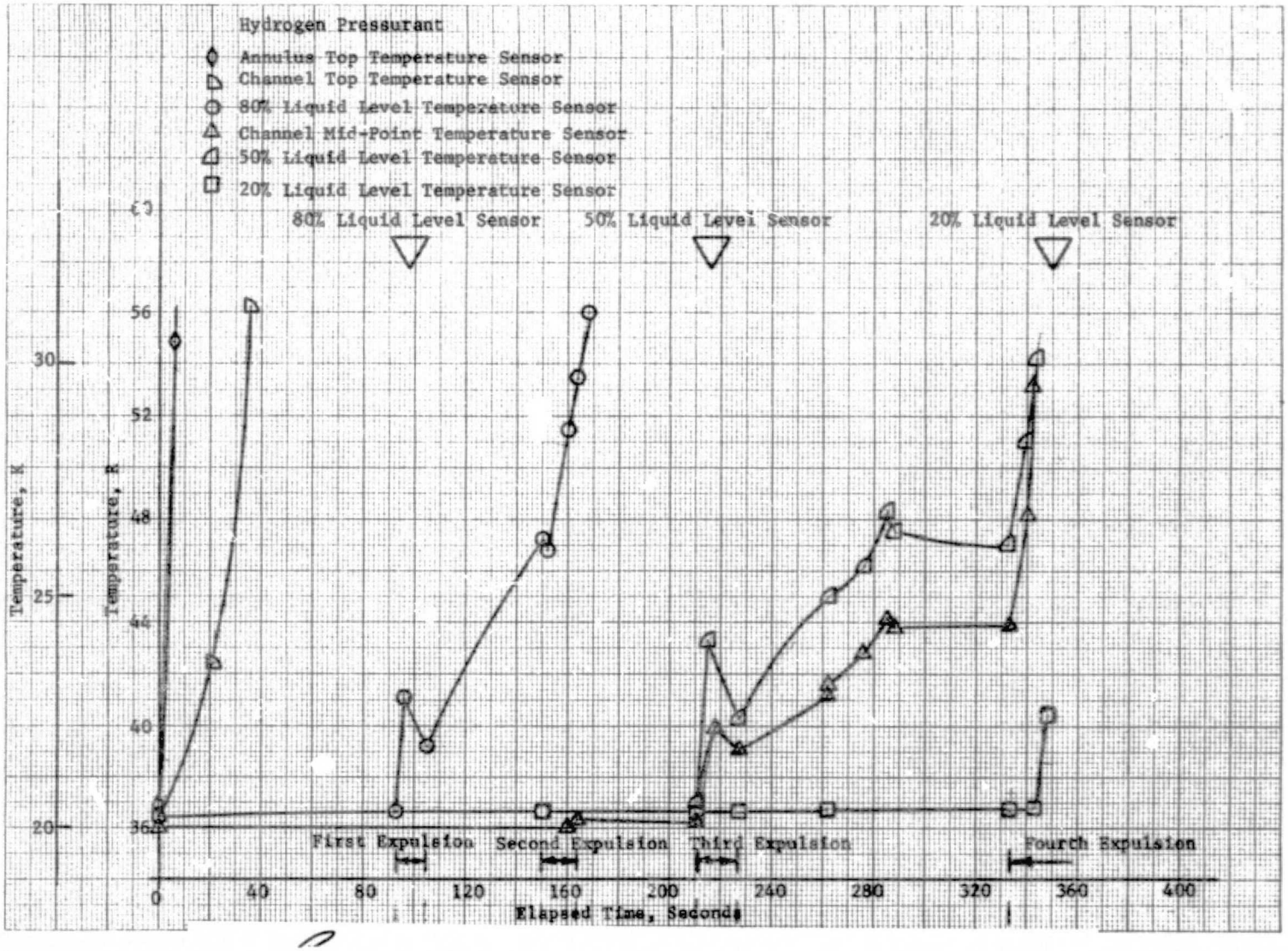

Figure 5.19: Temperature History for Test Plus G-1 with Hydrogen Pressurant

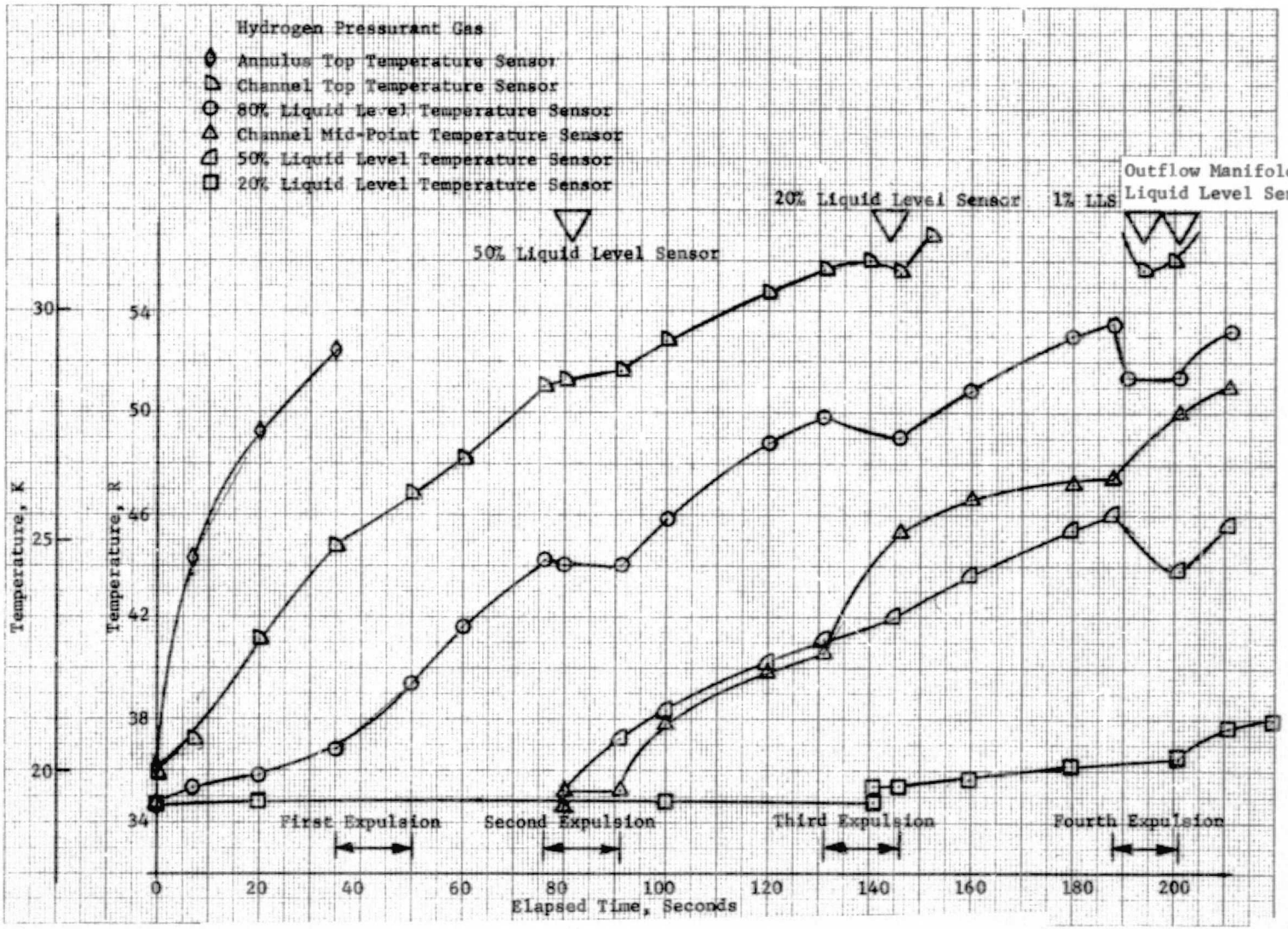

Figure 5.20: Temperature History for Test Plus G-4 with Hydrogen Pressurant

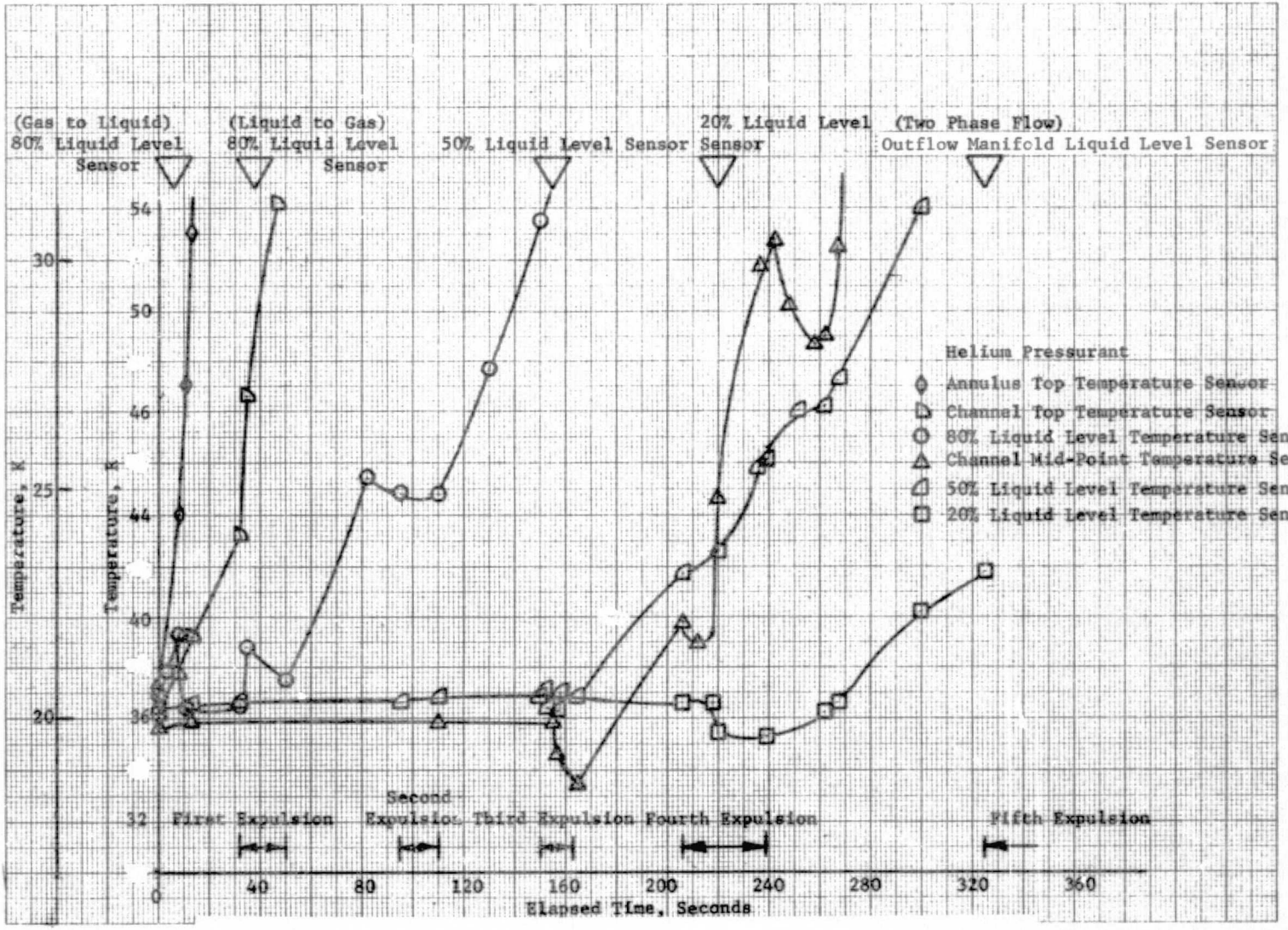

Figure 5.21: Temperature History for Test Plus G-2 with Helium Pressurant

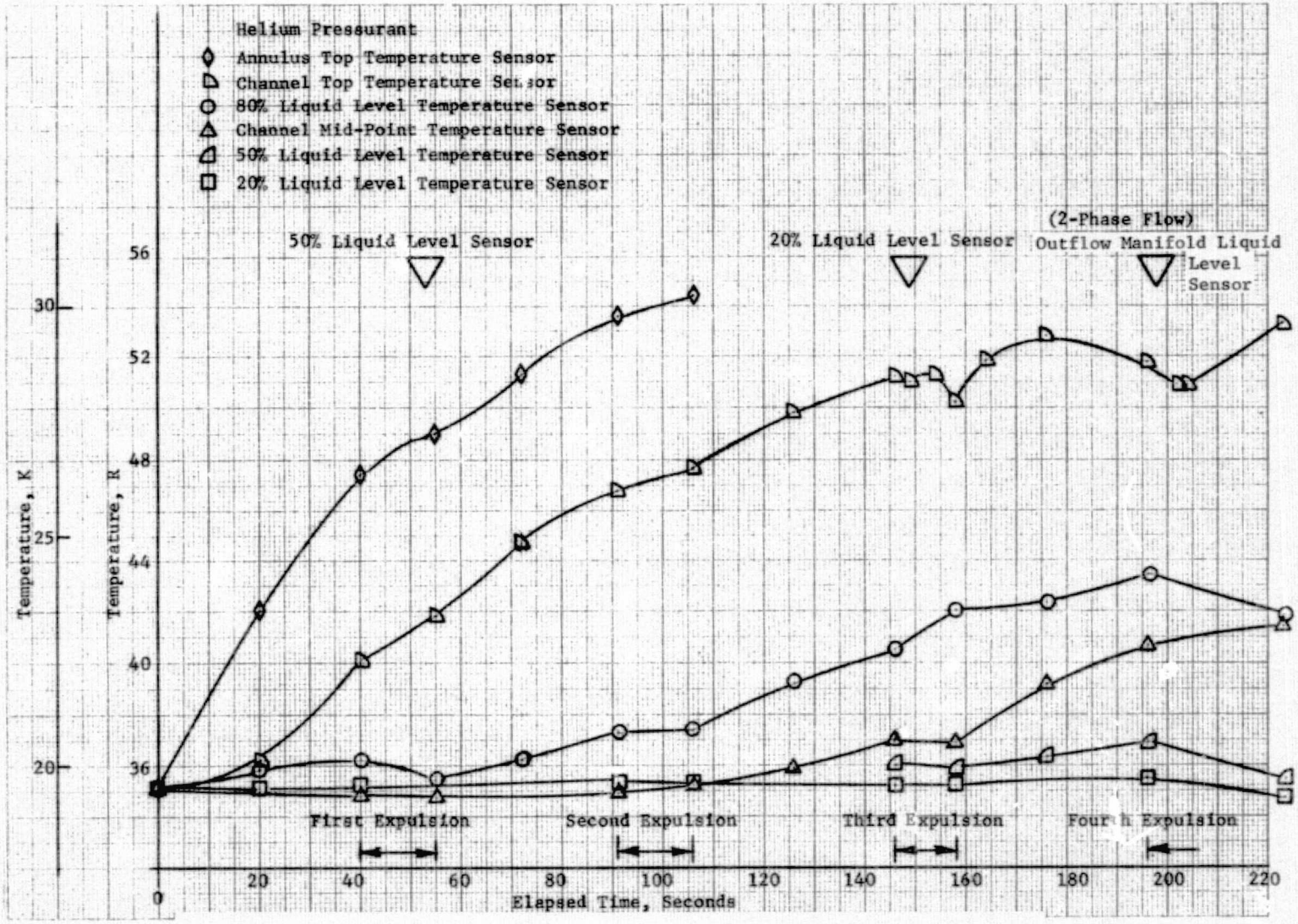

Figure 5.22: Temperature History for Test Plus G-3 with Helium Pressurant

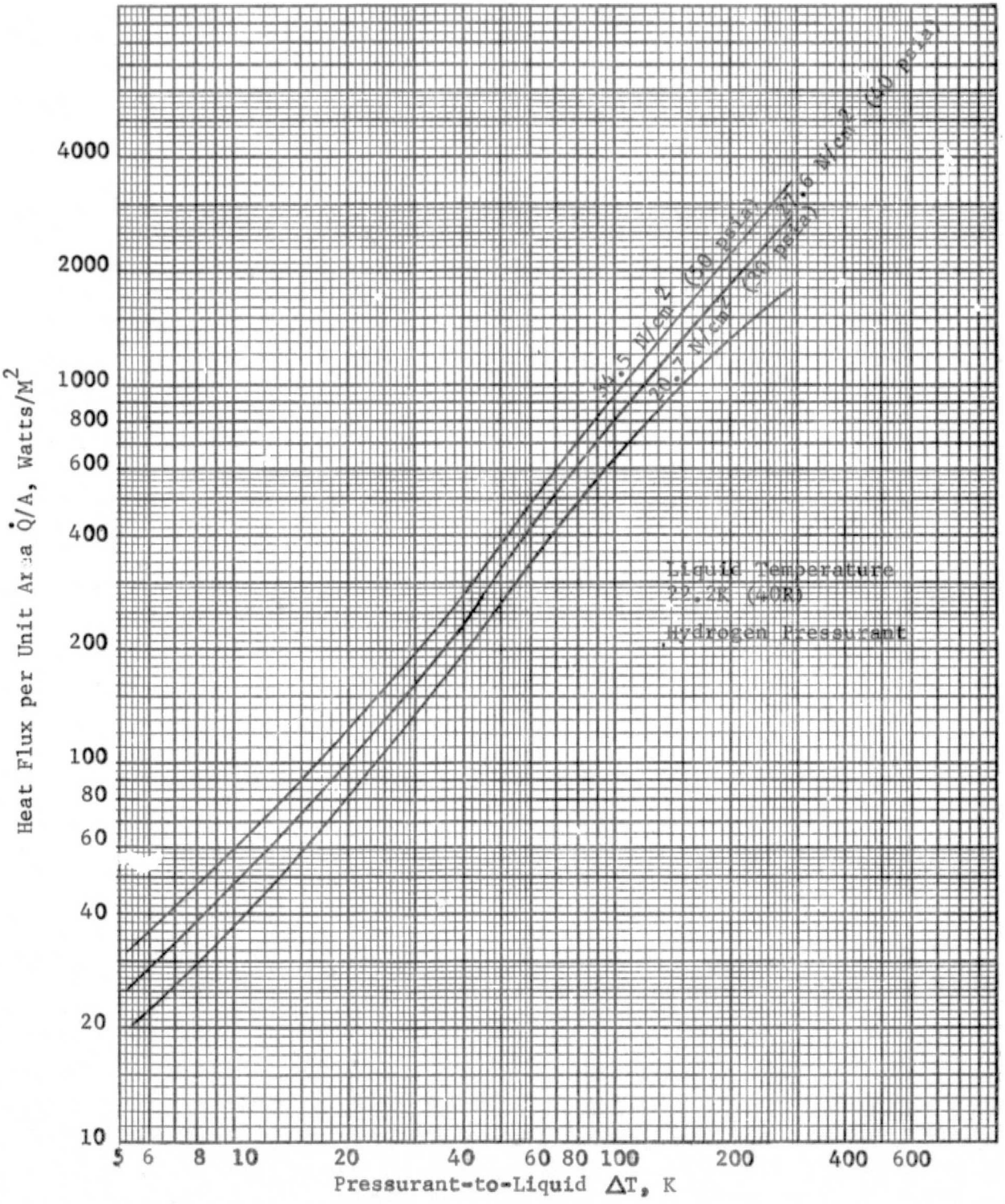

Figure 5.23a: Local Heat Flux Prediction at Screen Surface, Minus-G Attitude, Hydrogen Pressurant

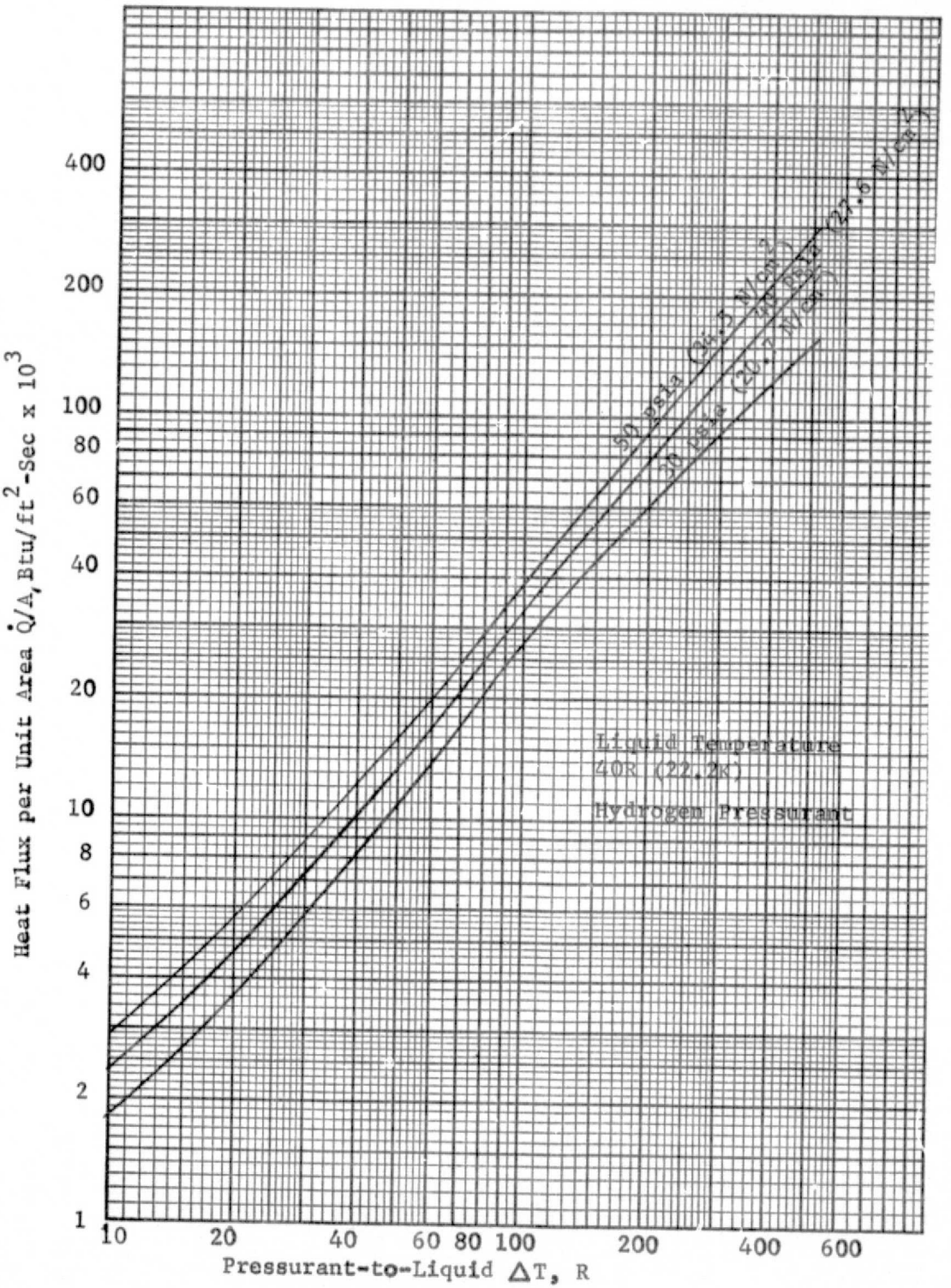

Figure 5.23b: Local Heat Flux Prediction at Screen Surface, Minus-G Attitude, Hydrogen Pressurant, English Units

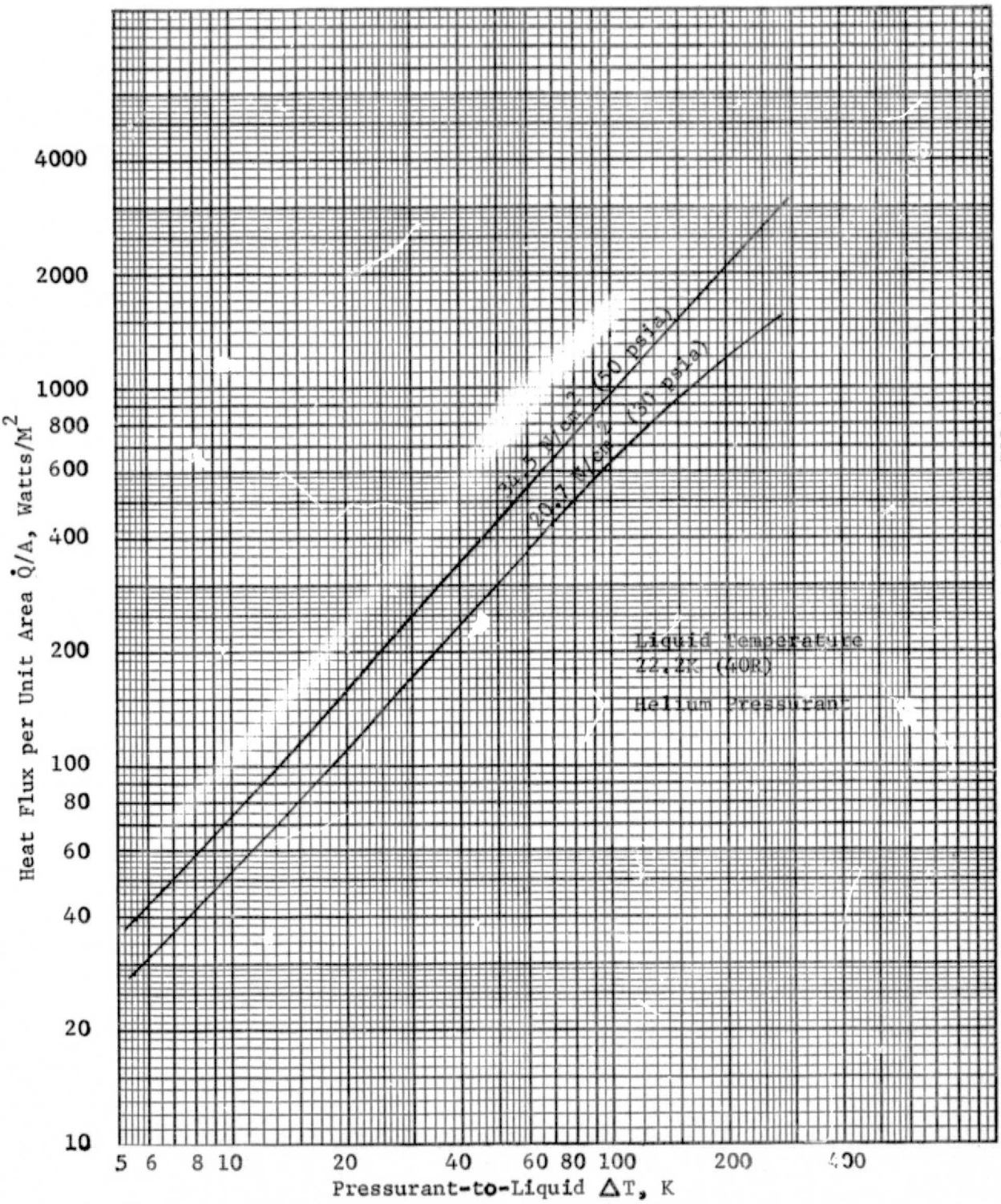

Figure 5.24a: Local Heat Flux Prediction at Screen Surface, Minus-G Attitude, Helium Pressurant

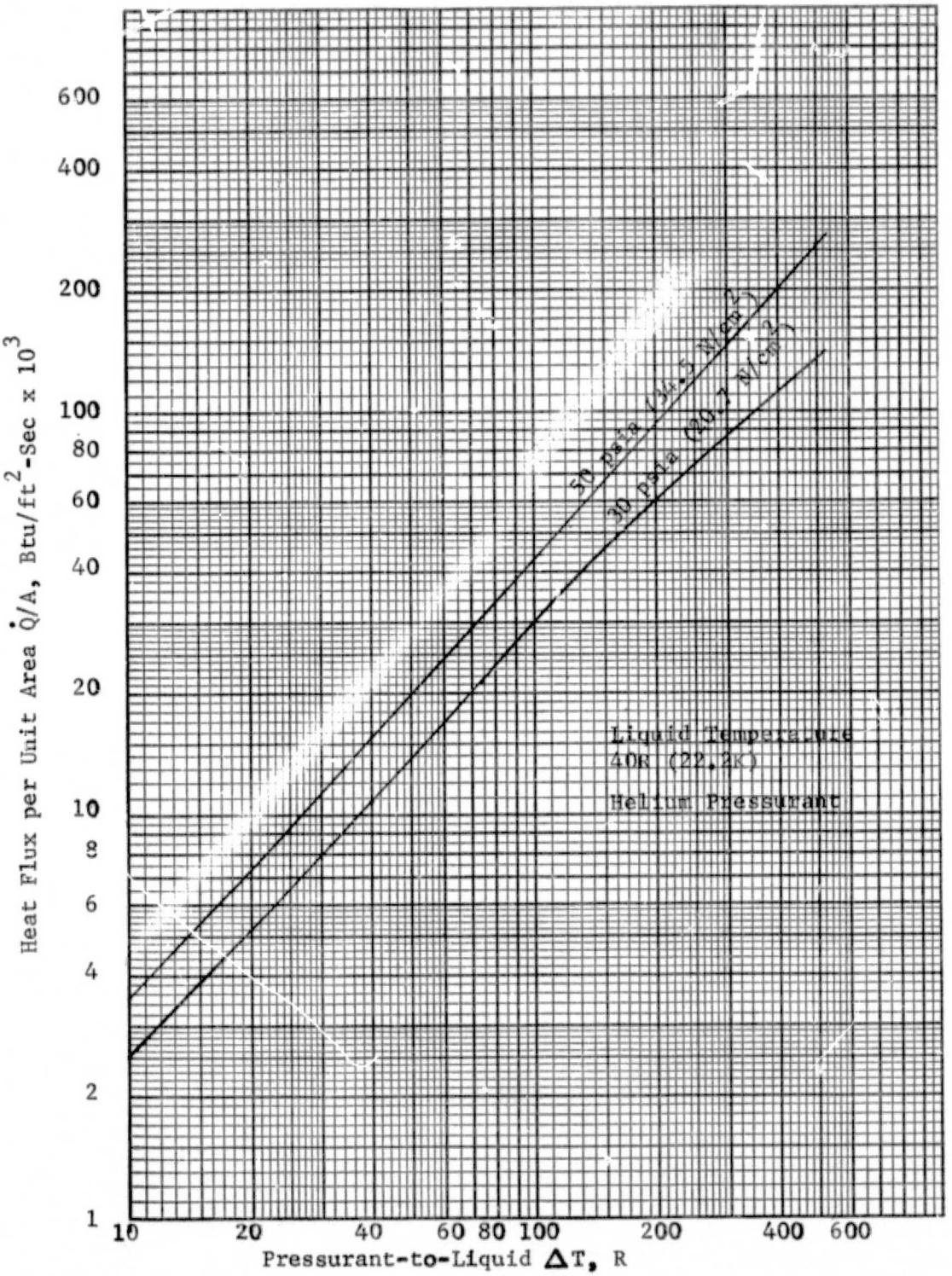

Figure 5.24b: Local Heat Flux Prediction at Screen Surface, Minus-G Attitude, Helium Pressurant, English Units

APPENDIX

The basic flow model, developed by F. M. Young under Contract NAS9-9313 (Ref. A-1), was modified to include nodes that simulate fine-mesh screen components of an acquisition system as well as a plotting routine and pressure and velocity time histories. The hydrualic transient model for a screen channel is illustrated in Figure A-1, and is described in the following equations. The equations describe a one-dimensional model that predicts the hydraulic transients between the bulk liquid and liquid in a flow channel that are separated by a fine-mesh screen. The nomenclature used is similar to that of Ref. A-1.

$$C_1 = V_1 - \frac{f}{2D_1} V_1 |V_1| \Delta t - \frac{S_1 g}{\rho a} P_1 \tag{A-1}$$

$$C_2 = \frac{S_1 g}{\rho A_1} \tag{A-2}$$

$$C_3 = V_2 - \frac{f}{2D_2} V_2 |V_2| \Delta t + \frac{S_2 g}{\rho a} P_2 \tag{A-3}$$

$$C_4 = \frac{S_2 g}{\rho A_2} \tag{A-4}$$

$$S_1 = +1 \text{ for left running wave} \tag{A-5}$$
$$= -1 \text{ for right running wave}$$

The conditions of a small time interval, Δt, are given by

$$VN_1 = C_1 + C_2 PN_1 \tag{A-6}$$

and

$$VN_2 = C_3 + C_4 PN_2 \tag{A-7}$$

Let the pressure drop across the screen satisfy the Armour and Cannon pressure drop condition (Ref. A-2) given by

$$f = \frac{\alpha}{N_{Re}} + \beta \tag{A-8}$$

where f is the friction factor and N_{Re} is the screen Reynold's

number.

$$f = \frac{\Delta P\ \varepsilon^2\ d}{L\ \rho\ U^2} \qquad \text{(A-9)}$$

$$N_{Re} = \frac{\rho U}{\mu a^2\ d} \qquad \text{(A-10)}$$

α = Viscous resistance coefficient (8.61) (Empirically Determined)

β = Inertial resistance coefficient (.52) (Empirically Determined)

P = Screen pressure drop

d = Screen pore diameter

L = Fluid path length = Q B

U = Fluid approach velocity

a = Surface area to volume ratio of screen

ε = Screen volume void fraction

μ = Fluid viscosity

ρ = Fluid density

B = Screen thickness

Q = Tortuosity factor

g = Acceleration

VN_1 = Upstream Velocity

VN_2 = Downstream Velocity

PN_1 = Upstream Pressure

PN_2 = Downstream Pressure

Using this form for the pressure drop data

$$-S_1\ VN_1 = -\frac{\alpha\mu a^2 d}{2\beta\rho} + \frac{1}{2}\sqrt{\left[\frac{\alpha\mu a^2 d}{\beta\rho}\right]^2 + \frac{4(PN_1 - PN_2)\ \varepsilon^2 d}{\beta L\rho}} \qquad \text{(A-11)}$$

for $PN_1 > PN_2$ and

$$S_1\ VN_1 = -\frac{\alpha\mu a^2 d}{2\beta\rho} + \frac{1}{2}\sqrt{\left[\frac{\alpha\mu a^2 d}{\beta\rho}\right]^2 + \frac{4(PN_2 - PN_1)\ \varepsilon^2 d}{\beta L\rho}} \qquad \text{(A-12)}$$

for $PN_2 > PN_1$

$$PN_1 = \left(\frac{VN_1 - C_1}{C_2}\right) \qquad \text{(A-13)}$$

$$PN_2 = \left(\frac{VN_2 - C_3}{C_4} \right) \tag{A-14}$$

Continuity implies

$$VN_2 = - VN_1 \frac{D_1^2 S_1}{D_2^2 S_2} \tag{A-15}$$

Let

$$A = \frac{\alpha \mu a^2 d}{\beta \rho} \tag{A-16}$$

$$B = \frac{\varepsilon^2 d}{\beta L \rho} \tag{A-17}$$

$$C = \left(\frac{D_1^2 S_1}{C_4 D_2^2 S_2} + \frac{1}{C_2} \right) \tag{A-18}$$

$$D = (C_3/C_4 - C_1/C_2) \tag{A-19}$$

$$E = S_1 A + B C \tag{A-20}$$

$$F = B D \tag{A-21}$$

From the above system it is seen that for $PN_1 > PN_2$

$$VN_1 = \frac{E \pm \sqrt{E^2 + 4 F}}{2} \tag{A-22}$$

and for $PN_2 > PN_1$

$$VN_1 = \frac{- E \pm \sqrt{E^2 - 4 F}}{2} \tag{A-23}$$

The appropriate sign is determined by substituting the results in equations (A-11) and (A-12). Thus, the pressures and velocity at the screen may be determined and the time increment advanced. The calculations are repeated as an iteration on time over the outflow period of interest.

Figure A-2 illustrates the nodal setup for the four channel model and test system.

The valve node is input as an array of orifice coefficients C versus time satisfying equation (A-24).

$$\dot{q} = C\sqrt{\Delta P} \qquad \text{(A-24)}$$

where $\dot{q}$ is the volumetric flow rate and ΔP is the pressure differential across the valve. The valve backpressure is also input. In the test system the flowmeter was located downstream of the valve; however, for this analysis it was located upstream of the valve and simply input as a series connection so that the flow rate may be printed out. The tank outlet and manifold are input as a series of two tee connections of very short length. The screen channels are input as lines of equivalent cross-sectional areas and length dependent on the liquid level. The hydrostatic pressure from the liquid level in the tank to various nodes is considered.

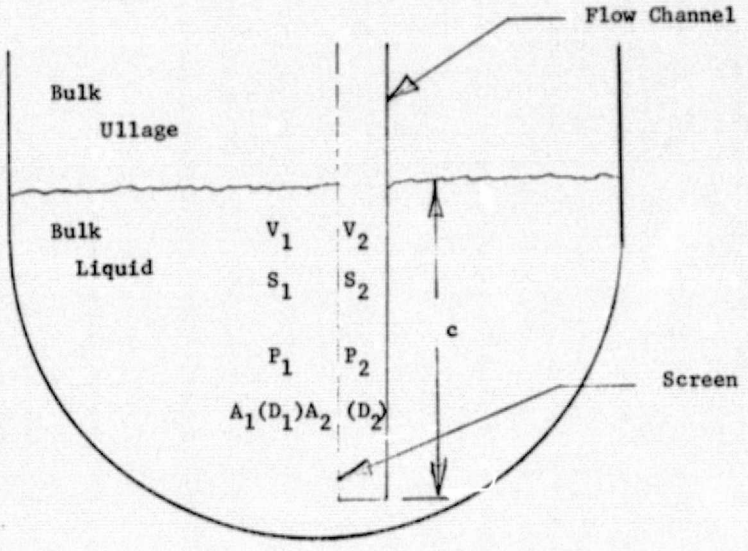

Schematic of Hydraulic Transient Model for Screen Channel

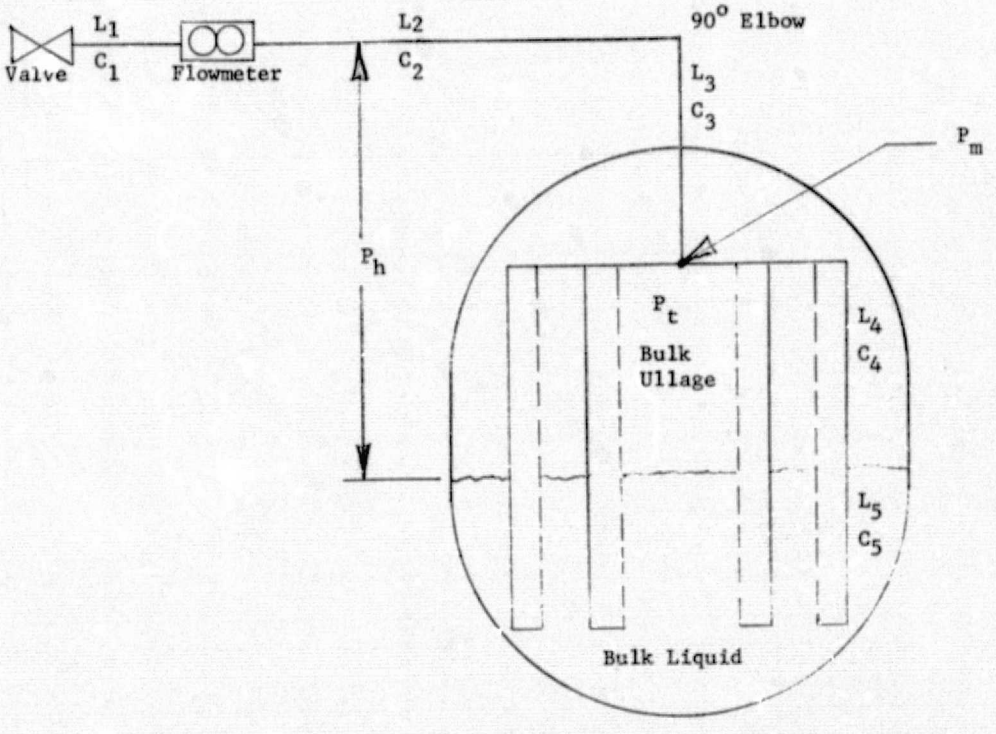

Schematic of Hydraulic Transient Model for Four-Channel Model and Test System

REFERENCES

1.1 G. F. Orton: Simulated Flight Vibration Testing of a Surface Tension Propellant Expulsion Screen. Thesis, Saint Louis University, 1971.

1.2 G. W. Burge, J. B. Blackmon: Study and Design of Cryogenic Propellant Acquisition Systems, Vol. II, Supporting Experimental Program, McDonnell Douglas Astronautics Co., Huntington Beach, California, December 1973, MDC G5038, Contract NAS8-27685.

1.3 G. R. Page: Final Report, Acquisition/Expulsion System for Earth-Orbital Propulsion System Study - Cryogenic Design, Vol. II. MCR-73-97. Martin Marietta Corporation, Denver, Colorado, October 1973. Contract NAS9-12182.

1.4 D. F. Gluck, et al: Transient Flow in Capillary Systems. SD-73-SA-0041. Rockwell International, Los Angeles, California, March 1973. Contract NAS7-200.

1.5 G. R. Page: Final Report, Acquisition/Expulsion System for Earth-Orbital Propulsion System Study - Cryogenic Test, Vol. III. MCR-73-97. Martin Marietta Corporation, Denver, Colorado, October, 1973. Contract NAS9-12182.

1.6 J. B. Blackmon: Design, Fabrication, Assembly and Test of a Liquid Hydrogen Acquisition Subsystem, McDonnell Douglas Astronautics Company, Huntington Beach, California, May 1974, MDC 5360, Contract NAS8-27571.

3.1 Theodore Baumeister and Lionel S. Marks: Standard Handbook for Mechanical Engineers, McGraw Hill Book Company 7th Edition, 1967, Pg 5-102.

3.2 ASME Boiler and Pressure Vessel Code, Division 2, Section VIII, Article 4-9, 1968.

4.1 D. F. Gluck: Transient Flow in Capillary Systems. SD73-SA-0041. Rockwell International, Space Division, Downey California, March 1973. Contract NAS7-200.

5.1 G. R. Page: Final Report, Acquisition/Expulsion System for Earth Orbital Propulsion System Study, Volume III - Cryogenic Test. MCR-73-97. Martin Marietta Corporation Denver, Colorado, October 1973. Contract NAS9-12182.

5.2 Lundberg, Reynolds and Kays: Heat Transfer with Laminar Flow in Concentric Annuli with Constant and Variable Wall Temperature and Heat Flux. NASA TND-1972.

A-1 F. M. Young: Hydraulic Transient Analysis Program. LME-1-71. Mechanical Engineering Department, Lamar State College of Technology, Beaumont, Texas. Contract NAS9-9313.

A-2 J. C. Armour and J. N. Cannon: "Fluid Flow Through Woven Screens", AIChE Journal, Vol. 14, No. 3, May 1968.